Master's thesis

NTNU
Norwegian University of Science and Technology
Faculty of Information Technology and Electrical Engineering
Department of Electric Power Engineering

Ragnhild Petterteig Mo

Analysis of Micro Hydropower Plant Connected to Microgrid in Island Mode Operation Consisting of Pump-as-Turbine, Self-Excited Induction Generator and Induction Generator Controller

Modeling and Laboratory Testing

Master's thesis in Energy and Environmental Engineering
Supervisor: Elisabetta Tedeschi
Co-Supervisor: Trond Leiv Toftevaag & Torbjørn Kristian Nielsen
July 2020

NTNU
Norwegian University of Science and Technology

Ragnhild Petterteig Mo

Analysis of Micro Hydropower Plant Connected to Microgrid in Island Mode Operation Consisting of Pump-as-Turbine, Self-Excited Induction Generator and Induction Generator Controller

Modeling and Laboratory Testing

Master's thesis in Energy and Environmental Engineering
Supervisor: Elisabetta Tedeschi
Co-Supervisor: Trond Leiv Toftevaag & Torbjørn Kristian Nielsen
July 2020

Norwegian University of Science and Technology
Faculty of Information Technology and Electrical Engineering
Department of Electric Power Engineering

NTNU
Norwegian University of
Science and Technology

Abstract

The aim of this thesis have been to analyze a cheap, robust, and simple micro hydropower plant consisting of a pump-as-turbine (PAT), a self-excited induction generator (SEIG) and an induction generator controller (IGC) connected in an islanded microgrid, supplying a varying single-phase village load. The long-term aim has been to prepare the evaluated system for implementation in decentralized villages in developing countries without connection to the main grid.

Some of the main obstacles when using an induction generator (IG), directly connected to an uncontrolled PAT, in stand-alone operations in an islanded microgrid are the difficulties of determining the excitation capacitance requirements, as well as ensuring stable voltage and frequency as the village load connected to the system varies. The objective of the IGC is to ensure a constant total consumed power seen from the generator, by dissipating surplus power to a ballast load, for the purpose of keeping the voltage and frequency deviations within a limited range. The necessary theory of the different components of the evaluated system is presented. The operating conditions of the tested system were defined so that it could be tested with the components which was already selected. Additionally, the power quality requirements of the microgrid were defined, under the assumption that the village load is purely resistive.

The IGC was first tested in the Electrical Machine Laboratory at the Norwegian University of Science and Technology (NTNU) without the PAT, to characterize its behavior. Thereafter, the whole stand-alone system was tested in the Waterpower Laboratory at NTNU, with the PAT as the prime mover. A simulation model of the tested system was also created in the SIMSCAPE environment in SIMULINK and MATLAB, for the purpose of verifying the laboratory test results. By creating a realistic, yet simplified simulation model, the system can, as further work, be analyzed for different topologies and with different parameters, for instance for other load power factors or with distribution lines.

The three-phase IG used, is converted to a single-phase IG by connecting the excitation capacitors in a C-2C connection. Depending on the operating frequency and the operating voltage, there exists one total load power ensuring a balanced operation of the generator in such a connection. The operating conditions for the tested system were therefore set mainly for obtaining a balanced operation of the IG. Both the laboratory tests and the simulations show that the tested system is able to supply a single-phase resistive load within the voltage and frequency requirements defined for the tested isolated system, at the defined operating conditions. However, the components used are not optimal. The test results show that the excitation capacitors integrated in the IGC cabinet are oversized. Both the PAT and the SEIG were operating in overload. The PAT has to operate far from the best efficiency point (BEP), because the BEP at the required head, is at a speed which is much higher than the operating speed. However, the behavior of the PAT seems good. As a result of the overloading of the generator, the line currents were measured to be up to 43 % higher than the rated current during the laboratory tests. This results in extra power

losses and a significant reduction of the efficiency. Overloading also result in a lower expected lifetime of the SEIG, which would contradict the requirement of robustness of the system.

Another concern for the tested system is that the IGC does not manage to ensure exact 230 V across the village load, thus it does not manage to ensure constant power seen from the generator, when the village load is varying. Due to the characteristic of the PAT and the IGC, both the frequency, voltage, and total load power increases when both the village load and the ballast load are consuming. This results in an unbalanced system and a further increase in two of the generator line currents. However, the voltage variation is only measured to be 2.6 $\%$ from the rated voltage, 230 V. The maximum frequency deviation is measured to be 6.6 $\%$ from the rated frequency 50 Hz, but the system frequency is never below 50 Hz. Because of the phase angle control method of the IGC, there are significant harmonics in the signal when both the ballast load and the village load are consuming. The maximal total harmonic distortion (THD) of the village load voltage and village load current is found to be 4.34 $\%$ and 4.33 $\%$ respectively. This is also within the power quality requirements defined.

Both the laboratory tests and the simulations show that the tested system, consisting of the pre-selected PAT, the pre-selected three-phase SEIG and the available IGC, is able to supply a varying single-phase resistive load within the voltage and frequency requirements defined for such isolated system, at the operating conditions defined. However, it is proposed to either reduce the excitation capacitor size in the IGC or that the SEIG in the tested system should be changed to a SEIG with a different magnetizing curve or higher rated current, in order to reduce the overloading of the SEIG and increase the efficiency.

Sammendrag

Målet med denne masteroppgaven har vært å analysere et billig, robust og enkelt mikro-vannkraftverk bestående av en pumpe-som-turbin (PAT), en egenmagnetisert asynkrongenerator (SEIG) og en asynkrongenerator-kontroller (IGC) koblet i et mikronett, som opererer i øydrift og forsyner en 1-fase landsby-last. Hensikten med denne masteroppgaven har vært å klargjøre det evaluerte systemet for å bli implementert i avsides landsbyer i utviklingsland, som ikke har tilknytning til sentralnettet.

Noen av de største utfordringene ved å bruke en asynkrongenerator (IG) alene i frittstående mikronett, er å bestemme størrelsen på magnetiseringskondensatorbankene, samt å sikre stabil spenning og frekvens når landsby-lasten varierer. Målet med IGCen er å sikre en konstant total effekt sett fra generatoren, ved å dumpe overskuddseffekt i en ballast-last. Formålet med dette er å holde spennings- og frekvensvariasjonene innenfor et begrenset intervall. Den nødvendige teorien om de forskjellige komponentene i det evaluerte systemet er presentert. Driftsbetingelsene til det testede systemet ble definert slik at det kunne testes med de komponentene som var tilgjengelige. I tillegg er kravene til el-kvaliteten i mikronettet definert. Først ble IGCen testet i Elektro-maskin-laboratoriet ved Norges Teknisk-Naturvitenskapelige Universitet (NTNU) uten PAT, for å kartlegge oppførselen dens. Deretter ble hele det frittstående systemet testet i Vannkraftlaboratoriet ved NTNU, med PATen som den primære kraftkilden. En simuleringsmodell av det testede systemet er også opprettet i SIMSCAPE i SIMULINK og MATLAB. Formålet er å verifisere laboratorieresultatene. Ved å lage en realistisk men forenklet simuleringsmodell av det testede systemet, kan videre arbeid være å analysere systemet for forskjellige topologier og med forskjellige parametere, som for eksempel ved andre effektfaktorer eller ved å inkludere overføringslinjer.

3-fase IGen som blir brukt i dette systemet konverteres til en 1-fase IG ved å koble magnetiseringskondensatorene i en C-2C kobling. I en slik kobling eksisterer det bare én totallast som sikrer balansert drift av generatoren, for en gitt driftsfrekvens og driftsspenning. Driftsbetingelsene for det testede systemet ble derfor satt hovedsakelig for å oppnå balansert drift av IGen. Både laboratorietestene og simuleringene viser at det testede systemet er i stand til å forsyne en varierende 1-fase resistiv last innenfor de spennings- og frekvenskravene som er definert, ved de definerte driftsforholdene. Kombinasjonen av de komponentene som blir brukt i dette systemet er imidlertid ikke optimal. Testresultatene viser at magnetiseringskondensatorene som er integrert i IGC-skapet er overdimensjonert. Både PATen og SEIGen blir derfor overbelastet. PATen må operere langt fra driftspunktet for beste virkningsgrad (BEP), fordi BEP ved den nødvendige fallhøyden oppnås ved en hastighet som er mye høyere enn driftshastigheten. Oppførselen til PATen er imidlertid bra. Overbelastningen av generatoren resulterer i at linjestrømmene blir målt til å være opp mot 43 % høyere enn den nominelle strømmen for generatoren. Dette resulterte i ekstra effekttap og en betydelig reduksjon i virkningsgraden av generatoren. Overbelastning resulterer også i en lavere forventet levetid for SEIG, noe som harmonierer dårlig med kravet om at systemet må være robust.

IGCen klarer ikke å sikre helt konstant 230 V over lasten og dermed klarer den heller ikke å holde en helt konstant totaleffekt sett fra generatoren når landsby-lasten varierer. Når både landsby-lasten og ballast-lasten konsumerer, øker både frekvensen, spenningen, samt den totale effekten, på grunn av karakteristikken til PATen og IGCen. Dette resulterer i et ubalansert system og strømmen i to av generatorlinjene øker ytterligere. Samtidig ble spenningsvariasjonen bare målt til å være 2.6 % høyere enn den definerte operasjons spenningen på 230 V. Det maksimale frekvensavviket ble målt til å være 6.6 % fra den definerte driftsfrekvensen på 50 Hz. Frekvensen ble aldri målt til å være under 50 Hz. Når både ballast-lasten og landsby-lasten konsumerer er det en betydelig andel med harmoniske komponenter i signalene på grunn av kontrollmetoden til IGCen. Den maksimale totale harmonisk forvrengningen (THD) i spenningen og strømmen i landsby-lasten er målt til henholdsvis 4.34 % og 4.33 %.

Både laboratorietestene og simuleringene viser at det testede systemet, som består av den forhåndsvalgte PATen, den forhåndsvalgte 3-fase SEIGen og den tilgjengelige IGCen, er i stand til å forsyne en varierende 1-fase resistiv landsby-last innenfor de spennings- og frekvenskravene som er blitt definert for et slikt isolert system, ved de driftsbetingelsene som også har blitt definert. Det blir imidlertid foreslått at størrelsen på magnetiseringskondensatorene integrert i IGCen bør reduseres eller at SEIG bør blir byttet ut, til en annen SEIG med en annen magnetiseringskurve eller høyere nominell strøm enn den som blir brukt i dette systemet. Dette er anbefalt for å redusere overbelastningen av SEIG og bedre virkningsgrad.

Preface

The following master thesis is my last work as a master student at the Department of Electric Power Engineering at the Norwegian University of Science and Technology (NTNU). The work is carried out the spring of 2020, in the Electrical machine laboratory at the Department of Electric Power Engineering and at the Waterpower laboratory at the NTNU.

In relation to the process of writing this thesis I wish to express a sincere appreciation to my supervisor professor Elisabetta Tedeschi, my co supervisor professor Torbjørn Kristian Nielsen and docent emeritus Trond Leiv Toftevaag for giving me guidance, helping me understand the different parts of the system considered and encourage me through laboratory testing of the system. In relation to the laboratory testing I want to show my appreciation to the technical staff at the Department of Electric Power Engineering, Bård Almås, Svein Erling Norum and Aksel Andreas Reitan Hanssen for the technical and physical contribution to my test setup and giving me assistance whenever there were a problem or uncertainties regarding the electrical equipment and test setup. I am also gratefully for the technical staff at the Department of Energy and Process Engineering Joar Grilstad, Halvor Haukvik and Trygve Opland for the assistance and support with the connection of the rig in the Waterpower laboratory, answering all my questions along the way and putting in the extra effort for ensuring easier control of the system to make me more comfortable with the laboratory testing. I also want to thank Johannes Opedal Kverno and Bård Aslak Brandåstrø for teaching me how to control the rig and some smart tricks for logging the measurements, which came in handy.

I also want to show my gratitude to my colleague for generously spending time to familiarize themselves to my problems and giving me input. I also want you to know that I am grateful for the sharing of knowledge in all the good discussions and conversations you all have given me both at school and after school, whenever I needed a second opinion. I also want to thank Olve Mo for giving input to the simulation model and for many good discussions. Finally, I want to give a huge thanks to my family and my partner Eirik Haugen Lillefosse for the love and moral support this year. I am thankful for your input and many helpful discussions throughout the day, both during the specialization project and this thesis. This master thesis would not have been possible without everyone's support and input. Thank you!

Trondheim
Ragnhild Petterteig Mo

TABLE OF CONTENTS

LIST OF FIGURES

LIST OF TABLES

LIST OF ABBREVIATIONS

AC	Alternating Current
BEP	Best Efficiency Point
ELC	Electric Load Controller
CFD	Computational fluid dynamics
DC	Direct Current
H-Q	Head (H) versus flow rate (Q)
IGC	Induction Generator Controller
IM	Induction Motor
IG	Induction Generator
NTNU	Norwegian University of Science and Technology
PAT	Pump-As-Turbine
PLL	Phase Lock Loop
PI	Proportional-Integral
PID	Proportional-Integral-Derivative
pu	Per-unit
RMS	Root Mean Square
SEIG	Self-Excited Induction Generator
VFD	Variable Frequency Drive
Δ	Delta connection
Y	Star connection

CHAPTER 1

INTRODUCTION

This thesis is part of an ongoing collaboration project between the Norwegian University of Science and Technology (NTNU) and the University of Tanzania, where the long-term aim is to design a simple, low-cost, and robust micro hydropower plant that can operate in stand-alone operations in an islanded microgrid. The purpose of the plant is to supply decentralized villages in developing countries, which do not have access to the main grid. To achieve a low-cost hydropower plant, a pump-as-turbine (PAT), a self-excited induction generator (SEIG) and a simple control unit, named induction generator controller (IGC) are used.

This thesis continues the work done in a specialization project carried out by the same author, at NTNU, during the fall of 2019. Therefore, parts of the background section are the same as in the specialization project [1].

1.1 Background

A cheap, robust and simple micro hydropower plant can play an important role in solving the issue related to access to electricity, focusing on decentralized villages in developing countries. For many locations in developing countries, grid connection is not available or too expensive. According to the world bank data, as much as 11 % of the world's population did not have access to electricity in 2017 [2]. The lack of electricity is mostly widespread in Sub-Africa and developing Asia. According to the same study presented by the world bank data, the number of people gaining access to electricity is increasing. At the same time, a report from the International Energy Agency states that between year

2012 and 2015 over 65 % of the gained access has come from fossil fuels [3]. Hydropower and other renewable energy sources can therefore be an essential and more sustainable source for low-cost power in these areas.

Hydropower is a robust and renewable power source, which in some areas are more continuously available than wind and solar power. Hydropower may also more feasible than other renewable sources. The technology of using a PAT and an induction generator (IG) in stand-alone operations is well known, but recently there has been a renewed interest in making this technology simple, both to implement and to maintain in areas short of expert knowledge and equipment. Hydropower systems are often expensive and require expensive control systems such as turbine governors. By using pumps and induction motors, which are easily available and low-cost due to mass production, micro hydropower systems become cheap and more robust. By reducing the initial cost of micro hydropower plants, the technology becomes more accessible, and the knowledge about such systems becomes distributed.

Some studies on different components used in the evaluated system have already been done in earlier theses and specialization projects at NTNU, by students with different backgrounds. S. Skjoldli and Ø. Albert have in [4] performed testing of a PAT. The same PAT is used in the tested system in this thesis. N. M. Whal has in [5] done laboratory tests and a literature study of an SEIG operating in stand-alone mode. The induction machine (IM) used in the tested system in this thesis, is the same as N. M. Whal studied. A. Andersson and E. Bye have in [6] done a literature study of an SEIG in stand-alone operations and evaluated different electronic load controllers (ELC) suitable to control the frequency and voltage in such stand-alone systems consisting of an SEIG. In relation with the specialization project an IGC was ordered. The working principle of a PAT is well established by A. A. Williams in *"Pumps as turbines for low cost micro hydro power"* [7] and *"Pumps as Turbines, A user's guide"* [8]. Using a motor as a generator together with an IGC has been explained thoroughly in *"Motors as generator for Micro-hydro power"* [9] by N. Smith. The working principal of a SEIG is thoroughly explained by J. Björnstedt in *"Island Operation with Induction Generators - Frequency and Voltage Control"* [10].

In addition to ensuring access to electricity in decentralized villages, the long-term goal of the system is to merge this micro hydropower plant with another ongoing project at the Department of Energy and Process Engineering at NTNU. The mentioned ongoing project aims to collect heat from the sun into an oil heater. The oil will be used for cooking purposes instead of the current solution of burning biomass. The control unit of the micro hydropower plant consists of a dump load, which is connected or disconnected to the plant as the surplus power of the plant varies. The idea is to integrate the dump load in the oil heater, such that the surplus power of the plant is not wasted. The oil heater is made for the purpose of reducing deforestation in developing countries [11].

1.2 Objective

The aim of this thesis is to analyze and test a low-cost, simple and robust micro hydropower plant as presented above, for different operating conditions with a varying village load. The test setup consists of the components available: a small induction machine is provided by the Department of Electric Power Engineering at NTNU, a small end-suction radial centrifugal pump and a control unit are both provided by the Department Energy and Process Engineering at NTNU. Voltage and frequency stability are the primary concerns of a stand-alone micro hydropower plant consisting of an SEIG, as well as the determination the size of the excitation capacitor. The main objective of this thesis is to provide a deeper understanding of the behavior of the plant based on laboratory tests, for the purpose to determine if it is possible to operate the system consisting of the selected low-cost components. The aim is to clarify conditions for achieving efficient operation in a location in Tanzania that is not yet selected. Another objective is to create a simulation model of the tested system in the SIMSCAPE environment in SIMULINK and MATLAB, for the purpose of verifying the laboratory test results. By creating a realistic, yet simplified model, the system can as further work be analyzed for different typologies and with different parameters for instance for different load power factor and with distribution lines.

A theoretical description of the PAT will be given as well as the disadvantages that this comes with. The IM is robust and cheap, but has some challenges with frequency and voltage regulations when it is used in stand-alone operation in an islanded microgrid. The main challenge is to control the voltage and frequency when the electrical power consumption varies. The main challenge of using a PAT, is to predict the operation point of the PAT. The aim is to decide the size of the loads that can be connect and determine the excitation capacitor size in order to obtain the desired voltage level and frequency in the tested system.

Generally, the produced power in a microgrid is changed in order to meet the load power. This requires accurate control of the power supply, and many electronic components, which are expensive. The plant is also typically, designed to meet the peak load demand of the consumer. In the evaluated microgrid system the load must meet the total power generated by the PAT and SEIG, and not the opposite.

1.3 Scope of Work

The scope of work is itemized below.

- Study the theoretical description, the working principles and the behavior of a PAT.
- Study the theoretical description, the working principles and the behavior of an SEIG.
- Study the most common exciting control techniques for the IGC.
- Define the operating conditions of the evaluated stand-alone micro hydropower

plant, consisting of the pre-selected PAT, the pre-selected SEIG and the available IGC.

- Define the power quality requirements for the evaluated isolated system.
- Perform laboratory testing of the IGC in the electrical laboratory at NTNU, in order to get to know its behavior.
- Perform laboratory testing of the evaluated micro hydropower plant, consisting of the available PAT, the SEIG and the IGC, in the Waterpower laboratory at NTNU.
- Create a simulation model of the system in SIMULINK and compare the test results with the simulation results.

1.4 Limitations

The limitation of work in this thesis is itemized below.

- Transients in the evaluated system is not considered.
- The distribution lines are not included, either in the simulation model nor in the test setup.
- The characteristics of the PAT is not known, and neither elaborated during the tests.
- The PI-regulator in the IGC is not tuned. The vendor of the IGC has not provided much information about the IGC, thus some assumptions were made. A lot of time was spent on trying to contact them.
- The power quality criteria only concern small-distribution voltage stability.
- The simulations only observe steady stare operations. The dynamic of the PAT is not included.
- The loads connected to the microgrid is assumed purely resistive.
- The plant site is fictive, and it is assumed that the available head and flow rate at the final site are as high as necessary.
- The system is assumed temperature invariant and all the machine parameters are assumed constant, except the magnetizing reactance which is affected by magnetic saturation.
- The efficiency of the IM used as an IG in the laboratory tests, is assumed to be equal to 80 %, since accurate data was not available.
- The power factor of the IG is assumed equal to the power factor when operating as an IM.
- Iron losses are neglected in the simulation model.
- Regarding the limitations in the practical implementation of the work of this thesis, it's worth mentioning that due to guidelines at NTNU, during the pandemic of the

COVID-19 virus, it was not allowed to perform laboratory testing at campus in March and April. The author applied for laboratory access, and the testing started in the mid-May, which resulted in a limited period for laboratory testing.

1.5 Relation to Specialization Project

The specialization project *"Analysis of a self-excited induction generator used in a micro hydropower plant"* [1], written in the fall of 2019 by the same author, is functioning as a pre-project for this thesis, and is therefore essential for the work to be conducted.

The same three-phase IG evaluated in the specialization project is evaluated in this thesis. The difference is that in the specialization project the IG was connected in star and supplied power to a balanced three phase load without a functioning IGC. Now the three-phase IG is connected with excitation capacitors in a configuration that allows single-phase load.

The basic work done in the specialization project, that included finding the circuit parameters of the machine and the magnetizing curve, also known as the no-load curve, are used in this thesis as well. The circuit parameters were found by preforming a DC-test, a no-load test and blocked rotor test. The obtained results are presented in table 2 in Appendix C. The magnetizing curve was found by a no-load test, and the obtained result is shown in table 1 in Appendix B.

In order to analyze the behavior of the SEIG in the evaluated system, some of the fundamental theory presented in the specialization project will be reused in this thesis. Some sections are directly reused, and some sections are shorted or modified in order to better present the theory. Some of the limitations of the thesis are also the same. An overview of the relation to the specialization project are given in the list below.

- The first paragraphs of Section 2.2 present a modified version of the theory presented in the specialization project.
- Subsection 2.2.1 is reused, with minor adjustments.
- The first two paragraph of Subsection 2.2.2 are reused, only shorted.
- In subsection 2.2.2.1 the first six paragraphs are reused. Some are shorted and some have smaller adjustments. The rest of the subsection is original work.
- In Subsection 2.4.1 the first paragraph is a modified version of a similar paragraph presented in the specialization project, and the second paragraph is reused with smaller adjustments.

1.6 Outline

Chapter 2 contains a description of the evaluated system, and covers the necessary theoretical background of each component, in order to be able to analyze the tested system.

Chapter 3 presents the defined operating conditions of the evaluated stand-alone system when using the available IGC, PAT and SEIG.

Chapter 4 presents the defined power quality requirements for the evaluated isolated system.

Chapter 5 presents a description of the test setup, and the test procedure when testing the IGC and SEIG without the PAT. The test results are also presented and discussed.

Chapter 6 presents a description of the test setup, and the test procedure when testing the evaluated system, consisting of the PAT, the SEIG and the IGC, in the Waterpower laboratory. The test results are also presented and discussed.

Chapter 7 presents a description of the created simulation model of the evaluated system, consisting of the PAT, the SEIG and the IGC. The simulation results are also presented, discussed and compared to the test results from the laboratory.

Chapter 8 sums up the work presented and the main findings in this work.

Chapter 9 presents suggestions on further work.

CHAPTER 2

SYSTEM DESCRIPTION

A cheap and robust micro hydropower plant consisting of a pump-as-turbine (PAT), an induction generator (IG), and an induction generator controller (IGC) will be evaluated and analyzed throughout this thesis. The IGC is a type of electric load controller (ELC) used together with an induction generator.

Micro hydropower plants are defined as power plants with a capacity of 100 kW or less [12]. The evaluated micro hydropower plant will be operating in stand-alone operation in an islanded microgrid, supplying a single-phase village load. An islanded microgrid is a power network delivering power to a local area without any connection to the main grid [13]. By stand-alone mode, it means that the micro hydropower plant is the only energy source in the microgrid. This also means that the produced power by the plant must meet the consumed power, for the purpose of ensuring stable voltage and frequency.

The circuit diagram of the micro hydropower plant in the studied microgrid is shown in Figure 2.1.

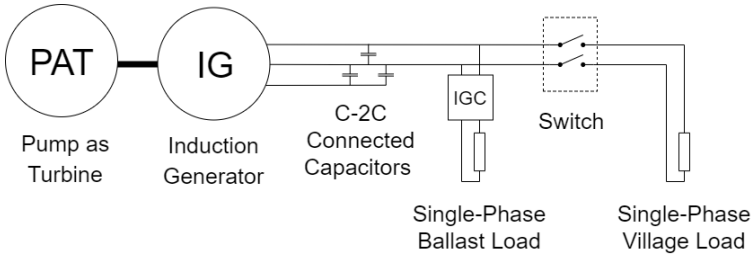

Figure 2.1: Circuit diagram of the micro hydropower plant and the microgrid evaluated in this thesis

In this chapter, the working principles and the necessary theory for each component in the evaluated system will be presented.

2.1 Pump-as-Turbine

A pump used in reverse is referred to as PAT. A PAT works by using the outlet of the pump as inlet, and the inlet of the pump as outlet. This way the PAT converts the hydraulic energy from the water to mechanical energy at the shaft. Different types of pumps can be used as PAT, but the conventional centrifugal pump with an end-suction is the most suitable [8]. The PAT which will be used throughout this thesis is an end-suction, radial, centrifugal pump. Figure 2.2 shows a sketch of such a pump, showing the inlet and the outlet in pump mode.

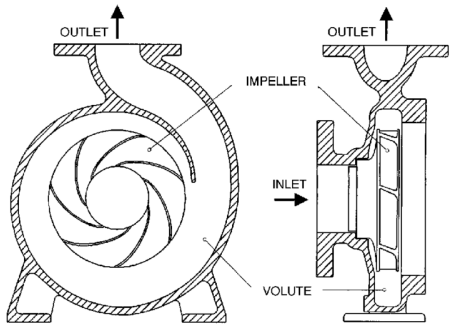

Figure 2.2: Sketch of a regular, radial centrifugal pump with end-suction. Obtained from [14]

A PAT is used as the turbine in this micro hydropower plant because of the aim of a low-cost power plant. Centrifugal pumps are mass-produced and used in widespread applications, and because of this, both the PAT and the spear parts are easily available and cheap [7]. The use of a PAT compared to a typical hydro turbine may reduce the capital cost of the plant, of the order of 10-1 [15]. Pumps are commonly used and available in

many sizes and for different heads and flows. It is, therefore, possible to self-pick the right pump for a specific site. The PAT is also easy to install, operate and maintain, compared to a typical turbine, and for a low capacity plant (less than 500 kW) a PAT can hence be a big advantage seen from an economical point of view [16]. Even though the simplicity of the PAT has many advantages, there are some disadvantages as well. The efficiency is far from the efficiency of a turbine. Skilled manufactures can achieve an efficiency equal to 96 $\%$ for a hydro turbine. A PAT may be able to achieve the same efficiency as the pump in pump mode, but the PAT efficiency is often some percentages lower than the pump efficiency [17]. A small centrifugal pump usually has an efficiency between 50-70 $\%$, while medium or larger pumps have an efficiency between 70-90 $\%$ [18]. Another disadvantage is that the PAT has a more limited range of flow rates in which the unit can operate, which will be further explained later in this chapter.

The amount of potential and kinetic energy, one kilogram of water delivers when passing through the plant, is defined as the gross specific energy of the plant [Nm/kg]. The gross specific energy, E_{gr} is shown in equation (2.1), where g is the acceleration of gravity [m/s^2], and H_{gr} is the gross head [m]. The gross head is defined as the level difference between the water surface of the upper reservoir or the forebay tank and the outlet of the turbine measured in meter. The forebay tank is illustrated in Figure 2.6.

$$E_{gr} = g \cdot H_{gr} \tag{2.1}$$

The gross power of the plant, P_{gr}, also known as the available power from nature is defined as shown in equation (2.2). Where Q is the flow rate, which is defined as the amount of water passing through a point, during a specific time, measured in cubic meters of water per second [m^3/s]. ρ is the water density [kg/m^3], which is approximately equal to 10^3 kg/m^3.

$$P_{gr} = Q \cdot H_{gr} \cdot g \cdot \rho \tag{2.2}$$

The available hydraulic power of the plant, P_{net}, shown in equation (2.3), depends on the net head, H_n. The net head considers the specific hydraulic energy loss, H_l between the forebay tank and the inlet of the turbine [19], shown in equation (2.4). The hydraulic losses include friction loss within the pipeline, which is proportional to the length of the pipeline, and singular losses due to valves, bends and changes in cross-section [20].

$$P_{net} = Q \cdot H_n \cdot g \cdot \rho \tag{2.3}$$

$$H_n = H_{gr} - H_l \tag{2.4}$$

The available power at the shaft, $P_{turbine}$, also known as the extracted power by the turbine or delivered power by the turbine, depends on the net head, flow rate, and the efficiency

of the turbine. The equation for the extracted power by the turbine is shown in equation (2.5). Where η_t is the efficiency of the turbine,

$$P_{turbine} = Q \cdot H_n \cdot g \cdot \rho \cdot \eta_t = P_{net} \cdot \eta_t \tag{2.5}$$

The developed torque at the turbine shaft, the mechanical torque, τ_m, can be expressed as shown in equation (2.6). Where w_r is the mechanical angular speed of the rotor [rad/s].

$$\tau_m = \frac{P_{turbine}}{w_r} \tag{2.6}$$

The hydraulic efficiency of the PAT, η_t, is calculated as shown in equation (2.7).

$$\eta_t = \frac{P_{turbine}}{P_{net}} = \frac{\tau_m \cdot w_r}{Q \cdot H_n \cdot g \cdot \rho} \tag{2.7}$$

The turbines used in hydropower plants are divided into two main groups based on their operation, reaction turbines, and impulse turbines. The impulse turbine converts kinetic energy from high-velocity water flow to mechanical energy, by changing the direction of the flow and create an impulse force that spins the turbine [19, 20, 21]. The reaction turbines are enclosed in a pressure casing, and it is a pressure difference between the inlet and the outlet of the turbine. The mechanical energy in a reaction turbine is produced both by the pressure difference, because of the head, and the impulse force, because of the chance of direction in velocity [20]. A PAT is categorized as a reaction turbine [8, 21].

A typical head - flow rate characteristic, later referred to as a H-Q characteristic, of a pump both in pump mode and in turbine mode is shown in Figure 2.3. The reference flow rate, Q is positive in pump mode, as indicated in the small figure in the top right corner. This means that the right side of the graph represents the pump in pump mode and the left side of the graph shows the characteristic of the pump in turbine mode. The upper characteristic shows the behavior at different net heads, H_n, and flow rates, Q, for a constant speed *n*. The speed has positive rotation in pump mode and will rotate in the opposite direction when operating as a turbine. The bottom graph shows the turbine efficiency and the extracted power by the pump or turbine as a function of the flow rate at a constant speed. In pump mode, the power represents the consumed power, and in turbine mode, the power represents the extracted power from the PAT. The dotted line shows the best efficient point (BEP) on the H-Q curve in both modes. The BEP represents at which flow rate and head, at constant speed, the efficiency is the highest.

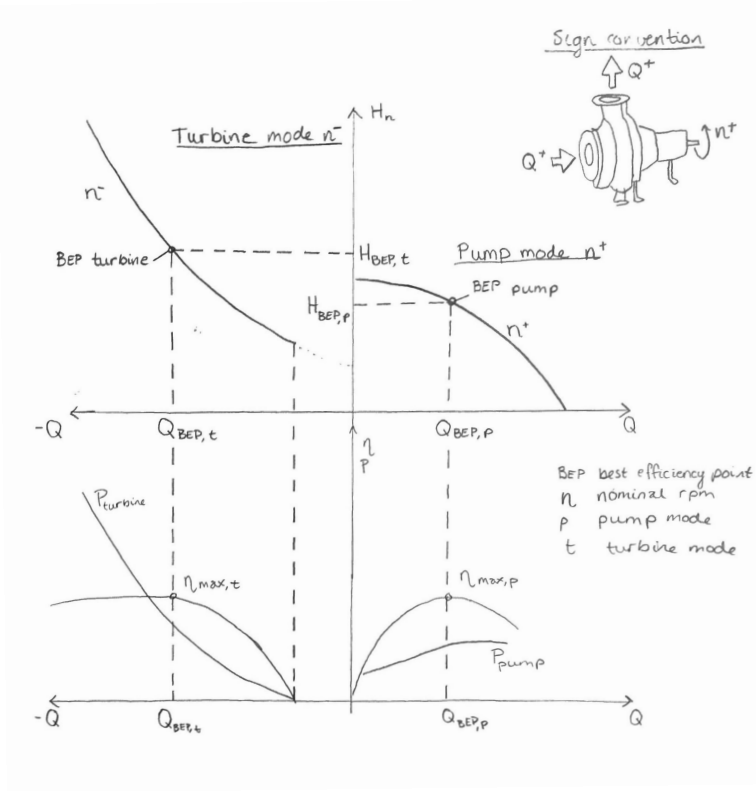

Figure 2.3: General characteristics of the behavior of a pump in both pump mode and turbine mode. Showing the net head vs the flow rate, the extracted power vs the flow rate, and the efficiency vs the flow rate. Reproduced from [17]

The relationship between the behavior in pump mode and the behavior in turbine mode depends on the flow pattern in the pump, the efficiency and the pump design (vane angles, number of impeller vanes, etc.). These are not the same for all pump types and sizes, and the behavior can differ considerably from one PAT to another [17]. The characteristic in Figure 2.3 is only a general behavior.

The ideal fluid theory would say that the BEP would be at the same head and flow when operating as a pump and when operating as a turbine at a constant speed. This is not the case, because of the hydraulic losses, the head and often the flow in turbine mode must be higher at the BEP, than in pump mode, for a radial pump [17, 22].

It can also be seen that, when the pump is operating as a turbine at low flow rates, the pressure head is lower than in pump mode. This can be seen in Figure 2.3 at low flows.

The rate of change in the mechanical angular rotor speed in the system, $\frac{dw_r}{dt}$ can be expressed by equation (2.8), also known as the rotational motion equation or the torque balance equation [10, 23]. Where J is the moment of inertia of all rotating mass [kgm^2], including both the PAT and the induction machine. τ_m is the mechanical torque at the shaft [Nm], τ_e is the generator electromagnetic torque [Nm], D is the friction factor, and w_r is the mechanical angular rotor speed [rad/s].

$$J\frac{dw_r}{dt} = \tau_m - \tau_e - D \cdot w_r \tag{2.8}$$

Figure 2.4 shows a general description of how the characteristic curve for a radial flow PAT changes at different speeds. The operating point for the PAT is at the intersection of the characteristic curves of the PAT and the site curve, the dotted vertical line. The site curve, also known as the system resistance curve, represents the characteristic of the site, which is the available net head [17]. Here the site curve is shown as a constant head, which is a simplification. In reality, the available net head is reduced for increasing flow rates because of penstock losses. The site curve has a parabolic form because the losses are a function of the flow rate square [8, 17]. The operating point will move along the site curve as the speed of the PAT changes, and thus the flow rate will change. Figure 2.4 therefore shows both the change of flow rate and the change of operating point as the speed changes, at constant head.

The dotted line to the left in the figure with legend τ = *0* shows the no-load line, where the torque on the shaft is zero. The intersection between the no-load line and the site curve give the runaway speed of the PAT. The runaway speed is defined as the speed of the turbine at a fixed head when the power output is zero, also known as the maximum speed of the PAT. The corresponding flow at this intersection is called the runaway flow. The runaway speed of a PAT is usually between 120 -160 % of the nominal speed [8, 17]. After full load rejection, grid failure, or voltage collapse the system may accelerate to runaway speed. There is a probability that this can happen, and all the rotating elements connected to the PAT should, therefore, withstand the runaway speed. The bottom line in the H-Q graph is the characteristic curve at standstill, where the rotating speed is zero and the torque is maximum, also known as the standstill line. At high heads, all the performance curves will eventually merge with the standstill line. The figure also shows 4 operating points at different speeds of the PAT, corresponding to different efficiencies and thus, different extracted power.

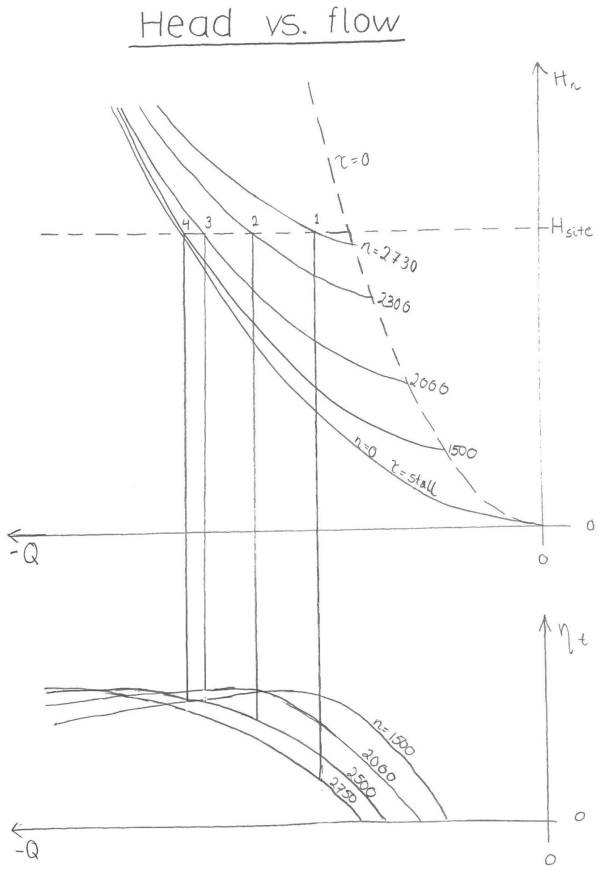

Figure 2.4: Shows the change of operating point for the PAT, when the turbine speed changes with constant head. Reproduced from [17]

It can be seen from Figure 2.4 that the flow rate chances with speed, and so does the efficiency. If both the flow rate and the efficiency changes with speed, so does the power extracted by the PAT, seen from equation (2.5). A typical relationship between the turbine power and speed is shown in Figure 2.5. The amplitude and the maximal speed, known as the runaway speed, will chance with the head. If the net head is increased, both the extracted power peak and the runaway speed would increase. This power-speed characteristic corresponds to the example in Figure 2.4. Operating point 1, 2, 3 and 4 represent the same operating point as shown in Figure 2.4.

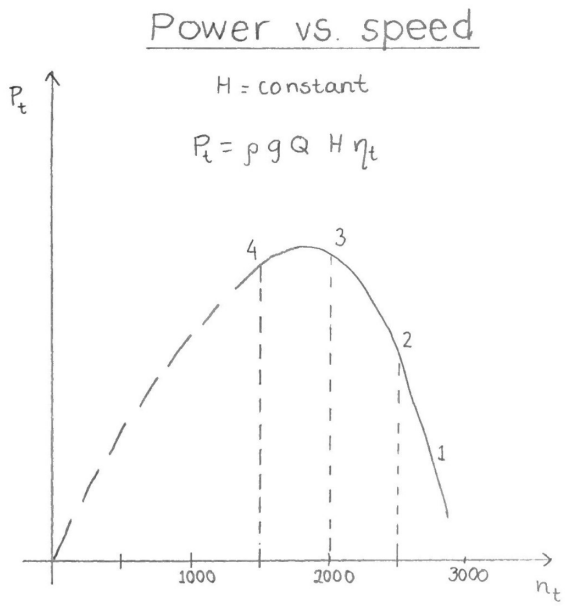

Figure 2.5: Power-speed characteristics of the PAT, with constant net head. Operating point 1, 2, 3 and 4 is the same as in Figure 2.4. Reproduced from [17].

The power-speed characteristic is relatively flat around the maximum power output, here between point 3 and 4, compared to characteristic between point 2 and 3. This is the case for all reaction turbines. If the turbine is operated far away from the maximum power point, an increase or a decrease in speed will result in a relatively higher change in power. A PAT is usually operated near operating point 4.

The performance curves of a PAT presented in Figure 2.3, 2.4 and 2.5, are usually not available. Usually, the only available data is the pump performance data or only the BEP in pump mode at specified speeds. The challenge is therefore to predict the performance of the pump used in revers as a turbine, in order to pick the right PAT for a specific site. There have been developed several methods of predicting the performance of a PAT, based on the pump data. The prediction methods usually concentrate on the prediction of the PAT BEP and not the whole PAT performance curve. In [24], eight different prediction techniques were investigated and compared to test results by A. A. Williams. The comparison was done for 35 different pumps, and the results show that no method predicted the behavior with 100 % certainty. The results also show that the prediction method named Sharma, proposed by K. R. Sharma is the recommended prediction method. The designer should have in mind that also the results from this prediction method can divert with $\pm$ 20 % from the actual values [8].

The prediction method Sharma combined by the affinity laws, predicts the head and flow rate at the BEP when running the PAT with a turbine speed n_t [8]. Equation (2.9) shows the equation to predict the head and equation (2.10) shows the equation to predict the flow rate. When using the affinities laws, it is assumed constant maximum efficiency for all speeds.

$$H_{BEP,t} = (\frac{n_t}{n_p})^2 \frac{H_{BEP,p}}{\eta_{max}^{1.2}} \tag{2.9}$$

$$Q_{BEP,t} = \frac{n_t}{n_p} \frac{Q_{BEP,p}}{\eta_{max}^{0.8}} \tag{2.10}$$

Where $H_{BEP,p}$ $[m]$ and $Q_{BEP,p}$ $[m^3/s]$ is the head and flow rate at the pump BEP at nominal pump speed n_p $[rpm]$. η_{max} is the maximal efficiency for the pump at nominal speed. The calculated head and flow rate are only approximations and it is important to remember that the real head and flow rate for the PAT BEP can divert from the calculated values. The only way to achieve reliable results is through testing of the PAT. This may, on the other hand, offset the low-cost advantages of using a PAT.

It can be seen from Figure 2.3 that the efficiency curve of the PAT keeps a high value for higher flow rates than the flow rate at the BEP [22]. A general tip when selecting the PAT is to select a PAT with a bit lower BEP than the designed net head and flow rate for the site. This way it will operate in the overload range. By doing this the errors and uncertainties in the prediction of the behavior of the PAT become less severe [17]. If the PAT absorbs a head and flow which is lower than the designed site head or flow, the available power will be lower, but the operating point will be nearer the BEP so the efficiency increase, resulting in a minimal change in extracted power. If the same had happened when the PAT was operating in under load range, both the available power and the efficiency would decrease, resulting in a decreased extracted power. If the PAT absorbs the designed head and flow or higher, the efficiency will be lower than at BEP, but the amount of power will be almost the same.

As mentioned earlier, one of the disadvantages of the PAT is that it has a limited range of flow rates in which the PAT can operate. A conventional turbine is designed to operate at variable flow rate, and still match the turbine power with the load power [17] and ensuring a constant speed. This can be done by adjusting the guide vanes at the inlet of the turbine. The guide vanes are adjustable blades that can change the flow rate in the turbine, by changing the angle of the vanes. This is done to adjust the turbine power when the electrical load changes, in order to operate efficiently at varying conditions [4, 19, 25]. The guide vanes make it possible to regulate the turbine output and still operate efficient and at stable speed in order to obtain constant frequency in the grid. A pump, on the other hand, is usually designed for one particular operation, at a constant head, flow rate, and speed, known as the BEP. Because of this, the pump has no guide vanes, which means that the energy from the PAT is not controllable.

Since the PAT does not have these guide vanes, the water flow cannot be controlled. If the load changes, so does the speed and the operating point of the PAT. This will also affect the frequency and the voltage in the system. The PAT is therefore not suitable for a plant with varying flow conditions into the turbine. The PAT is often used in hydropower plant which is run by the river, ensuring a constant water flow to the turbine. Figure 2.6 shows a typical run-of-river scheme, showing the main elements such as the intake, channel, forebay tank, the penstock, and the powerhouse. The scheme will depend on each site topology and hydraulic conditions, but the principle will be general [26]. In a run-of-river micro hydropower plant, the intake diverts some of the water from the river to the forebay tank through the channel. The forebay tank operates as a buffer and ensures a constant flow rate thus constant head to the turbine, as well as a transition from open channel to low-pressurized flow in the penstock. The excessive water will flow over the edge because of a free water surface. The penstock supplies the water to the turbine. The penstock is enclosed, and the water is under pressure. Both the PAT and the induction generator are located in the powerhouse. In such a scheme, no expensive water storage is required [21], and by avoiding this, the cost of the plant reduces and a big encroachment in nature is avoided. The construction of the plant beside the powerhouse will not be in focus in this thesis but is mentioned to get a perspective of the planned plant.

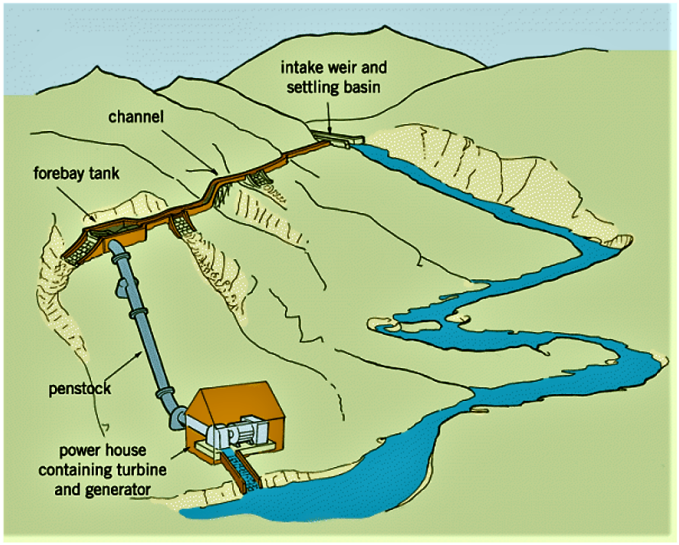

Figure 2.6: Typical scheme of a run-of-river micro hydropower plant. Showing the intake, channel, forebay tank, penstock, and the powerhouse. Obtained from [26]

The PAT that will be used in the micro hydropower plant evaluated in this thesis is named Pedrello FG 32/160 B and is shown in Figure 2.7. The technical data for this pump can be found in [27] and some of this data is also listed in table 2.1 below.

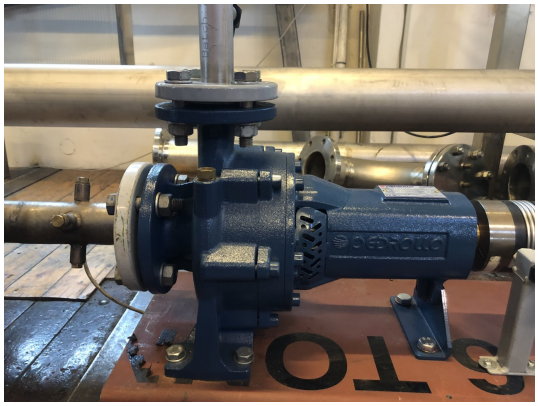

Figure 2.7: Picture of the pump-as-turbine which will be considered throughout this thesis

Table 2.1: Some of the available technical data for the pump that will be used as a turbine in this thesis. Obtained from [27]

Technical data		
Pump speed 2900 rpm		
Head [m]	H_{BEP}	23.5
Flow rate [m^3/h]	Q_{BEP}	18
Efficiency	η_{max}	58 %
Pump speed 1450 rpm		
Head [m]	H_{BEP}	6.2
Flow rate [m^3/h]	Q_{BEP}	8.7
Efficiency	η_{max}	55 %

2.2 Induction Generator

The generator aims to convert the mechanical power, delivered by the PAT to electrical power, which can be transmitted to the village. In this micro hydropower plant, a three-phase AC squirrel cage induction motor (IM) will be used as an induction generator. The induction generator is preferred over the DC generator and synchronous generator, because:

- It is a commonly used motor, which means it is easily available
- It is robust
- It has cheap production costs
- It has low maintenance demand
- It is easily installed

- It has self-protection against short circuit
- It has a wide power range
- It has simple control demands

The induction generators disadvantages, on the other hand, are the consumption of reactive power, and the difficulties of deciding the required excitation capacitor size. In stand-alone operations it is also difficult to control the voltage and frequency of the IG, during variation in load. Even so, in this system, the arguments that the machine is cheap, less complex, and easily maintained are heavily weighted, and an IM will hence be used as a generator in this micro hydropower plant.

The induction generator will supply a single-phase load, but a single-phase induction machine generally cost more per kW than a three-phase induction machine [28]. Hence a three-phase generator is used and converted to a single-phase generator by connecting the excitation capacitors in a certain way, which will be presented later in this section.

The IM used as a generator in the tested micro hydropower plant is shown in Figure 2.8, and the nameplate data is given in Table 2.2 and in Figure A in Appendix A.

Table 2.2: The nameplate data of the induction machine which will be used and evaluated in this thesis. Reused from [1]

Machine parameters	
ID number	A03-0107
Nominal speed	1420 [rpm]
Rated frequency	50 [Hz]
Number of poles	4
Nominal RMS line voltage in Y-connection	400 [V]
Nominal RMS line voltage in Δ-connection	230 [V]
Power in motor mode	1.5 [kW]
Power factor	0.81
Nominal RMS line current in Y-connection	3.45 [A]
Nominal RMS line current in Δ-connection	6 [A]
Assumed efficiency	0.85

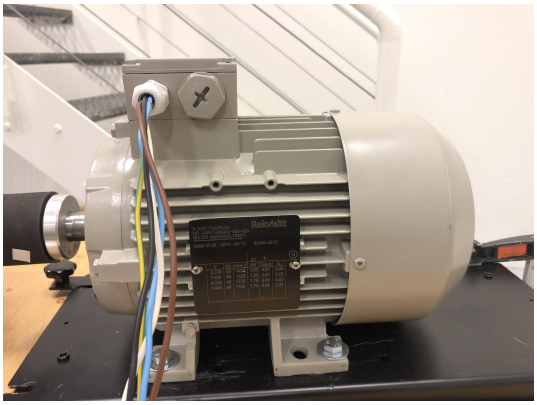

Figure 2.8: Picture of the induction machine which will be used and evaluated in this thesis. ID number: A03-0107. Reused from [1]

To be able to understand the behavior of this system, it is necessary to know the basic operations of the induction machine. In this section the behavior of an IM is briefly explained. This is done to easier understand the operations of a stand-alone induction generator, which will also be explained in this section.

2.2.1 Working Principle

By applying three-phase sinusoidal current at the stator terminals of an IM, there will be produced a rotating magnetic field in the air gap of the motor. The rotor conductors motion relative to the magnetic field produced by the stator, also known as the slip speed, leads to an induced voltage in the conductors in the rotor. The angular velocity of the magnetic field produced by the alternating stator currents, w_s, is dependent on the frequency of the stator current, f_1, as shown in equation 2.11. Equation 2.12 shows the rotating speed of the stator field in [rpm], where p is the number of pole pairs in the machine. This is also defined as the synchronous speed of the machine, n_{sync}.

$$w_s = 2 \cdot \pi \cdot \frac{f_1}{p} \tag{2.11}$$

$$n_{sync} = \frac{60 \cdot f_1}{p} \tag{2.12}$$

Due to the shorted rotor conductors, the induced voltage in the rotor will lead to a flow of alternating current in the rotor. The frequency of the produced current, f_2, depends on the relative speed, slip speed, between the magnetic field wave produced by the stator with respect to the rotor, and the frequency of the rotor current, seen in equation 2.13. Where s is the slip of the machine defined as shown in equation 2.14, where n_{sync} is the synchronous speed of the motor in [rpm] and n_r is the rotor speed in [rpm], calculated as

shown in equation 2.15.

$$f_2 = s \cdot f_1 \tag{2.13}$$

$$s = \frac{n_{sync} - n_r}{n_{sync}} = \frac{w_s - w_r}{w_s} \tag{2.14}$$

$$n_r = (1 - s) \cdot n_{sync} \tag{2.15}$$

The rotor current will lag behind the induced voltage because the rotor conductors are inductive. Furthermore, the rotor currents will also produce a magnetic rotating field, which will interact with the magnetic field from the stator and produce a torque. The magnitude of the induced torque, τ_{ind} is given by equation 2.16.

$$\tau_{ind} = kB_r B_{net} \cdot sin(\delta) \tag{2.16}$$

Where k is a proportional factor, B_R is the magnetic field produced by the rotor current [T], B_{net} is the magnetic field in the motor, which is the net magnetic field of the rotor field and the stator field [T], and δ is the angle between the magnetic field produced by the rotor current and the net magnetic field in the motor, which depends on the slip thus the size of the load [29]. This can be seen from Figure 2.9, which shows a machine with light and heavy load.

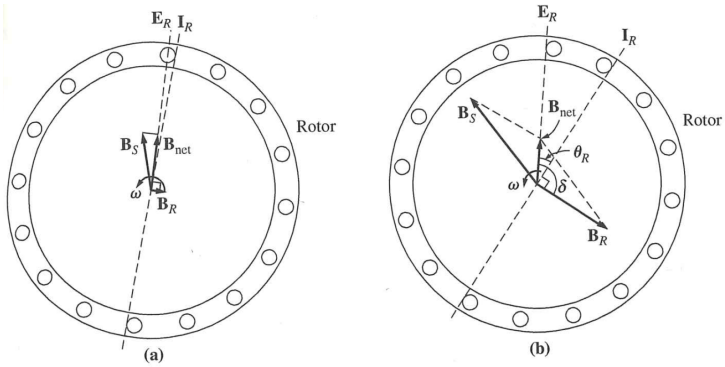

Figure 2.9: The magnetic fields in an induction machine under heavy load (b) and lights load (a). Obtained from [29]

As the load increase meaning the induced torque increase, the rotor slip increases at constant supply frequency. As the slip increase, so does the rotor current, the magnetic field produced by the rotor, the rotor frequency seen from equation (2.13), and the rotor inductance which is proportional to the frequency. The increase in the rotor inductance makes the rotor current lag the rotor voltage even more, hence δ increase with increasing load.

Figure 2.10 shows the induced torque as a function of the speed and the slip, which is referred to as the torque-speed characteristics of an induction machine. This characteristic gives information about the operation of the machine when operating as both motor and generator. The characteristic shows that the induced torque is zero at no-load, that the motor operation region is when the speed is between $0 < n_r < n_{sync}$, and that the machine operates as a generator when the speed is higher than n_{sync}.

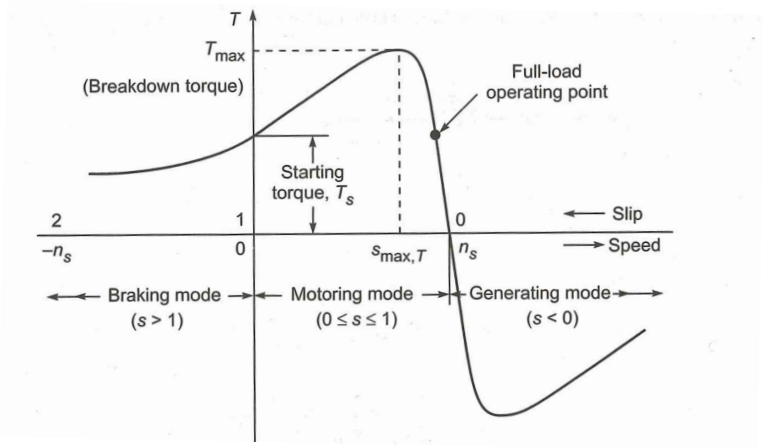

Figure 2.10: The relation between the speed and an induced torque in the induction machine. Obtained from [30]

It is clear that the frequency of the machine is mainly a result of the rotor speed, but is also affected by the load because the difference between the mechanical load and the electrical load affects the speed shown in equation (2.8). However, it is sufficient to say that due to the steep torque-speed characteristics of the induction machine the total frequency variation at nominal operations is limited, at constant mechanical angular velocity. This limitation will be within 5 $\%$ [29, 31]. The voltage magnitude, on the other hand, is mainly decided by the external reactive power source connected to the machine terminals.

The negative peak in Figure 2.10 represents the maximum torque which can be developed in generator mode. The generation will collapse, and the operation will be unstable if the electric load increase beyond this point.

Two other important phenomena of the torque-speed characteristic, is firstly that with a constant voltage-frequency ratio, the curve will be staggered to the left or right depending on the stator frequency as illustrated in Figure 2.11 (a). The figure illustrates the behavior of a machine with one pole pair. Secondly, the torque at a given speed for a given stator frequency will vary with the square of the terminal voltage [29] as illustrated in Figure 2.11 (b).

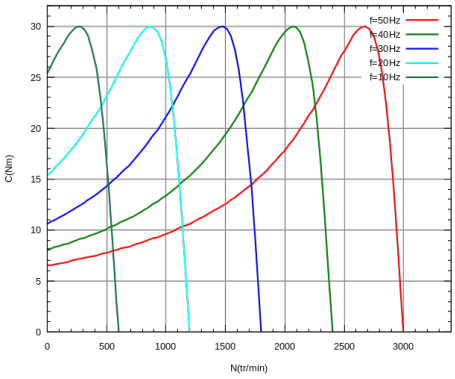

(a) General torque-speed characteristic for an induction motor at different frequency with a constant voltage-frequency ratio. Obtained from [32]

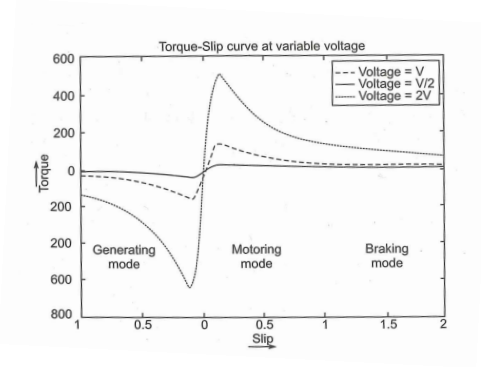

(b) General torque-speed characteristic for an induction machine for different voltage levels at constant frequency. Obtained from [30]

Figure 2.11: Torque-speed characteristics for varying frequency with constant voltage-frequency ratio (a) and varying voltage at constant frequency (b)

2.2.2 Self-Excited Induction Generator

An induction generator operating in stand-alone mode in an islanded microgrid is often referred to as a self-excited induction generator. This is because the generator needs to build up its own voltage before it can operate as a generator, and this process is called self-excitation, which will be explained here. The generator requires an external reactive power source in order to self-excite. The reactive source is generally capacitors connected to the generator terminals, referred to as excitation capacitors.

The most crucial parameters for the self-excitation of the generator is the speed of the shaft, the residual magnetism in the rotor and the size of the capacitor [33]. When the rotor shaft starts to rotate due to the prime mover, the residual flux in the rotor will rotate. Due to the relative movement between the stator coils and the rotating magnetic field, there will be induced a small voltage in the stator conductors. Since the capacitor is connected to the stator terminals the induced voltage produces a small capacitive current. This current leads the induced voltage by 90 degrees, and will, therefore, generate a magnetic field in the same direction as the residual flux in the rotor. This means the flux is reinforced and the induce voltage increases, thus the circulating current in the stator increase as well. This will go on until the machine voltage is built up. The final voltage value is based on the machine saturation characteristic in the magnetic circuit and the size of the capacitor. The magnetic characteristics of the machine are represented by the magnetizing curve, which will be more explained in the section below. Whether there exists some residual flux in the rotor or not depends on how the excited generator was stopped last time it was used. Björnstedt shows in [10], that the residual flux in the rotor can be lost if a

fault accrue, depending on the fault circuit current. It was also observed during testing in the project thesis [1] that the residual flux was too low to excite the generator after tests where the voltage collapsed because the prime mover torque was to low compared to the electrical load torque. In order to increase this residual flux, a DC source or a battery can be connected to two of the stator terminals for a short period of time.

2.2.2.1 Magnetizing Curve and Excitation Capacitors

As already mentioned, the magnetic field will be produced by the stator always lead the current in the rotor. Hench the induction machine will always consume reactive power in order to excite, both in motor operations and in generator operations. This reactive power must be delivered from an external source. Initially charged capacitors are therefore connected to the stator terminals in order to supply reactive power to the machine, to make the voltage-buildup possible as explained. Since there is no control of the rotor currents there is also no control of the output voltage of the induction generator in stand-alone mode. The capacitors will therefore have some control of the terminal voltage of the generator [29].

The magnetization curve, also known as the no-load curve or the excitation curve, represents the saturation of the iron in the machine. The curve shows the relation between the airgap voltage and the magnetizing current I_M at a given frequency. This curve is usually found by a no-load test. The magnetization curve for the induction machine which is used in the evaluated system in this thesis was found in the specialization project [1], and is shown in Appendix B. This curve is directly related to the geometry of the machine, the type of iron, the dimension of the core and the windings of the machine [34]. The magnetization curve is highly frequency-dependent, and a typical magnetizing curve at different frequencies is shown in Figure 2.12 (a), where w_1<w_2<w_3. Figure 2.12 (b) shows a magnetization curve along with three per phase capacitor curves for a given frequency. The capacitor curves show the capacitive current, I_c, which is produced as a function of the applied voltage, V_t, for a given capacitor size, C_{phase}, and frequency f_1, shown in equation (2.17). X_c is the excitation reactance. Capacitor Small C < Medium C < Large C, which also means that $X_{m,small} > X_{m,medium} > X_{m,large}$.

$$V_t = X_c \cdot I_c = \frac{1}{2\pi f_1 \cdot C_{phase}} \cdot I_c \tag{2.17}$$

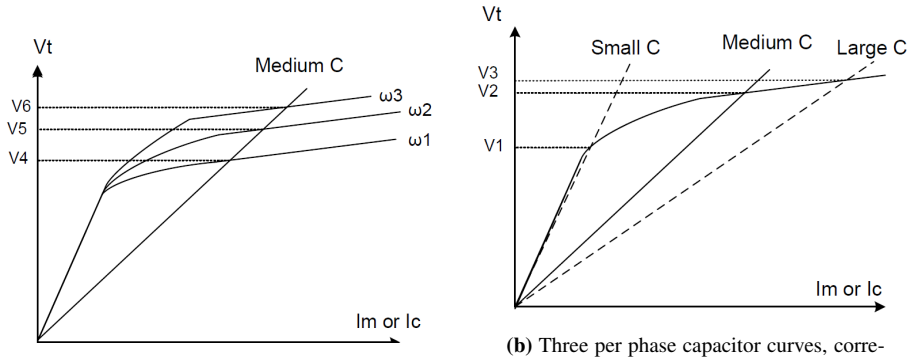

(a) The magnetization curve of an induction machine at different frequencies

(b) Three per phase capacitor curves, corresponding to three different capacitor sizes, and the magnetization curve of an induction machine for a given frequency

Figure 2.12: The magnetizing curve for different frequencies (a) and capacitor curves for different capacitor sizes (b). Obtained from [31]

Choosing the right size of the capacitor is crucial and will together with the magnetizing curve, determine the terminal voltage and the self-excitation. This is because the intersecting point between the capacitor curve and the magnetizing curve of the machine will be the steady-state value for the generator voltage and capacitor current, for a given frequency and capacitor size, at no-load. The capacitor line for the small capacitor is aligning with the linear part of the excitation line of the machine, so self-excitation will not be certain. If a smaller capacitor than the small capacitor shown in Figure 2.12 (b) is connected to the terminals of a generator, the generator would not excite. The generator would not excite because the capacitor would be too low and would not supply enough reactive power. The amount of reactive power supplied by the capacitor is dependent on both the frequency and the square of the voltage as shown in equation (2.18).

$$Q_{phase} = V_t \cdot I_c = 2\pi \cdot f_1 \cdot C_{phase} \cdot V_t^2 \tag{2.18}$$

When using the medium capacitor, the steady-state voltage will be where the intersection of the capacitor curve and the magnetization curve occur. This intersection gives a no-load terminal voltage, V_4 for w_1, V_5 for w_2 and V_6 at w_3, as shown in Figure 2.12 (a). By changing the capacitor connected to the induction machine, the terminal voltage can be adjusted to the desired value. The intersection point between the capacitor and the magnetization curve must not correspond to a current higher than the rated current given in table 2.2. If the operating capacitor current is higher than the rated current, the winding current will also be high, and saturation in the windings of the generator can occur which will result in decreased efficiency caused by heat dissipation.

Figure 2.12 (a) does not illustrate the fact that the capacitor curves also are frequency dependent. X_m is inversely proportional to the frequency, and the curve will, therefore, become steeper as the frequency decrease. If the speed is reduced, higher capacitors are

needed in order to both excited the machine and to obtain a desired voltage level.

The capacitor size is here referred to as the capacitor size in each phase. For a star-connected generator, excited by a delta-connected capacitor banks, the capacitor size must be one third the per phase capacitor size. For a delta-connected generator excited by a star connected capacitors, the size must be 3 times the per phase capacitor size. Normally the capacitors would be delta-connected because this would make the line currents more balanced [35].

The capacitor size per phase at no-load needed for ensuring rated voltage at rated frequency at no-load can easily be found by rearranging equation (2.17) and using the no-load current from the no-load test at 230 V. Assuming the no-load apparent power equals the machine consumption of reactive power, hence the reactive power the capacitor must deliver, the capacitor size can be calculated as shown in equation (2.19).

$$C_{phase} = \frac{I_{no-load}}{2\pi f_1 \cdot V_{no-load}} \tag{2.19}$$

Another way of estimating of the needed excitation capacitor can be done if the full load line current, I_{fl}, the full load power factor, pf_{fl}, and the machine rated power, P, the rated line voltage, V_l and rated frequency, f are known. They are typically presented in the data sheet of the machine. The estimate of the total amount of reactive power, Q_{tot}, required can be calculated as shown in equation (2.20). Where S_{tot} is the total apparent power and P_{tot} is the total active power. It is assumed that the load connected is restive, the generator power factor is equal to the motor power factor and that the generator produces rated power at rated voltage and frequency. The per phase capacitor can then be calculated using equation (2.21).

$$Q_{tot} = \sqrt{S_{tot}^2 - P_{tot}^2} = \sqrt{(\sqrt{3} \cdot V_l \cdot I_{fl})^2 - (\sqrt{3} \cdot V_l \cdot I_{fl} \cdot pf_{fl})^2} \tag{2.20}$$

$$C = \frac{Q_{phase}}{2 \cdot \pi \cdot f \cdot V_{phase}^2} \tag{2.21}$$

This way of calculating the capacitor is an approximation because the full-load current and the cos phi in generator mode is not necessary the same as in motor mode. This calculation does not take the magnetization curve of the machine into account, and will therefore not necessarily be close to the actual needed capacitor size.

As the connected load increase, the voltage decreases which again decreases the reactive power supplied from the capacitor, as shown in equation (2.18). On the other hand, will the needed reactive power in order to supply active power will increase with an increase in active power load, at constant voltage. This relation between the active and reactive power for an induction machine at constant voltage can be seen in Figure 2.13. The voltage will drop if the supplied reactive power is not high enough.

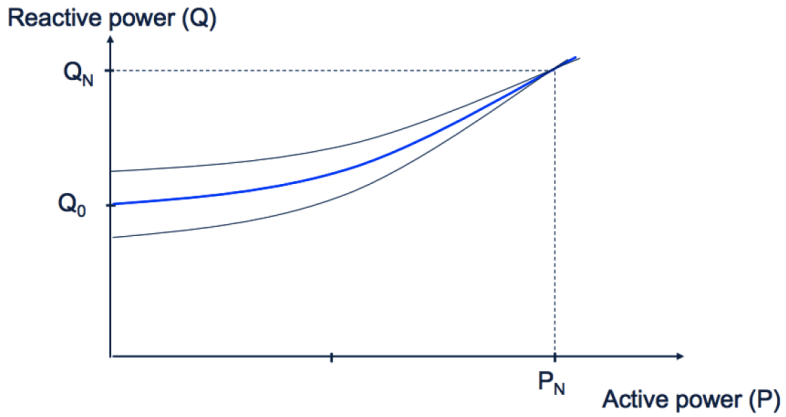

Figure 2.13: The reactive power consumption versus the active power load for an induction motor. Obtained from [6]

It can be seen that the required excitation capacitor must increase with increased load in order to keep the voltage and frequency constant. This also means that it is not enough to determine the capacitor size using the no-load curve. This because, when the generator is loaded the required reactive power increase. J. Björnstedt explains in [10] how to obtain the magnetizing curve for a machine connected to a balanced three-phase load. Figure 2.14 shows the per phase equivalent circuit of an induction machine, with a load resistance R_{load} and excitation capacitor, X_c connected to the terminals. R_s and R'_r are the per phase stator and rotor resistance (referred to the stator side) of the machine. X_s and X'_r are the per phase stator and rotor (referred to the stator side) leakage reactance of the machine. X_m is the magnetizing reactance of the machine, and the core loss resistance is neglected. The curve can be found by considering the load resistance, R_{load} together with the generator, as shown as Z_{tot} in the figure. The circuit parameters of the machine considered was found in the specialization project and can be found in Appendix C.

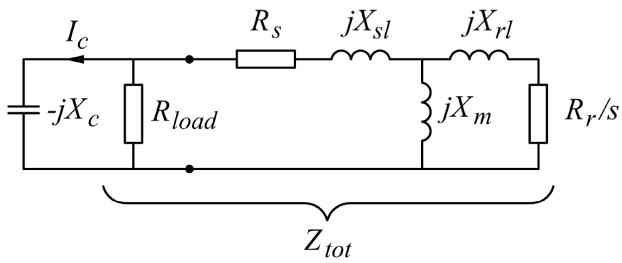

Figure 2.14: The per phase equivalent circuit of the induction generator with a load resistance and excitation capacitor connected to the terminals. Obtained from [10]

Finding the loaded curve for the machine can be done by a similar test as the no-load test. This is done by connecting the generator to the grid using a variable transformer as shown in Figure 2.15 and driving the generator by a controllable pendulum or DC motor. Then the generator slip is adjusted so that the grid current, I_{tot} is 90 °lagging, leading to a purely inductive I_{gen}. The curve is then obtained by reading the generator current at each voltage level. In stand-alone mode I_{tot} can be compensated by the excitation capacitor.

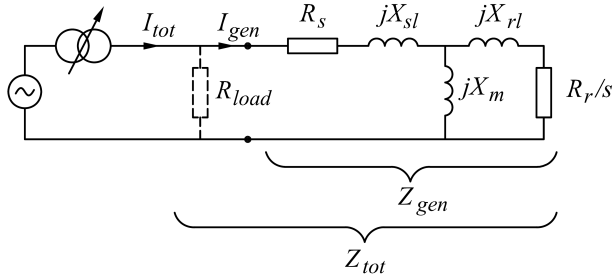

Figure 2.15: The per phase equivalent circuit of the induction generator connected to the grid via a variable transformer and a load resistance. Obtained from [10]

The magnetizing curve of a loaded generator can also be found by calculations using the known circuit parameters and known relation between the magnetizing reactance and the voltage. This is done by calculating the I_{tot} for a given voltage and a low slip, and then increase the slip until the real part of I_{tot} is lower than 0.01 A. At this slip I_{gen} is calculated and saved together with the corresponding voltage. This is done for all voltage levels where X_m is known. The MATLAB script for this calculation is given i Appendix D. The pseudo code for this script is shown in Figure 2.16 below. This calculation is based on a similar calculation done by J. Björnstedt in [10].

```
slip = -0.002;
for every Voltage
    Xm = Xm(V)  %from no-load calculation
    Calculate Zgen
    Calculate Itot
        while real(Itot)>0.01
            slip = slip - 0.0001
            Calculate Zgen
            Calculate Itot
        end

    Calculate Igen
    Save Igen
end
```

Figure 2.16: Pseudo code for finding the magnetizing curve for the loaded generator, using the circuit parameters, known relationship between the magnetizing reactance and the load resistance. Inspired by [10]

The result will depend on the connected R_{load}, but a general result is shown in Figure 2.17, where the solid curve is the magnetizing curve at no load and the blue dashed curve is the magnetizing curve for a loaded generator at the same frequency. The yellow dashed line represents the rated current of the machine.

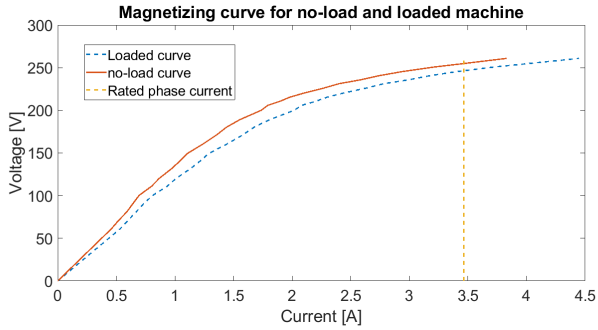

Figure 2.17: The magnetizing curve for no-load and loaded machine, at the same frequency.

It can be seen from the figure, that when a resistive load is connected to the SEIG, the generator requires more reactive power in order to maintain the voltage level. The voltage will drop more for higher loads, when a fixed capacitor is connected. The required per phase excitation capacitor size should therefore be found by implement the magnetizing current at 230 V, found by the loaded curve, in equation (2.19). This is the procedure for calculating the per phase capacitor for a three-phase balanced generator.

As mentioned earlier will the three-phase generator be converted into a single-phase machine. This is done by connecting the capacitors as shown in Figure 2.18, and neither in delta nor in star configuration. This connection is referred to as a C-2C connection, because capacitor C_2 is twice the size as capacitor C_1. The capacitor size C_1 is the same as the required per phase capacitor size needed for normal operation for a delta connected generator at nominal voltage.

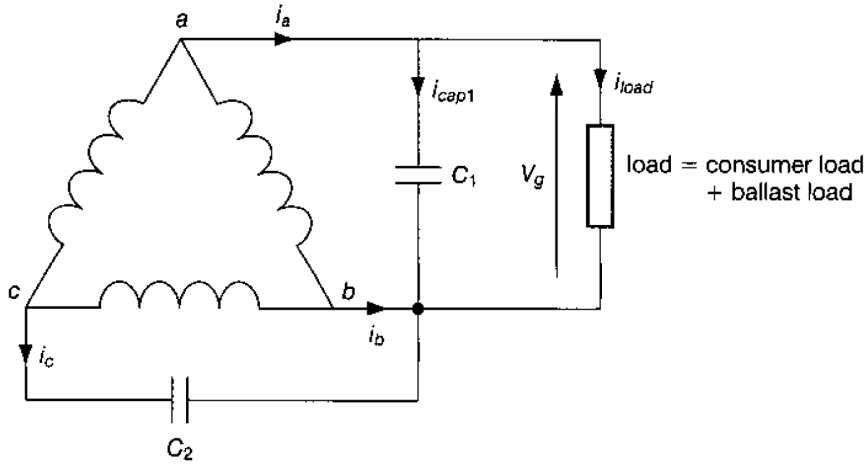

Figure 2.18: C-2C connection of the excitation capacitors in order to convert a three-phase generator to a single-phase generator. Obtained from [28]

Where i_a,i_b and i_c is the line currents. Where the sum of i_{cap} and i_{load} is equal to i_a. The relation between the line currents are as shown in equation (2.22) and (2.23).

$$\bar{i_a} = \bar{i}_{load} + \bar{i}_{cap} \tag{2.22}$$

$$\bar{i_b} = -(\bar{i_a} + \bar{i_c}) \tag{2.23}$$

It is desired to operate the machine as a balanced three-phase machine, even though the load is connected across only one phase. By detailed analysis it can be seen that the unbalanced arrangement of the capacitors can cancel out the unbalanced load, if the condition shown in equation (2.24) is met, when assuming the load is constant and resistive [9, 28]. This condition is equivalent to equation (2.25). Were Q_{tot} is the total reactive power of the capacitors at the rated voltage and frequency. P_{load} is the load power, consumed by the single-phase load.

$$P_{load} = \frac{Q_{tot}}{\sqrt{3}} \tag{2.24}$$

$$\bar{i}_{load} = \sqrt{3}\bar{i}_{cap} \tag{2.25}$$

The phase sequence is very important when connecting the system as shown. If the capacitors are connected to the wrong phases an unbalanced system occurs and the generator may overheat.

The needed capacitor size per phase in order to ensure a specific phase voltage, can either be found by estimation, by knowing the no-load current or by finding the magnetizing

curve for a loaded machine as explained earlier. Assuming a purely resistive village load, and that the system fulfills the condition shown in equation (2.25), the load power and the per phase excitation capacitor should have the relationship shown in equation (2.26), in order to have minimum unbalance in the system. Equation (2.26) is a rewritten version of equation (2.24).

$$P_{load} = \sqrt{3} \cdot V_t^2 \cdot 2\pi \cdot f \cdot C_{phase} \tag{2.26}$$

Where V_t is the terminal phase voltage [V], I_{load} is the load current [A], C_{phase} is the per phase capacitor, I_{cap} is the capacitive current through capacitor, and f is the frequency. This means that in the evaluated system, the total power consumed by both the ballast load and the village load must be equal to P_{load}.

2.3 Induction Generator Controller

As already mentioned, the operating point of the PAT will change if the system is submitted to a load variation. This will also affect the voltage, frequency and the generated power in the microgrid. In order to retain an output voltage and frequency within acceptable limits, when the system is exposed to load variations, two types of control methods are usually used and suitable for a micro hydropower plant. Either mechanical control or electrical control [36].

When using mechanical control, a governor is used to control the speed and the hydraulic power extracted by the turbine [37]. This is done by sensing the speed of the turbine and regulate the water flow into the turbine by adjusting the guide-vanes. By controlling the water flow, the turbine power is controlled, and can be matched to the varying consumed power by the connected loads. Used together with a synchronous generator, the governor ensures a constant frequency by matching the turbine power and the generator power, to ensure constant synchronized speed. Mechanical control can be done automatically, which requires expensive speed sensors, or it can be done manually. Both methods will result in a slow reaction to variation in the village load, because it takes time to adjust the mechanical components properly. Since this plant is in stand-alone operations, a slow reaction will affect the voltage and frequency much, due to fast variation in the village load and low inertia off the generator and PAT. The moving parts controlling the water flow will also cause more maintenance. Mechanical control is often expensive and not usually used for small scaled hydropower plants [16], like the micro hydropower plant considered in this thesis.

In addition to the fact that governors are complex and costly, the PAT does not have guide-vanes, which makes the mechanical control difficult. The micro hydropower plant in this thesis is therefore controlled electrical. An induction generator controller (IGC) is mostly used in stand-alone systems with an uncontrolled turbine running with an induction generator [38]. The name suggests that the IGC controls the generator directly, which it does not. Instead the IGC control the generator indirectly by controlling the load

connected to the generator, like an ELC. The main different of the IGC and the ELC is that the IGC measure and controls voltage and the ELC measure and controls the frequency. The ELC is used in stand-alone systems with an uncontrolled turbine running with a synchronous generator. The aim of an ELC and an IGC are to compensate the variation in the main load, by varying the amount of power consumed by an additional dump load connected to the system. The ideal feature is thus, that the IGC ensure that the generator experiences a constant load. If both the load power factor and the total load seen from the generator are constant, the system will be in steady state and ideally there will be no fluctuations in voltage and frequency, even with varying main load. This means that the voltage and frequency can be held within desired limits. The main load in this system is referred to as the village load, and the dump load is also known as the ballast load.

The rated full load village load is designed to consume the rated generated power. As the village load decrease from the rated full load, the surplus power, generated by the hydropower plant will be dumped in the ballast load. When the village load is zero, the ballast load must be able to consume the total amount of generated power. It is therefore necessary that the ballast load is designed to consume equally or more than the maximum generated power by the plant. The principle of operation of the ELC and IGC is shown in Figure 2.19. As the village load change, the power consumed by the ballast load also changes to ensure that the sum of the two is constant. By ensuring that the sum of the village load and ballast load always is equal to the constant generated power, the generator will not see a change in the system load. This way the torque balance shown in (2.8) will be equal to zero and the rotational speed is constant and thus the voltage and frequency will maintain the same.

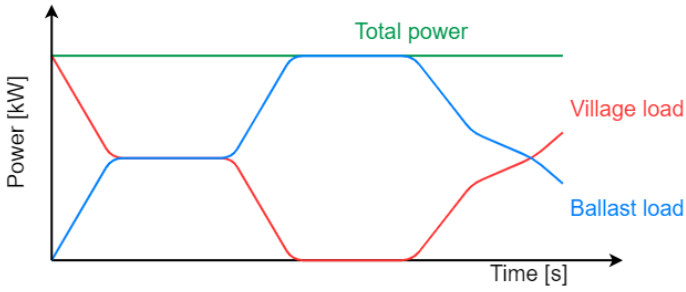

Figure 2.19: The principle operation of the IGC and ELC. As the village load change, the power consumed by the ballast load also changes to ensure that the sum of the two is constant.

Typically, there are three different control techniques for varying the size of ballast load connected to the system; phase-angle control, binary-weighted load control and variable mark-space ratio control [9, 39]. Each technique can have different methods of sensing the voltage, but it is the main operation which will be in focus in this section [40]. The three techniques will here be explained briefly.

The binary-weighted load control produces a variable ballast load by connecting different combinations of fixed resistors elements to the system. The resistor elements are weighed according to their size. By combining different elements, it is possible to achieve several ballast load-steps. Two back-to-back thyristors are used as switching device for each fixed load element, and the loads are connected in parallel to each-other, as shown in Figure 2.20 (a). The different load steps are connected from the start of each period of the signal. Meaning that the triggering happens at the beginning of each period, causing no waveform distortion. Figure 2.20 (a) and (b) shows an example, when 3 different load size are used to achieve seven load steps. The different combinations of loads and the seven load-steps are shown in Figure 2.20 (b). Here the load resistance R_1 = R, R_2 = 2R, and R_4 = 4R. The size of the ballast load changes by controlling which resistor-thyristor circuits is "on".

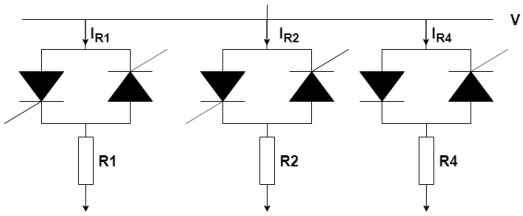

(a) Connection diagram of the three fixed load resistors. Showing the back-to-back connection of the thyristors. Where R_1 = R, R_2 = 2R, and R_4 = 4R.

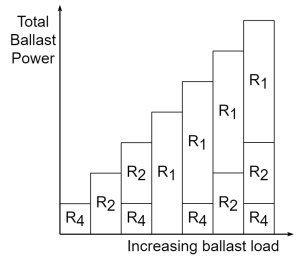

(b) The seven possible load steps when using the switched binary-weighted load control with 3 recessive elements. Where R_1 = R, R_2 = 2R, and R_4 = 4R.

Figure 2.20: The connection (a) and load-steps (b) when using a binary-weighted load control of the system

Using this method, the waveform distortion is minimum because the load is switched "on" the whole period. This means that the generator does not need to be overcompensated because of the losses due to the waveform distortion [41]. The disadvantage is that there is only a certain numbers of ballast load steps which is available. Meaning that the sum of the ballast load and village load will not always be constant, for example if the needed ballast load consumption exists between to load steps. The voltage and frequency can thus not be controlled precisely but will vary within a certain range.

The phase angle control produces a variable load by controlling the current to a fixed resistive ballast load. When using this control method, the effective size of the ballast

load is increased or decreased by switching in the load early or late in each sinusoidal half cycle. This is done by changing the triggering angle, α between 0° and 180°. By changing the gate triggering point, the power dissipation also changes. When α is 0° the full current passes through the ballast load, which leads to maximal ballast load power. Figure 2.21 (b) shows the general concept, where the sinusoidal curve represent the current through the ballast load at different triggering points, α = 0°, α = 90°, and α = 180°. The time of the triggering pulse in each half cycle are marked with arrows. In order to both trigger during the positive half cycle and the negative half cycle, two anti-parallel thyristors are used, and connected as shown in Figure 2.21 (a).

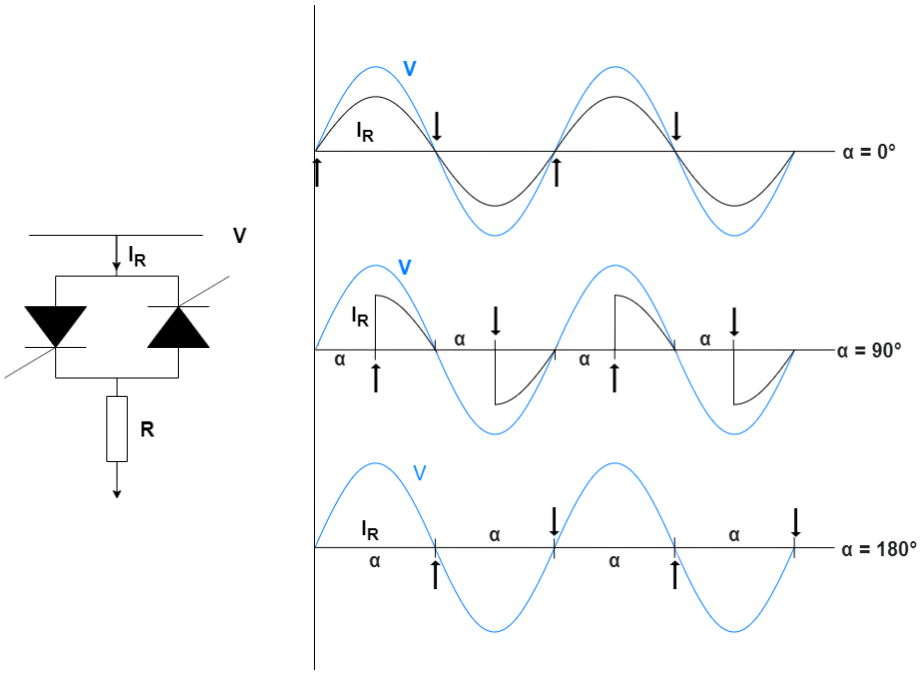

(a) Connection of the ballast load when using phase-angle control. R represent a fixed load and the triggering pulse of the anti-parallel thyristor can be controlled in order to control the effective size of ballast load.

(b) The current and the voltage across the ballast load at three different triggering angles, α = 0°, α = 90°, and α = 180°. Triggering points are marked with arrows.

Figure 2.21: The wave form of the power dissipation in the ballast load, using a phase angle control at different triggering points

Phase angle control make it possible to achieve any necessary ballast load, but it affordably also leads to distortion of the waveform and may lead to high di/dt [40]. Especially when the switching appears at the peak of the AC wave [42]. If the di/dt exceed a certain limitation value, it can damage or destroy the thyristor [43]. The switching during the sinusoidal curve also leads to variable lagging power factor. The reactive consumption of

the thyristors increases with increasing α. This will result in a reduction in the generator output voltage, because the effective size of the capacitor reduces. The generator is often oversized with 20 $\%$ when using phase angle control, to compensate for power loss due to wave distortion [41].

The variable mark-space ratio control can smoothly vary the size of the ballast load, without waveform distortion and lagging power factor. This control uses a rectifier bridge to convert the AC current to rectified AC current and a transistor switches the signal on and off at high frequency, in order to get a variable RMS current thorough the ballast load. The rectifier bridge and the transistor are connected as shown in Figure 2.22(a). The signal across the ballast load is shown in Figure 2.22 (b). The electronic switch can be either a transistor, MOSFET or an IGBT. The IGBT is mostly uses, but it is easily damage so care must be taken against transients during switching.

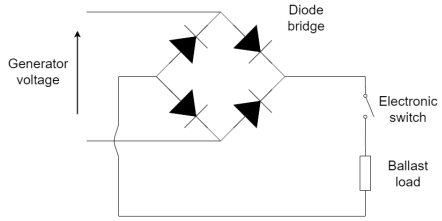

(a) Connection of the ballast load, the diode bridge and the transistor.

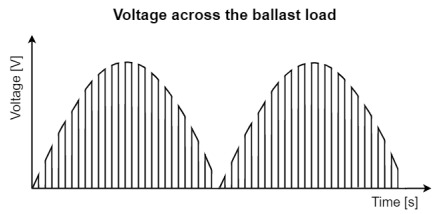

(b) Shows the ballast load voltage at a 50 $\%$ of the generator voltage.

Figure 2.22: Connection of the ballast load (a) and the voltage across the ballast load (b) in a mark-space ratio controlled single-phase system.

This is a smooth control technique, with little waveform distortion because of the inductance of the generator. The disadvantage is that this control generates high frequency noise at the supply side, which has a negative effect on radio, TV and wireless telephones. The components in this controller can also be a bit more expensive than the components in the other two methods, due to the use of MOSFET or IGBT.

Both the ELC and the IGC uses the principal of proportional-integral-derivative (PID) control [41]. In an IGC the phase voltage is compared to a desired voltage, and the error is feed into the PID controller connected to the system in a feedback loop. For the ELC the variation of the frequency from the desired frequency is be feed into the feedback loop PID controller. The advantages of using an electric controller compared to a mechanical control is that the electrical control is less costly and can provide regulations of the frequency and the voltage with minimal delay. Further benefits are that the IGC and the ELC have no moving parts, are very reliable and virtually maintenance free.

The IGC used in this thesis is manufactured by a vendor named Preesu Electronics PVT

LTD located in Nepal and is phase angle controlled. The IGC consist of three 50 μF capacitors, a center-tapped step down transformer, a thyristor with heatsink and a main board. Figure 2.23 shows a picture of the IGC, where the village load switch is located in the blue box, the three capacitors are located in the green box, the main board and the thyristor is in the yellow box. The coupling rail for the generator, village load and ballast load is shown in the purple box, where the three connections to the left are for the generator and the four connections to the right are for the ballast and village load. The circuit diagram of the IGC is shown in Figure 2.24 and in Figure 3 in Appendix F.

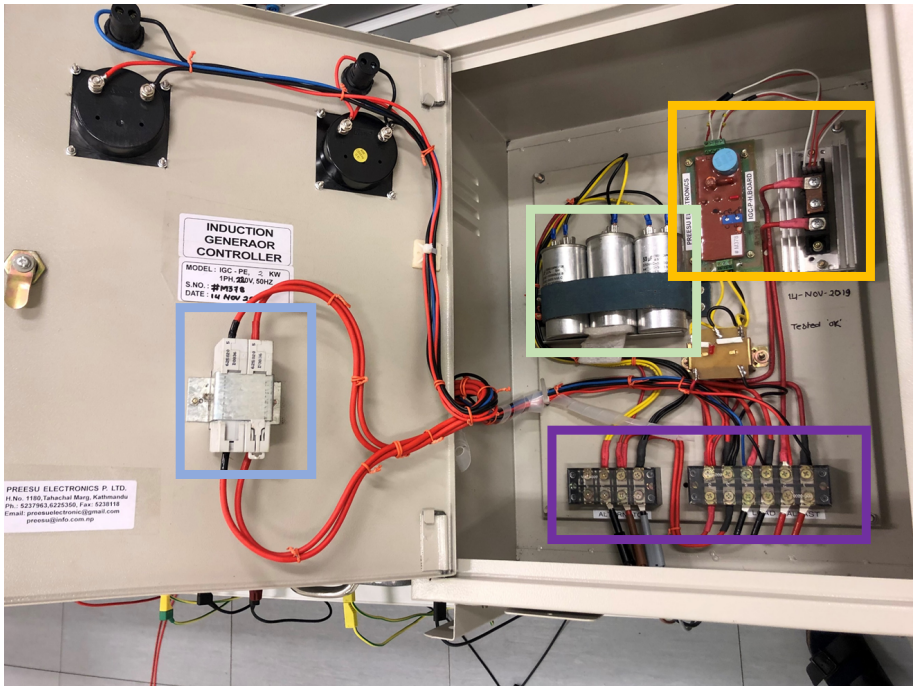

Figure 2.23: Picture of the inside of the electric load controller, showing the connection ports to the generator, the ballast load and village load in the purple box. The capacitors are shown in the green box, the thyristor and main board are shown in the yellow box, and the backside of the switch are shown in the blue box below two voltage measurement are at the door

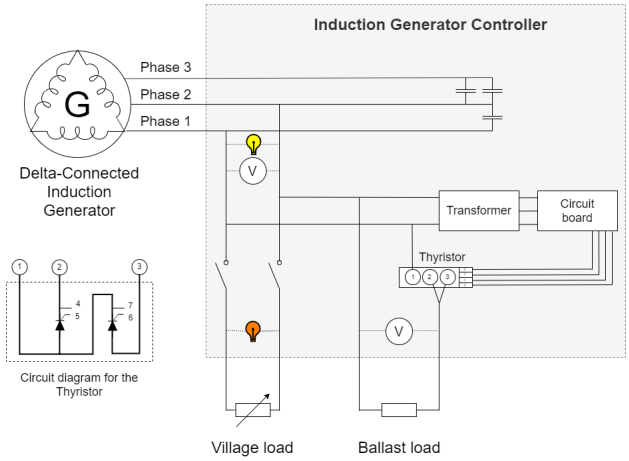

Figure 2.24: The circuit diagram of the connection and the components of the electric load controller. Reused from [1]

The exact behavior and operation of the IGC is not known, because the vendor has not answered the request for such information. It is therefore assumed that the triggering point of the triac, α is decided by using a proportional-integral (PI) regulator. The RMS phase voltage in per-unit (pu) across phase 1 and phase 2, *Y*, is compared to the desired phase voltage, Y_{ref}, i.e. the reference voltage, 230 V, equal to 1 pu. The obtained error, e, between the voltages is the input of the PI regulator. The error input will be multiplied by the proportional gain, K_p, in parallel to being multiplied by the integral gain, K_i which also is integrated. The output is the sum of the two terms. The block diagram of the Pi regulator is shown in Figure 2.25, and the equation of the PI regulator can be seen in equation (2.27).

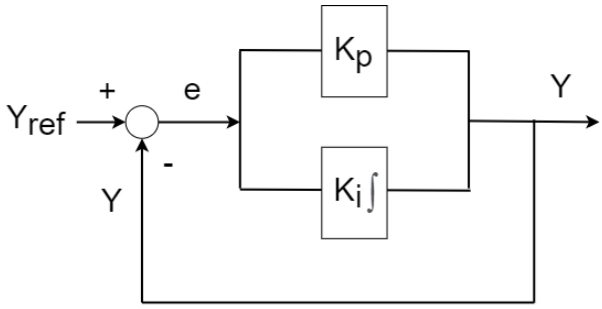

Figure 2.25: The block diagram of the PI regulator used in the IGC

$$Y = e \cdot K_p + e \cdot \frac{K_i}{s} \tag{2.27}$$

The main advantage of the PI regulator is that, if tuned correctly, the error will become zero, and hence the measured value will become equal to the reference. This way, the IGC can ensure that the phase voltage is equal to the desired phase voltage, 230 V.

2.4 Load

The main load of this system is defined as the power consumption of the consumers connected to the plant, which in this case is a small village, and is named the village load. The secondary load is the ballast load. Both the village load and the ballast load are assumed resistive. The village load will be light bulbs. The ballast load is typically an air heater or water heater. The long term-goal for this system is to use the ballast load as heating elements in oil, in an oil heater. The oil and the oil heater will be used for cooking purposes.

A micro hydropower plant can either have a single-phase or three-phase distribution system. Three phase system cuts the cost of the distribution cable and has lower losses than a single-phase system, for long transmission lines. If a three-phase motor is connected to the system, three-phase distribution is required. If the village load is more than 500 meters from the powerhouse a three-phase distribution system should also be considered [8]. The disadvantage of a three-phase distribution system is that the loads connected to the system should be split into three equal parts, partitioned between the three phases. If not, the system becomes easily unbalanced, which is not desired. Unbalanced load can give extra losses in stator, rotor and the distribution lines. An unbalanced system can also damage equipment connected to the grid, because the voltage in one or two phases can exceed the operating voltage. In an unbalanced system the produced unbalanced currents, produces unbalanced voltage drop in the lines, which result in extra power loss. The consequences of an unbalanced system can therefore be summarized as higher power losses, lower efficiency, reduce motor life, vibration and reduced efficiency.

Single-phase distribution is often preferred if the system is smaller than 15 kW. In a single-phase system, there is no need to split the load into three equal parts, since there only is one phase. For supplying a single-phased system, both a single-phase and a three-phase induction generator can be used, as explained earlier. Due to the characteristics of the IGC the load in this system will be single-phase.

In order to avoid system-breakdown, the consumed power must always meet the produced power. The load power can never become higher than the maximum output power of the turbine, but if to low resistance is connected to the system, the voltage will decrease. If the load is increased further, the system voltage may collapse. If the load power becomes lower than the turbine power, the speed of the PAT and SEIG changes, as described in the torque equation (2.8). The micro hydropower plant should be designed to meet the peak power demand, including distribution losses and safety margins [17].

2.4.1 Power Factor

The excitation capacitors must supply all the reactive power needed in the system. If an inductive load is connected to the stator terminals and the capacitor size is constant, the voltage decreases. This because both the machine and the load will demand reactive power, and the available reactive power for the generator decrease. Meaning that the connection of inductive load to the induction generator has the same effect as decreasing the capacitor size as shown in Figure 2.12 (b). Without the IGC and with a constant total load, the voltage level would therefore move downwards to the left along the magnetization curve, as more inductive loads were connected to the system instead of resistive loads. In worst case the voltage will collapse. Inductive loads can for example be motors, fans and heaters. The connection of inductive loads are as decreasing the capacitors size. The IGC can manage to keep the voltage up, but this affects the total load power. Figure 2.26 shows different characteristics for different types of loads connections to a standalone system without an IGC. Leading power factor, means there is a capacitive load connection, lagging power factor means inductive loads are connected, and a power factor equal to 1 means only pure resistive loads are connected to the system.

For a given speed and capacitor size, the output voltage versus the load current in pu at different power factors are shown in Figure 2.26 a). The voltage versus power in pu, also known as nose curves, at different power factors are shown in Figure 2.26 b). Figure 2.26 c) shows the frequency as a function of the load power in pu for different power factors of the load.

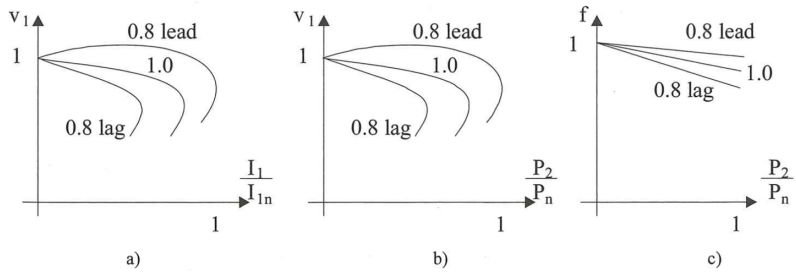

Figure 2.26: Steady state curves for a SEIG connected to a fixed capacitor and constant speed. Obtained from [44]

The characteristic in Figure 2.26 b) can also be seen from the magnetization curve. Connecting a capacitive load, leading to leading power factor is the same as increasing the size of the capacitor. This means that the load can be increase, in order to get the intersection point of the loaded magnetizing curve and the capacitor curve, rated voltage, compared the situation with purely resistive load. This will also lead to a higher current at the intersection point, as shown in Figure 2.26 a). Connecting an inductive load, leading to lagging power factor is the same as decreasing the size of the capacitor. This means that the load must be decrease, in order to get the intersection point of the loaded magnetizing curve

and the capacitor curve, rated voltage, compared the situation with purely resistive load. This will lead to a lower current at the intersection point, as shown in Figure 2.26 a).

CHAPTER 3

OPERATING CONDITIONS FOR TESTED SYSTEM

In this chapter the operating conditions of the system will be evaluated. The operating conditions are primarily chosen in order to achieve balanced three-phase operation of the generator using the available IGC, SEIG and PAT. The selection of the PAT, the SEIG and the IGC where made in earlier separate master thesis and specialization projects. The selections were done without regards to the other components in the system. Suggestion on an improved selection of the SEIG and PAT is also presented in this chapter.

3.1 Self-Excited Induction Generator

In the micro hydropower plant evaluated, an induction machine designed as a motor is used as a generator. There are some different considerations when designing a motor, compared to designing a generator. An induction machine designed as a motor but operated as a generator at the voltage and frequency ratings of the motor, will run at lower efficiency and with higher temperatures than when operating as motor [9]. In order to achieve optimum efficiency when operating a motor as generator, the motor ratings should be reduced by 5 - 10 %. This will decrease both the capacitor costs and endure an improved insulation lifetime [9]. In this section the operating voltage, frequency, power and excitation capacitor will be decided.

3.1.1 Voltage

The maximum and minimum voltage level at synchronous speed depend on the magnetizing curve. The upper voltage limit is the voltage at which the excitation current corresponds to the rated current of the machine. The lower voltage limit at synchronous speed is where the generator is just enough saturated to operate stably. If the operating voltage would be close to the upper limit the maximum load which can be connected to the generator is reduced due to winding temperature restrictions, and the high current coming from the capacitors. If the operating voltage would be close to the lower limit the excitation capacitors are reduced, making the system vulnerable to inductive loads. By decreasing the operating voltage, the load current must increase in order to achieve rated power, thus the power losses increase as well [9].

In the micro hydropower plant considered, the IGC is designed to retain 230 V at the phase terminals of a delta connected machine. The rated voltage of the machine in delta-connection is also 230 V. Ideally the generator should be operated at least 6 $\%$ lower voltage than the rated voltage [9], as mention above. On the other hand, operating at rated motor voltage is also acceptable. Since the IGC will try to achieve a terminal voltage equal to 230 V, and the standard voltage at the consumers in Tanzania is also 230 V, the voltage in this system is desired to be 230 V at the stator terminals of the generator. If the selection of the generator would have been done all over again, an induction machine with some percentage higher rated voltage in delta-connection should have been considered.

An additional voltage drop must be considered when implementing the distribution lines to the system. This because of the line impedance, in the line. The distribution lines will also affect the power factor of the load, since the lines are inductive. This will affect the system voltage as well, as explained earlier. Since the site is not located, it is not known if there will be need for long distribution lines, distribution lines are not considered in this thesis.

3.1.2 Frequency

The standard frequency in both Tanzania and Norway, as well as many other countries, is 50 Hz. The motor data is also presented at 50 Hz. The operating frequency for the microgrid is therefore chosen to be 50 Hz. The effects of operating the system at a higher or lower frequency will be discussed in Chapter 4.

3.1.3 Power

The generated power depends on the available flow, head, the PAT efficiency, and the SEIG efficiency. In order to ensure steady operation of the system, the designed full load power must meet the generated power at the chosen operating conditions. Under loading will cause higher speed in no time, causing higher frequencies, higher voltages and higher currents. Overloading can cause a collapse of the voltage in the system. As the load power increases the needed reactive power increase, as shown in Figure 2.13, and the capacitors

will not be able to supply it, and the system voltage may collapse. As mentioned earlier in this section should the generator power be derated to 80 % of the rated motor power. If the generated power is higher than the motor rated power, a motor with higher power ratings should be chosen as generator.

Since the capacitor are C-2C connected there is one total load power which gives balanced three-phase operations of the generator for the chosen capacitors. The size of the capacitors are 50 μF, the phase voltage is 230 V, and by using equation 2.26, the load power is calculated to be 1440 W at 50 Hz, in order to achieve balanced three-phase operation. The rated load power is therefore, chosen to be 1440 W. It is assumed that the power factor of the generator is the same as the rated power factor of the motor. The selection of the capacitor size will be explained in the next section.

3.1.4 Capacitor Size

In the specialization project [1] the size of the per phase excitation capacitor was calculated to be 33 μF at no-load. The size was found by first finding the no-load current at 230 V phase voltage and using equation 2.19, to calculate the required per phase capacitor size. This excitation capacitor size ensured a phase voltage of 230 V at no-load during testing in the specialization project [1]. During these tests, the machine was connected in star, and the line voltage was 400 V. The excitation capacitor is the same per phase, when connected in star as when connected in delta, in order to achieve 230 V phase voltage. From the previous chapter it was clear that the required no-load capacitor is not enough for ensuring 230 V when the machine is fully loaded. The loaded magnetizing curve can be found by a simple algorithm in MATLAB, using the known no-load curve, parameters of the machine, the known variation of X_m with the voltage, and desired load power. The pseudo code for this calculation is shown in Figure 2.16 and the MATLAB script is shown in Appendix D. The magnetizing curve for the machine connected to a 110 Ω resistance per phase, equivalent to a total load power of 1440 W, can be seen n Figure 3.1 together with the no-load curve obtained in the specialization project [1].

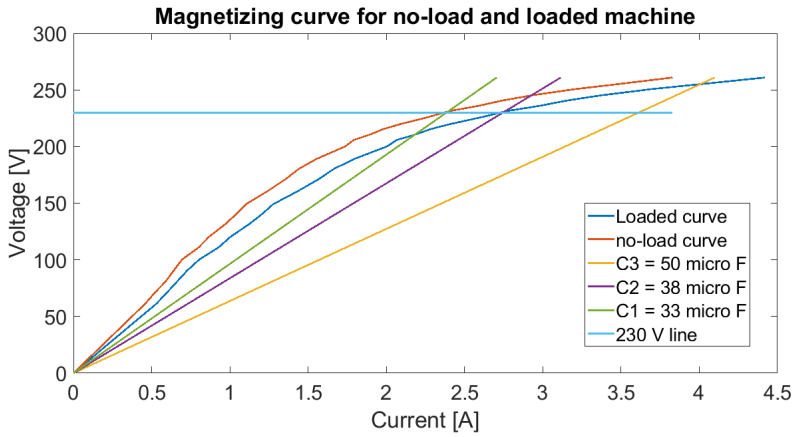

Figure 3.1: Magnetizing curve at no-load (orange) and full loaded (blue) machine, where full load corresponds to 1440 W and R_{phase} = 110 Ω. Three capacitor curves are also included, C1 = 33 μF (green), C2 = 38 μF (purple), C3 = 50 μF (yellow).

From the no-loaded magnetizing curve, it can be seen that the needed excitation capacitor must be 33 μF, in order to ensure 230 phase voltage, as already tested. From the loaded magnetizing curve, it can be seen that the needed excitation capacitor must be 38 μF, in order to ensure 230 phase voltage. The capacitor curve corresponding to 50 μF is also included and will be explained later.

An estimate of the needed excitation capacitor of the system can also be calculated using (2.20) and the given parameters in the nameplate data given in table 2.2, as explained earlier in Chapter 2.2.2.1. The full load line current of the evaluated IM is equal to 6 A and the pf_{fl} is equal to 0.81. The rated line voltage is defined to be 230 V and the rated frequency is 50 Hz. The total reactive power required is then calculated to be 1402 VAR, which correspond to a per phase reactive power of 467 VAR. Using equation (2.21), the approximate needed size of the per phase excitation capacitor can be calculated to be 28 μF. The fact that the estimated per phase excitation capacitor is lower than the excitation capacitor needed at no-load, indicates that this is not the best way for deciding the capacitor size. This because this calculation do not take into account the magnetization curve or the characteristic of the machine.

The excitation capacitor size in the evaluated system is already determined, because they were integrated in the IGC. The vendor received the nameplate data of the induction machine used in the evaluated system, and they selected the capacitor size. The capacitors integrated in the IGC are 50 μF. From the loaded curve in Figure 3.1 the phase voltage will be 254.6 V when using the size 50 μF. Why the vendor chose 50 μF is not known. It can be seen that if equation (2.20) is used wrong, either:

$$S = 3 \cdot V_{line,star} \cdot I_{line,star} \text{ or } S = 3 \cdot V_{line,delta} \cdot I_{line,delta}$$

the estimated size then becomes 48.7 μF. This may be what has happened, but it is not known for sure.

If the capacitor size would have been determined ones more it would be chosen to be in between 33 μF - 38 μF. This because if 38 μF is chosen, this capacitor size corresponds to a lower load power than the one used to find the magnetizing curve for a loaded machine in Figure 3.1. Meaning that the magnetizing curve would be shifted slightly upwards closer to the no-load curve and the intersection of the capacitor curve and the magnetization curve for a loaded generator occurs at a slightly higher voltage level than shown in Figure 3.1. By using equation (2.26), the rated power corresponding to a 38 μF per phase capacitor would be 1094 W, which is below 80 $\%$ of the rated power of the motor.

However, the capacitors integrated in the IGC is the ones available and therefore the ones which is used throughout this thesis.

3.1.5 Mechanical Speed

The frequency is highly dependent on the mechanical speed of the system and the connected load. In the specialization project a method for calculating the approximated mechanical speed needed to archive 50 Hz, for a given load and known machine parameters was found. The MATLAB script for this calculation is shown in Appendix H.

In this calculation the total load power is assumed to be equal to the rated load power, 1440 W, corresponding to a per phase resistance of 110 Ω at 230 V, and the desired frequency is 50 Hz. The result from the calculation, is that the PAT and the SEIG should operate at 1569 rpm. It is therefore expected that the operating speed of the PAT and the generator will be close to 1569 rpm.

3.2 Pump-as-Turbine

In this thesis the PAT was already selected. The BEP of the chosen PAT can be found using equation 2.9 and 2.10 presented in Chapter 2.1. In this calculation the rotational speed when operating as a turbine must also be known. The PAT and the SEIG are directly connected, and the mechanical speed will be approximately 1569 rpm to obtain rated operating frequency in the microgrid, as stated in the previous section. The predicted head and flow rate at the PAT BEP when operating as a turbine at speed 1569 rpm is shown in table 3.1, together with the BEP of the pump operating at rated pump speed 1450 rpm.

Table 3.1: Predicted BEP for Pedrello FG 32/160 B operating as turbine with a turbine speed of 1569 rpm, using Sharma predicting method combined with the affinity laws, and the BEP of the pump at rated pump speed 1450 rpm.

Pump mode, 1450 rpm		
Head [m]	$H_{BEP,p}$	6.2
Flow rate [m^2/s]	$Q_{BEP,p}$	8.7
Efficiency	η_p	55 %
turbine mode, 1569 rpm		
Head [m]	$H_{BEP,t}$	14.9
Flow rate [m^2/s]	$Q_{BEP,t}$	15.2
Efficiency	η_t	55 %

Using the predicted BEP of the PAT and Equation 2.5 the extracted power by the PAT can be calculated to be 339.4 W. Assuming a generator efficiency of 80 %, the produced power by the plant is equal to 271.5 W. This power output is much lower than the needed power consumption in order to obtain balanced operation of the generator.

Since this hydropower plant is operating in stand-alone operations, the main design focus is to make sure the generated power equals the consumed power in order to avoid break-down. From Figure 2.3, it can be seen that, by increasing the head at the site, the extracted power by the turbine also increase. Since the H-Q characteristic of the PAT is not known, it is not easy to predict the operating point of the PAT which gives the right amount of power. Different operating points will therefore be tested in the laboratory.

It is important to remember, that when the head is increased the operating point at which the reaction turbine has maximum power output occur at higher speed than at rated head. Since the turbine will operate at a speed much lower than the speed corresponding to the maximum power output, a small variation in speed will also wary the extracted power by the turbine. When the head increases, the runaway speed also increases. The speed might be higher than 160 % of the nominal speed, as mentioned earlier.

The design procedure of this plant is a bit untraditionally, and the site is not known in forehand. Therefore, it is important that when selecting the site, the available head must be higher than the head found during testing. This because of penstock losses and hydraulic losses, as explained in the previous chapter. It is also important to know the variation in flow through the year, or several years in the river which will be used. This because the system is a run-of-river scheme and will behave poorly if there are variation in the flow during the year, as explained in Chapter 2. It is desired that the evaluated system works all year around and must therefore be scaled depending on the minimum flow rate of the river. After the evaluated system is implemented at a site, the flow to the turbine should be constant. If the flow rate becomes less than the designed flow rate of the system, the system should be stopped. This because the delivered power from the PAT reduces, the

frequency and voltage level will be poor, and the rated load must be decreased leading to an unbalanced system. A flow duration curve shows the flow rate against the probability of the flow being higher than a given value. Figure 3.2 shows a typical flow duration curve for a site. The minimum flow rate is noted as Q_{min}. In this Master Thesis there has not been chosen a specific site, so this will not be discussed further, but is it important to have in mind for the designer.

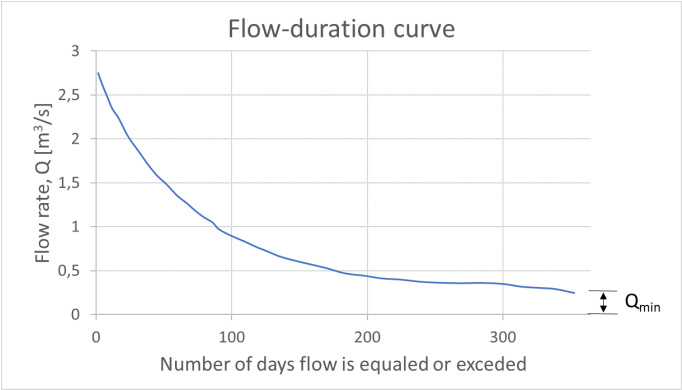

Figure 3.2: A typical flow-duration curve for a river used in a run-of-river scheme. Showing how many days the flow rate is above a certain flow rate with a given certainty. Where Q_{min} is the minimum flow rate in the river.

3.3 Recommendations

Designing a micro hydropower plant is a complex and iterative procedure. In this Master Thesis the components of the system are not the best fit but is used because they are available. Based on readings [45] [16] and the problems that accrued in the design of this plant, a procedure for selecting the right PAT, SEIG and IGC is here presented. The procedure assumes a run-of-river scheme with direct connection of the PAT and SEIG.

- Select a site.
- Estimate the available hydraulic power, by estimating the net head and water flow rate which is available at the site.
- Estimate the turbine speed, by deciding the number of pole pairs of the generator and the desired frequency. The PAT and the generator are direct connected, so the speed should be estimated to be equal to the synchronous speed of the induction generator. In reality the speed will be higher, but this is just an estimate.
- Select a PAT based on the estimated net head, flow rate and turbine speed. The PAT BEP should be at a lower net head and flow rate than available, at the estimated speed.

- Estimate the extracted power by the PAT and select the generator size and voltage ratings. (find the no-load curve of the machine if possible)
- Estimate the available power from the generator and choose a rated power a bit lower.
- Calculate the needed rotational speed to get rated frequency, with rated power. Check the PAT BEP point at this speed, and double check that everything is matching.
- Choose the capacitor size to archive the rated voltage at rated frequency for the rated load.
- Select the IGC for the rated values, with correct capacitor size.

This procedure recommends designing the system in the opposite order than what is done in this Master Thesis. This should be in mind if a new system is designed.

CHAPTER 4

POWER QUALITY FOR ISOLATED SYSTEM

When designing and analyzing the micro hydropower plant, it is important to define and evaluate the desired power quality of the system. The power quality of the system says something about a certain minimum standard the power supply must meet, even when it is subjected to disturbances. Design and operating criteria are an important part of the system to ensure safe operation for both the consumer and the producers, and for preventing and limiting damage to the plant and the equipment connected [9, 10, 46]. There are three important quantities to look at when considering the power quality [46]:

- Voltage stability
- Frequency stability
- Reliability

The needed quality of the system depends on the requirement of the end-user's applications, as well as requirements of the plant itself. In this chapter the listed quantities will be explained, and the operating criteria will be set and discussed. Additionally, this chapter will give a fundamental insight in transients and harmonic distortion in the system, which also says something about the power quality.

4.1 Voltage Stability

Voltage stability is defined as the ability of the system to maintain an acceptable root mean square voltage level in the microgrid after being exposed for a disturbance [47, 48]. Voltage stability can be classified in tow sub classes; large-disturbance voltage stability and small-disturbance voltage stability. Where system faults, short circuit of a distribution line and loss of a generator are examples of large disturbances. Small perturbations like minor load changes is an example of a small disturbances [46, 48]. The voltage stability criteria defined in this section is mainly the criteria for small-disturbance voltage stability. This because it cannot be expected that the stand-alone system keeps a certain voltage level if there is a loss of the only generator connected. Voltage instability can both occur over a short period of time (few seconds), or over a longer period of time (tens of minutes) [48]. High voltage levels compared to the manufactured rated voltage can both damage and reduce the lifetime of the equipment connected to the grid [9].

The standard EN 50160 states that the voltage level supplied to low- and medium voltage consumer should not deviate more than $\pm$ 10 $\%$ of the rated value, measured at the consumer.

When deciding the limit of operating voltage for the micro hydropower plant considered, it is important to remember that there will also be a voltage drop due to the distribution lines. Because of this the voltage limit at the generator terminals should be lower than $\pm$ 10 $\%$ which the standard claims. Remote Hydrolight produces ELC and has chosen to set the operating voltage limit to $\pm$ 4.35 $\%$ when testing a similar system [6]. The limit for the operational voltage will therefore be set to $\pm$ 4.35 $\%$ at the generator terminals here as well, which means the desired voltage range be within 220 - 240 V.

4.2 Frequency Stability

Frequency stability can be defined as the ability of the system to obtain the average frequency over a small time interval, within a limited range from the nominal frequency [49].

The synchronization of some domestic electrical applicants like electrical clocks and televisions were earlier dependent on the supply frequency and required well-regulated supply and stable frequency. Today, with more modern equipment, the acceptable frequency variation is set by transformers and motors connected to the grid [9].

To understand the consequences of a reduced operating frequency in both the induction generator and other machine and transformers connected to the microgrid, the transformer equation is presented, shown in equation 4.1. A rewritten version of the transformer equation is shown in equation 4.2. E_{ind} is the amplitude of the induced voltage in the windings, f is the flux frequency [Hz], N is the number of tuns of the stator winding and ϕ_{peak} is the

peak flux [Wb].

$$E_{ind} = \frac{2 \cdot \pi \cdot f}{\sqrt{2}} \cdot \phi_{peak} \cdot N \tag{4.1}$$

$$\frac{E_{ind}}{f} = \frac{2 \cdot \pi}{\sqrt{2}} \cdot \phi_{peak} \cdot N \tag{4.2}$$

It is desired to keep the relation between the induced voltage and the frequency in equation 4.2 constant, in order to keep the flux constant. If there is a decrease in the frequency, while the voltage is the same, the flux increases and thus the flux density increases. This could result in saturation of the core, thus lead to increased losses in the machines and reduce the efficiency. Small transformers used in electrical applications are also easily damaged at low frequencies [9].

An increase in frequency can be beneficial for the machine. It can be seen from equation 4.2 and the magnetizing curve at different frequencies in Figure 2.12 (a) that the flux, thus the flux density thus the magnetizing current decrease with increased frequencies at constant voltage. A reduced magnetizing current will reduce stator winding losses and increase insulation life.

The disadvantage of an increase in the frequency will mainly affect any motor loads connected to the system with power requirement that increase with speed, or speed dependent loads like fan and pumps. Even though highly speed dependent motors are connected to the system, they generally can handle up to 10 $\%$ increase in frequency. This because they are generally oversized, the increased shaft speed increases the cooling of the machine and the magnetizing current decrease as mentioned earlier [50].

The standard EN 50160 states that the frequency in the microgrid must be within 42.5 - 57.5 Hz all the time, and that the average mean frequency over 10 s should not range outside 49 - 51 Hz more than 5 $\%$ during a week.

One of the assumptions related to the load of the micro hydropower plant evaluated, is that the load is resistive and robust. In [9] it stated that if there are no high-speed motors connected the microgrid, the frequency can be varied from 50 Hz + 20 $\%$. As a general rule, the frequency should not fall far below 50 HZ. The limit for the frequency in this microgrid is therefore set to 49 - 60 Hz.

4.3 Reliability

The level of reliability for the system refers to its ability to serve satisfactory operation on a continuous basis, without many interruptions. The reliability considers the systems behavior over an appreciable period of time [48]. In the system evaluated in this Master Thesis, the reliability of the microgrid depends several factors:

- a constant water flow rate

- the robustness of the SEIG
- the robustness of the PAT
- the robustness of the IGC
- that the maximum consumed power by the village does not exceed the maximum produced power

If the SEIG or the PAT is damaged, or need maintaining, the power production stops. If the controller in the IGC stops working there will be no power dispatching in the ballast load, and the system will behave as if there were no controller. This could lead to either runaway conditions, if there are no village load, or instability in the voltage and the frequency as the village load varies.

One of the main objectives of the evaluated micro hydropower plant is the aim of a low-cost plant. High reliability is costly, and therefore not prioritized in this system.

4.4 Transients

Variations in the waveform which can cause over- or undervoltage as well as overcurrents are described as transients. An example is lightning strokes. Over voltage an over current can damage equipment connected to the microgrid if the peak is higher than the withstand capacity of the equipment. It is assumed that the equipment connected to the microgrid is robust, and further analysis will not be done in this Master Thesis, but it is recommended in the further work in Chapter 9.

4.5 Harmonic Distortion

Harmonics in the grid are sinusoidal voltage and current signals with frequency integer multiples of the operating frequency of the system, known as the fundamental frequency. Sinusoidal voltage and current signals, at the rated operating frequency is the ideal condition in the microgrid. When harmonics occur in combination with the fundamental signals it produces waveform distortion, called harmonic distortion. Harmonic distortion occurs because of the nonlinear characteristics of loads and devices in the system [51]. It is desired to have a low amount of harmonic distortion in the system because they have a negative effect on both motors, generators, transformers and capacitors [52]. The main disadvantages of harmonic distortion are the increased iron and copper losses in motors and generators, temperature rise risk in both transformers and capacitors, risk of system resonance between the inductive and capacitive parts of the network at higher frequencies. The losses in the capacitors will also increase because they are proportional with the reactive output which is proportional with the frequency. The lifetime of the capacitors will be reduced.

Total harmonic distortion (THD) is the measure used to indicate the magnitude of the harmonic distortion of the voltage or current signal. The THD is defined as the sum of ratio of the RMS voltage of all harmonic frequencies, over the RMS voltage of the fundamental harmonic frequency. The mathematical definition is shown in equation 4.3. Where $V_{n,RMS}$ is the RMS voltage amplitude of each harmonic. $V_{n,RMS}$ and $V_{1,RMS}$ can be change with the RMS current amplitudes, in order to find the THD of the current signal.

$$THD(\%) = \sqrt{\frac{\sum_{n=2}^{\infty} V_{n,RMS}^2}{V_{1,RMS}^2}} \tag{4.3}$$

The THD is measured in percentage, and $V_{1,RMS}$ is the RMS voltage amplitude of the fundamental frequency, and $V_{2,RMS}$ is the RMS voltage amplitude at frequency equal to the fundamental multiplied by two, and so on for n = 3, 4,.., ∞.

Two of the IGC designs mentioned in Chapter 2 includes power electronic equipment, which can cause harmonic distortion because of nonlinear behavior. The worst case occurs when the phase angle controlled IGC is triggered at the voltage or current peak of the signal. This will be further investigated in Chapter 5.

The recommended harmonic line to neutral voltage limit at a point of common coupling with rated voltage level lower than 1 kV, for an individual harmonic is 5 $\%$. The recommended voltage limit for the THD is 8 $\%$ [53].

The fact that the induction generator is connected in delta already ensure that third harmonic current will not cause problems for the consumer.

CHAPTER 5

LABORATORY TESTING OF INDUCTION GENERATOR CONTROLLER

In this chapter the IGC will be tested. The tests are done in order to characterize and get to know the behavior of the controller as the village load varies, before testing the SEIG and the IGC together with the PAT in the Waterpower Laboratory. The IGC was tested in the specialization project [1] as well, but at that time it was not able to work, and due to time limitations the IGC was not further investigated. It is also interesting to see how good the IGC will control the voltage and frequency. The variation of the village load will be done by varying a variable resistor. The voltage and frequency will be measured both as RMS and instantaneous values. The waveform of the signals as the load varies will be analyzed, and an estimation of the THD is calculated. The effect of tuning the IGC is also evaluated.

5.1 Test Setup

The test setup for this laboratory test is shown in Figure 5.1, and the equipment used are listed in table 3 in Appendix E. The variable frequency drive (VFD) is supplied with 230 V AC, and is controlling the induction motor (IM), which represent the prime mover of the system. The rotor shaft of the SEIG is direct connected to the rotor shaft of the IM as shown in Figure 5.2. A tachometer and a reflective tape are used to measure the rotational speed of the shaft, shown in Figure 5.1. The excitation capacitors were delivered as an integrated part of the IGC and is connected as shown. The village load switch is also

integrated in the IGC cabinet. Four variable resistors are connected in series to represent the village load. The village load resistance can be varied from 0 Ω to 80 Ω. Two variable resistors are connected in series to represent the ballast load. The ballast load resistance is constant equal to 35 Ω. The voltage and current measurements across the village load and the ballast load was done using a measuring instrument, named Power CASSY. Power CASSY also tracks the frequency and the active power. The Fast Fourier Transformation (FFT) of the measured signals is also available in Power CASSY. The phase voltages at the terminals of the generator were measured using three multimeters. The generator line currents were measured using a clamp meter, because it was uncertain if the currents would surpass the maximum current limit for the multimeters.

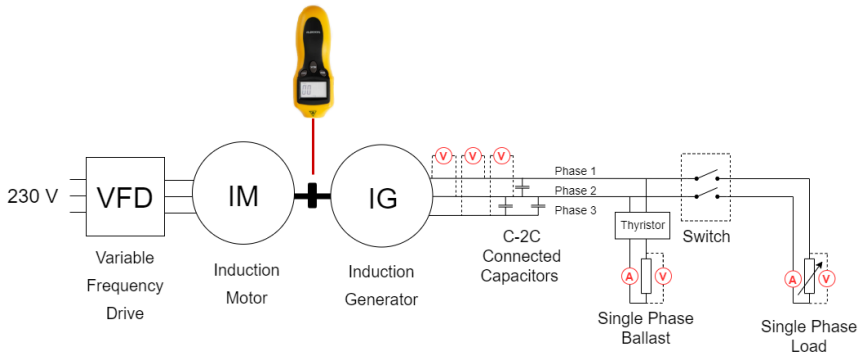

Figure 5.1: Test setup for testing the SEIG and the IGC, driven by an IM

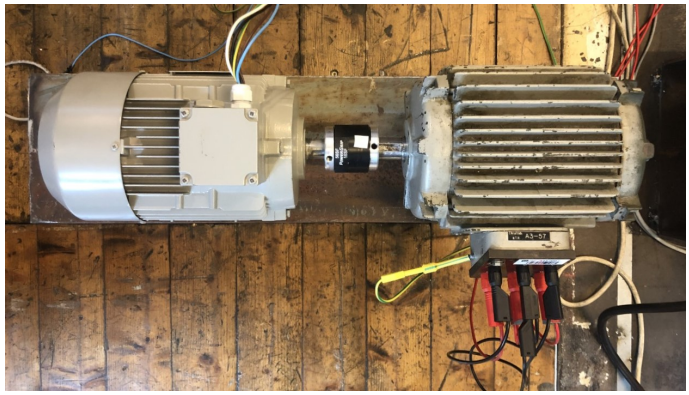

Figure 5.2: The direct connection of the SEIG and the IM. The reflective tape can be seen at the shaft.

The phase sequence and size of the load connected to the microgrid, is important in order to obtain balanced operations of the SEIG, as elaborated in Chapter 2.2.2.1. In order to know if the connection is correct, the currents must be measured during different tests.

If the currents are heavily unbalanced, another configuration should be tested. In this test setup the right connection were to connect the black, white and brown cords from the generator as shown in Figure 4 in Appendix G. From now on the black cord from the generator represent phase 1, the brown cord represent phase 2 and the white cord represent phase 3 as shown in Figure 5.1

5.2 Self-Excitation Procedure and Results

The self-excitation of the SEIG with the excitation capacitors implemented in the IGC is first tested. This test is performed by first making sure both the village load and the ballast load are disconnected from the IGC at startup. The VFD is then used to increase the rotational speed of the IM shaft until the phase voltage in phase 1-2 reached 230 V. This test is referred to as test 1.1. It is also tested to increase the rotational speed further, until the frequency reaches 50 Hz. This test is referred to as test 1.2. The measured RMS line currents, RMS phase voltages and frequency are noted and presented in table 5.1. The measured currents and voltages are also compared to the magnetizing curve found in the specialization project, shown in Figure 5.3. Where the solid curve is the magnetizing curve at 50 Hz, the red curve is the 50 μF capacitor curve at 50 Hz, the yellow curve is the 50 μF capacitor curve at 45 Hz, the purple line shows 230 V, the blue circle represent the tested result in test 1.1, and the red circle shows the test result in test 1.2.

Table 5.1: Test results when testing the self-excitation of the SEIG with the IGC

Measured data in test 1			
Test no.		1.1	1.2
SEIG			
Capacitor size	[μ F]	50	50
Rotational speed	[rpm]	1360	1525
RMS phase voltage 1-2	[V]	230.4	278.7
RMS phase voltage 2-3	[V]	213.6	254.0
RMS phase voltage 3-1	[V]	200.7	237.3
RMS line current 1	[A]	3.3	4.5
RMS line current 2	[A]	8.6	11.6
RMS line current 3	[A]	6.1	8.2
Frequency	[Hz]	44.9	50.2
$P_{village}$	[W]	0	0
$P_{ballast}$	[W]	0	0

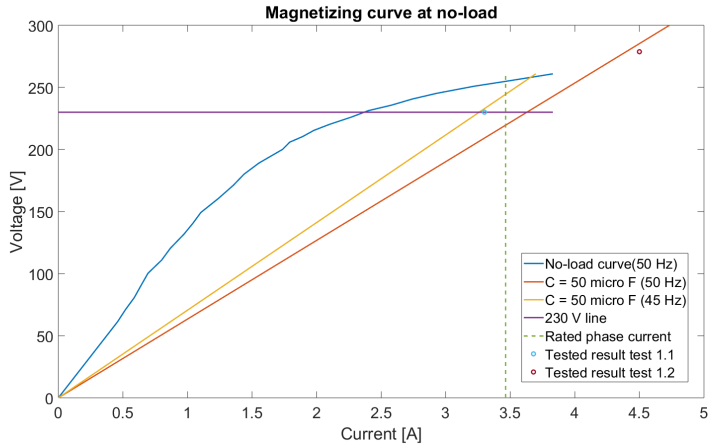

Figure 5.3: The magnetizing curve at 50 Hz obtained in [1] together with the tested no-load operating point at 45 Hz and 50 Hz, and the 50 μF capacitor curve at both 50 Hz and 45 Hz.

5.3 Load Connection Procedure and Results

After ensuring that self-excitation occur, a laboratory test with varying village load is performed. This test is referred to as test 2. In order to limit the unbalanced currents in the generator, shown in test 1.2, the village load is connected before reaching a phase voltage of 230 V. The rotational speed of the IM is afterwards increased further, until the voltage is 230 V across phase 1-2. It is not possible to achieve exactly 230 V, due to the working of the VFD. It is no fine tuning of the VFD, causing the voltage jumps between 227 V and 232 V when trying to adjust the VFD.

At first the village load resistance connected is equal to 37 Ω, which corresponds to the rated village load, 1440 W, at 230 V. The test results at this operating point is numbered 2.1 in table 5.2. Afterwards the village load resistance is increased to 79 Ω, corresponding to 669 W at 230 V. The test results at this operating point is numbered 2.2. in table 5.2. Then a test with full village load rejection is tested by switching out the village load. This corresponds to 0 W in the village load and a village load resistance equal to ∞ Ω. This test result is numbered 2.3 in table 5.2.

Table 5.2: The test results for running the SEIG together with the IGC when the village load connected to the terminal is varied.

Measured data in test 2			
Test no.	2.1	2.2	2.3
SEIG			
Capacitor size [μF]	50	50	50
Rotational speed [rpm]	1585	1612	1599
RMS phase voltage black-brown [V]	231.7	235.9	234.1
RMS phase voltage white-black [V]	232.2	228.3	230.2
RMS phase voltage brown-white [V]	233.7	241.4	236.9
RMS phase line black [A]	7.2	6.0	6.7
RMS phase line brown [A]	7.0	6.4	6.7
RMS phase line white [A]	7.6	8.3	7.9
Frequency	50.8	51.9	51.3
Village load			
Resistance [Ω]	37	79	∞
RMS voltage [V]	231.6	236.5	0.1
RMS current [A]	6.20	2.99	0.001
Consumed power [W]	1436	707	0
Ballast load			
Resistance [Ω]	35	35	35
RMS voltage [V]	30.4	134.9	216.7
RMS current [A]	0.82	3.76	6.1
Consumed power [W]	25	507	1322
Total consumed power [W]	1461	1214	1322

The IGC compensate the decreasing village load by disperse power to the ballast load. The ballast voltage and current through the ballast load varies as the village load varies. Figure 5.4 shows the RMS power consumed by the village load and the ballast load as the village load resistance is increased, meaning that the village power is decreased. Figure 5.5 shows the village voltage, the phase voltage across the loaded phase, phase 1-2, and the frequency of the microgrid, as the village load decreases. The y-axis to the left in the graph show voltage [V], while the y-axis to the right show frequency [Hz]. The x-axis shows the time in seconds. In both figures, the village load resistance is equal to 37 Ω from 0 s. After 15 s, the resistance is increased to 79 Ω. At 63 s, the village load resistance is disconnected, corresponding to a resistance equal to ∞ Ω.

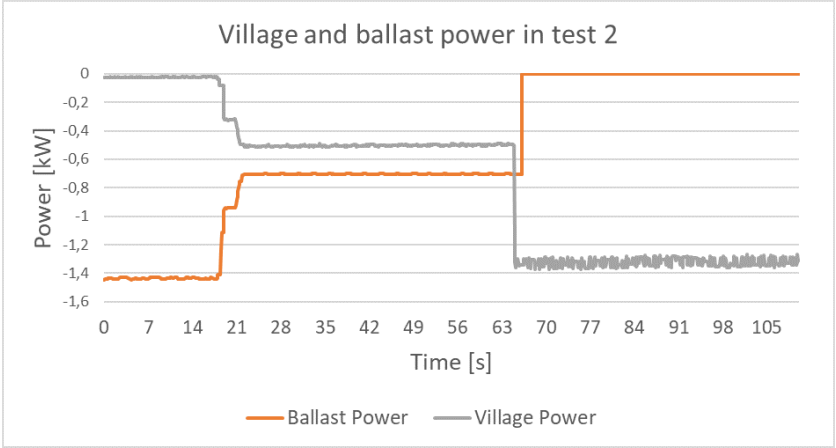

Figure 5.4: Shows the consumed RMS power by the village load (blue) and the ballast load (orange) as the village load decreases. $R_{village}$ = 37 Ω at 0 s. $R_{village}$ = 79 Ω at 15 s. $R_{village}$ = ∞ Ω at 63 s.

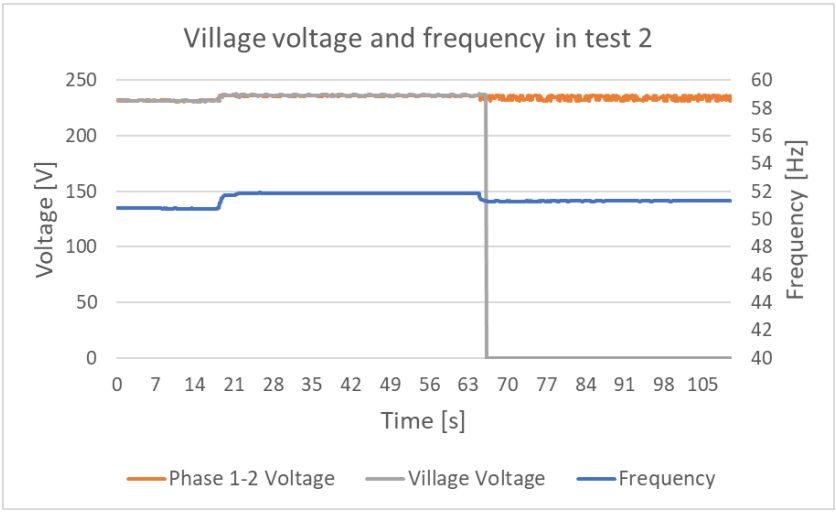

Figure 5.5: Shows the RMS 1-2 phase voltage (grey), village voltage (yellow) and frequency (orange) as the village load decreases. $R_{village}$ = 37 Ω at 0 s. $R_{village}$ = 79 Ω at 15 s. $R_{village}$ = ∞ Ω at 63 s.

5.3.1 Waveform distortion

When the ballast load is not consuming, the signals in the system are sinusoidal. As the ballast load is switcher on at different phase angles, the waveform of the signals changes.

In the tests where the village load resistance is equal to 37 Ω and 79 Ω, Power CASSY is used to track the instantaneous signals over both the village load, and the ballast load. The measured RMS results are the same as presented in table 5.2, but in this section the waveform of the signals are in focus. In order to see the waveform of the signals the sampling time in Power CASSY is set to 20 μs, and the sampling period is 600 ms. The figures presented the first 40 ms of the measured signals.

Figure 5.6a shows the instantaneous village voltage in blue and the instantaneous village current in orange, in test 2.1. Figure 5.6b shows the instantaneous ballast voltage in blue and the instantaneous ballast current in orange, in test 2.1. In this test the village load resistance is equal to 37 Ω, the village power is equal to 1436 W and the ballast power is equal to 25 W. In the next four figures, the x-axis show time [ms], the y-axis to the left in the graphs show voltage [V], while the y-axis to the right show current [A].

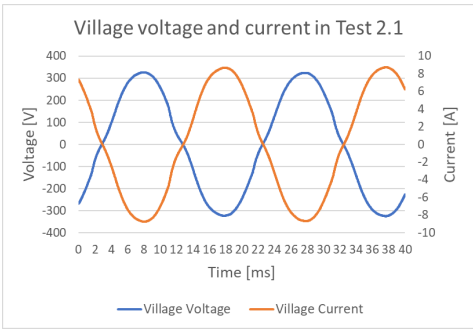

(a) The village voltage (blue) and the village current (orange) when the village load resistance is equal to 37 Ω, $P_{village}$ = 1436 W and $P_{ballast}$ = 25 W

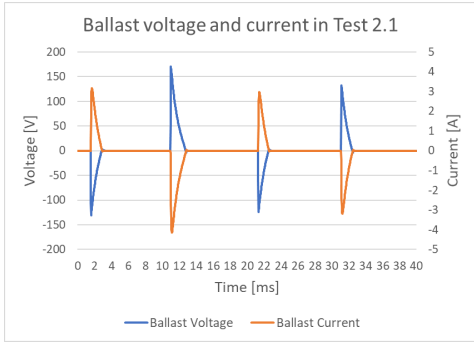

(b) The ballast voltage (blue) and the ballast current (orange) when the village load resistance is equal to 37 Ω, $P_{village}$ = 1436 W and $P_{ballast}$ = 25 W

Figure 5.6: Village voltage and current in Test 2.1 (a) and ballast voltage and current in Test 2.1 (b)

Figure 5.7a shows the instantaneous village voltage in blue and the instantaneous village current in orange, in test 2.2. Figure 5.7b shows the instantaneous ballast voltage in blue and the instantaneous ballast current in orange, in test 2.2. In this test the village load resistance is equal to 79 Ω, the village power is equal to 707 W and the ballast power is equal to 507 W.

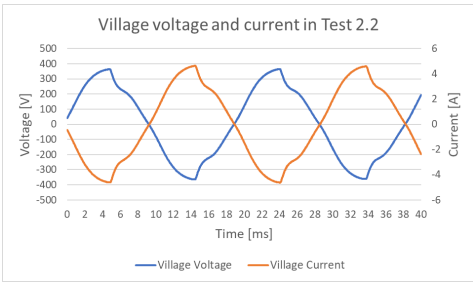

(a) The village voltage (blue) and the village current (orange) when the village load resistance is equal to 79 Ω, $P_{village}$ = 707 W and $P_{ballast}$ = 507 W

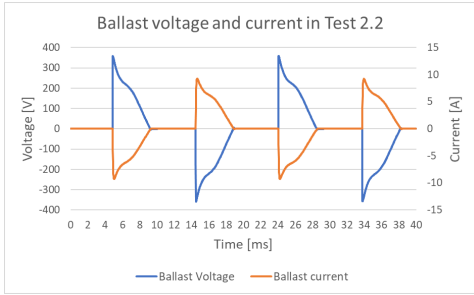

(b) The ballast voltage (blue) and the ballast current (orange) when the village load resistance is equal to 79 Ω, $P_{village}$ = 707 W and $P_{ballast}$ = 507 W

Figure 5.7: Village voltage and current in Test 2.2 (a) and ballast voltage and current in Test 2.2 (b)

5.3.1.1 Fast Fourier Transform

The FFT of a signal is a way of representing the signal by a sum of sinusoidal signals with different amplitude and frequency [54]. By investigating the FFT of the signal an estimate of the total harmonic distortion (THD) of the signal can be found, as explained in Chapter 4.5.

By using Power CASSY the FFT of the measured village voltage signal and village current signal is found, in both test 2.1 and 2.2. The village is disconnected in test 2.3, which means that the THD is not relevant for this test. The result is shown in table 5.3.

Table 5.3: The calculated THD [%] of the village voltage and current in test 2.1 and 2.2.

Calculated THD [%]		
Test no.	2.1	2.2
Voltage THD [%]	4.17	4.3
Current THD [%]	4.08	4.3

5.4 Fine Turning of Induction Generator Controller

From the tests it is clear that the IGC does not work as good as hoped. It can be seen that the voltage increases as the village load decrease, and the IGC allows the voltage to increase further than 230 V. It is desired that the voltage will remain constant equal to 230 V. After communicating with the vendor of the IGC, they proposed to run some tests where the effect of adjusting the finer control parameter in the main board of the IGC would be analyzed. A picture of the tuning opportunities of the IGC can be seen below in Figure 5.8. Where C is the coarse tuning and F is finer tuning. A test was therefore done both with

an increased F and an decreased the F. The vendor also said, not to change the position of C, so this is not done. Figure 5.8a shows the F in the state which has already been tested, from now on named *normal F*. Figure 5.8b shows the state of F when it is decreased, and Figure 5.8c shows the state of F when it is increased.

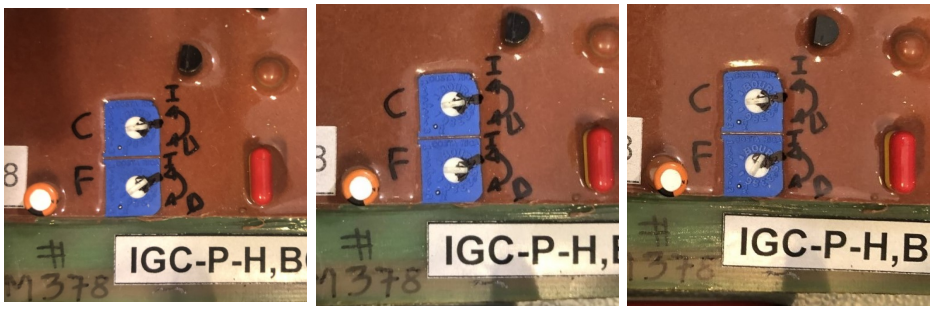

(a) Normal F **(b)** Decreased F **(c)** Increased F

Figure 5.8: The tuning opportunities of the IGC. Showing the variation of the fine tuning on the main board

The tests when changing the position of F are done exactly the same way as test 2. The tests with the name *F normal* are the same test as presented in in Table 5.2. The results when F is decreased are presented in table 5.4. The test results when F is increased, are presented in table 5.5.

Table 5.4: Test result for normal F and when F is decreased (test 2 and test 4)

	F normal			F decreased		
Test no.	2.1	2.2	2.3	3.1	3.2	3.3
Resistance connected [Ω]	37	79	∞	37	79	∞
Rotational speed [rpm]	1585	1612	1599	1580	1612	1605
frequency [Hz]	50.8	51.9	51.3	50.5	51.9	51.7
RMS Phase voltage 1-2 [V]	231.7	235.9	234.1	233.2	240.3	239.1
RMS Phase voltage 2-3 [V]	233.7	241.4	236.9	233.1	243.3	241.3
RMS Phase voltage 1-3 [V]	232.2	228.3	230.2	233.2	229.6	230.8
RMS Line Current 1 [A]	7.2	6.0	6.7	7.4	5.8	6.2
RMS Line Current 2 [A]	7.0	6.4	6.7	7.4	6.8	6.7
RMS Line Current 3 [A]	7.6	8.3	7.9	7.6	8.4	8.3
$P_{village}$ [W]	1436	707	0	1446	731	0
$P_{ballast}$ [W]	25	507	1322	0	429	1191
P_{tot} [W]	1461	1214	1322	1446	1160	1191

Table 5.5: Test results for normal F and when F is increased (test 2 and test 4)

	F normal			F increased		
Test no.	2.1	2.2	2.3	4.1	4.2	4.3
Resistance connected [Ω]	37	79	∞	37	79	∞
Rotational speed [rpm]	1585	1612	1599	1588	1612	1590
frequency [Hz]	50.8	51.9	51.3	51.0	51.9	51.0
RMS Phase voltage 1-2 [V]	231.7	235.9	234.1	230.6	233.2	231.9
RMS Phase voltage 2-3 [V]	233.7	241.4	236.9	234.2	240.1	234.1
RMS Phase voltage 1-3 [V]	232.2	228.3	230.2	232.1	228.0	231.1
RMS Line Current 1 [A]	7.2	6.0	6.7	7.2	6.2	7.1
RMS Line Current 2 [A]	7.0	6.4	6.7	6.8	6.3	7.0
RMS Line Current 3 [A]	7.6	8.3	7.9	7.7	8.1	7.6
$P_{village}$ [W]	1436	707	0	1421	687	0
$P_{ballast}$ [W]	25	507	1322	59	564	1441
P_{tot} [W]	1461	1214	1322	1480	1251	1441

5.5 Discussion

The first test results in test 1.1, shown in table 5.1, show that the SEIG is able to self-excite with the capacitors integrated in the IGC. The tests show that the system is able to archive 230 V across phase 1-2, when the rotor is rotating at 1360 rpm, with no load connected to the SEIG. When the system achieves 50 Hz, the voltage is much higher than 230 V. This was expected because the capacitor is much higher than the capacitor required for archiving 230 V at no-load, which was found to be 33 μF in the specialization project [1]. From Figure 5.3 it can be seen that the intersection of the no-load curve and the 50 μF capacitor curve at 50 Hz, occurs at a much higher voltage level than 230 V, more specific at ca 270 V. The results of test 1.2, show that the voltage is higher than 270 V. The reason for this is not known but may be a result of the frequency being slightly higher than 50 Hz, or it can be because the current measurements are somewhat inaccurate, because the clamp meter only shows one digit. It can also be a result of the uncertainty connected to the test when finding the magnetizing curve, or the uncertainty regarding the best fit line of the magnetizing curve. It can be seen that both the test results differ from the capacitor curve for the corresponding operating frequencies. This may indicate that the capacitor size is it a bit higher than 50 μF, but this may also be because the current measurements are somewhat inaccurate.

In test 1.1, the frequency is lower than 50 Hz, which is the frequency at which the no-load curve was found. In Chapter 2.2.2.1 it was shown that the magnetizing curve is lowered at lower frequencies. This correlates with the obtained result shown in Figure 5.3, where the test result is along the capacitor curve at 45 Hz, but lower than the no-load curve at 50 Hz. Since the magnetization curve for 45 Hz is not known, the test result cannot be verified for sure.

It can be seen from both table 5.2 and 5.1 that the line currents are not 100 % equal in magnitude, meaning that this connection does not ensure a balanced system. All the different phase connections were tested, and the sequence used in these tests, which is presented in Figure 4 in Appendix G was the best connection. The reason why the system is not balances is because the tested system does not satisfy the conditions for a balanced system, since the total load connected is not equal to the rated power. The applied power form the IM should have been decreased in test 2.1 in order to get a balanced system, but as already mentions was it very difficult to fine tune the VFD. The reason because the VFD was difficult to adjust is not known.

The active power in test 2.1 and 2.2 is not equal to the expected values. In test 2.1, the expected power is 1430 W, when there is 230 V across a 37 Ω resistor. Since the voltage is higher, the expected value of the village load power should be 1450 W. Instead the power is 1436 W, meaning that the resistance connected is not 37 Ω, but more like 37.36 Ω. In test 2.2 the expected active power is 670 W, when there is 230 V across a 79 Ω resistance. Since the voltage is increased in this test as well, the expected value pf the village power would be 708 W, which is equal to the measured value. The same happens for the ballast load. The value of the ballast load resistance changes for the different test, even though the resistance is not change. This indicates that the switching of the IGC may affect the power factor of the loads, which was expected. All in all, gives this an indication that the measuring of the load resistances may not be 100 % correct.

It is desired that the generator experiences a constant load connected to the generator terminals, even when the village load varies. From Figure 5.4 and table 5.2 highlighted in orange, it can be seen that this is not the case in these tests. As the village load varies, the IGC does not manage to keep the voltage in phase 1-2 equal to 230 V, highlighted in blue in table 5.2. The reason why there is an increase in the phase 1-2 voltage as the ballast load starts consuming and the power is divided between the two loads, is not known. It could be due to how the IGC measures the voltage, but the investigation of this has not led anywhere, but should be investigated in further work. As the village load power decrease, not enough power is consumed by the ballast load, and the speed of the system increase in order to match the motor torque and the generator torque. The increase in speed ensure a decrease in the mechanical torque from the IM, seen from the characteristic of the IM, shown in Figure 2.11. The workings of the VFD is not known for sure, but it is assumed that the VFD ensure that the IM torque match the SEIG torque at constant electrical frequency at the IM terminals. In this test it can be seen that the system may behaves as shown in figure 5.9. Where operating point 1 corresponds to test 2.1, operating point 2 corresponds to test 2.2 and operating point 3 corresponds to test 2.3. When the total load power and thus the load torque is decreased, the speed of the IM increases which decreases the IM torque, as shown in equation (2.8).

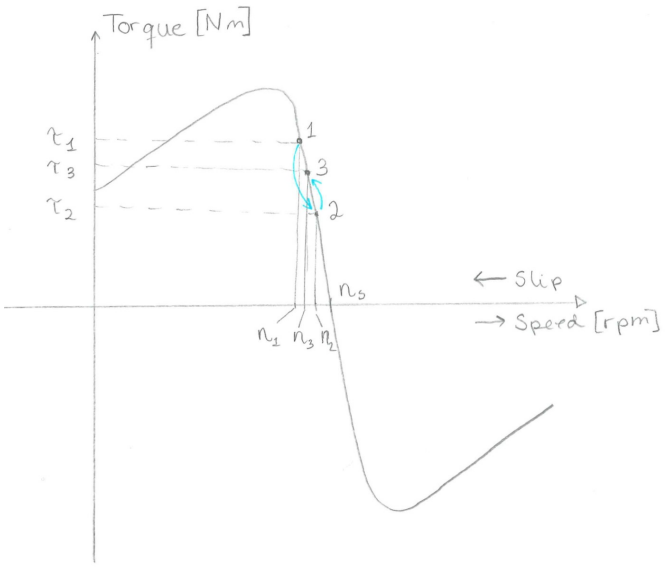

Figure 5.9: The behavior of the IM in this test, when the village load and the total load power is decreased

This test could have been done differently by adjusting the VFD after each village power decrease, to ensure constant rotational speed instead of constant electrical frequency in the IM. The test could also have been performed by using another VFD, ensuring constant rotational speed or constant torque.

Form Figure 5.4 it can be seen that the IGC manage to compensate the change in the village load power very quickly. However, it does not compensate a 100 %. This can also be seen from the small increase in village voltage and the system frequency in Figure 5.5. It can be noticed that there are some noise in the ballast power measurement after the village load is disconnected at time 63 s. The source of this noise is not known. Since the IGC does not keep the voltage equal to 230 V, and the total load power varies, the generator becomes more unbalanced. It can be seen from Figure 5.5 and table 5.2 that the IGC behaves best when the ballast load does not consume power, and second best when the ballast load is the only consumer, and the village load is disconnected.

The aim of this thesis is among other to study the changes in voltage and frequency in the system for different operating points of the system. From table 5.2 and Figure 5.5 it can be seen that the maximum village RMS voltage which is measured is 236.5 V. This is a deviation of +2.8 % of the rated voltage, which is within the defined voltage variation limits of the evaluated isolated systems. From the same table and figure, it can be seen that the maximum frequency and the minimum frequency which is measured is equal to 51.9 Hz and 50.8 Hz respectively. Which means the maximum frequency deviation is +3.8 %, which is

also within the defined frequency limits of the evaluated isolated system. It should also be noted that the frequency is never below 50 Hz. The voltage and frequency deviation could be higher for a village load resistance which is in-between the load in test 2.2 and 2.3, but it is not possible to increase the village load resistance further because there are no more resistors available. The system is also not tested for a higher village loads than in test 2.1, because it is assumed that the village load is not increased further than the rated power.

By evaluating the instantaneous voltage and current in the system during the different tests, it is clear that the waveform of the signals changes a lot for different village loads. It can be seen that the IGC behaves a bit differently than expected. The switching of the ballast load shown in Figure 5.6b and 5.7b is not as smooth as shown in Figure 2.21. It can be seen by compering Figure 5.6a and Figure 5.7a that the harmonics in test 2.2 is higher than in test 2.1, seen from the differences in the waveform. This is also shown in the calculations presented in table 5.3, which present the THD of the different signals. In Chapter 4 it was stated that the THD should not increase 8 $\%$. At almost the worst case, when the triggering is near the peak of the voltage and current signal, in test 2.2, the voltage THD is equal to 4.3 $\%$ and the current THD is equal to 4.3 $\%$.

The test result from the tests where the tuning of the IGC changes, shows that that the voltage becomes higher as the fine tuning is decreased, both at full village load and as the village load resistance is increased. It can also be seen that even if the phase 1-2 voltage is 233.2 V in test 3.1 the ballast load is not consuming, which it should have been, for ensuring 230 V. In test 4 the voltage is kept 230 V in test 4.1, and the voltage is not increase much, as the village load is decreased. In test 2 and 3, the village load voltage increases more than in test 4, as the village load is decreased. which also is good. On the other hand, the currents and the voltages are more balanced in test 3.1 than in test 2.1, but the system is again more balanced in test 2.1 than in test 4.1. However, this is manly a result of the fact that the total load power is different in each test, due to the trouble with the VFD. The currents in test 4.2 and 4.3 more balanced than the currents in the corresponding tests 2.2, 2.3, 3.2 and 3.2. In other words, decreasing F is not the solution.

It is important to point out that in reality, the village load is not connected to the system before the voltage in the loaded phase is 230 V and the ballast load is consuming the rated power.

CHAPTER 6

LABORATORY TESTING OF SYSTEM WITH PUMP-AS-TURBINE

In this chapter the SEIG, the village load, the ballast load and the IGC are tested together with the PAT in the Waterpower laboratory at the Norwegian university of Science and Technology. These tests are done in order to analyze and evaluate the behavior of the system as the village load varies. The test setup, procedure and results will be presented and discussed in this chapter. The power quality in the microgrid is also evaluated, by studying the voltage and frequency deviation from the rated values, the waveform of the measured signals and the THD of the village voltage and village current are also elaborated.

6.1 Test Setup

The test setup for this laboratory test is shown in Figure 6.1, and consist of the SEIG, the IGC, the village load and the ballast load evaluated in the previous chapter, in addition to two pumps, the PAT and an auxiliary one. The auxiliary pump is driven by a frequency drive. Which means that the auxiliary pump can provide and adjust the flow rate and the head of the rig. The flow map is also shown in Figure 6.1, together with the electrical setup. The water is pumped up from the reservoir to the inlet of the PAT. The water is then returned to the reservoir by the piping network. To obtain the right back pressure, the water is first led into a water container filled with a constant amount of water, with free water surface. When the water flows over the water surface of the container, it is led back

to the reservoir. The induction generator is connected directly to the shaft of the PAT, as shown in Figure 6.2. The IGC and the loads is connected as previously. All equipment used in these tests are listed in table 4 in Appendix E.

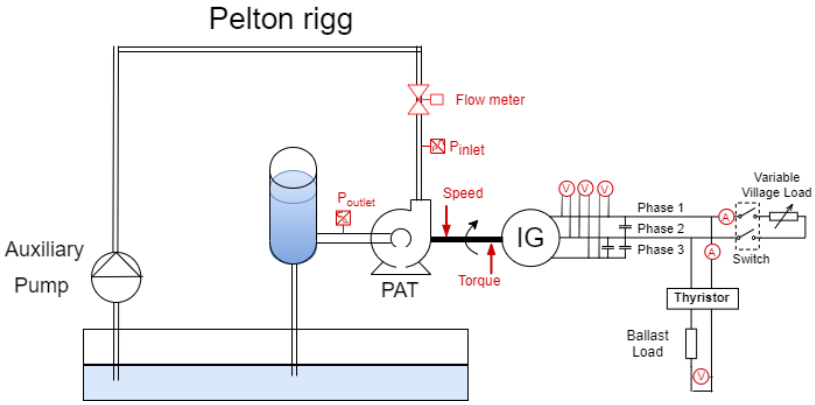

Figure 6.1: Figure showing the test setup in the Waterpower Laboratory. Showing the sensors, the measuring equipment, the pipeline system and the electrical connection of the SEIG, the IGC, the loads and the capacitors.

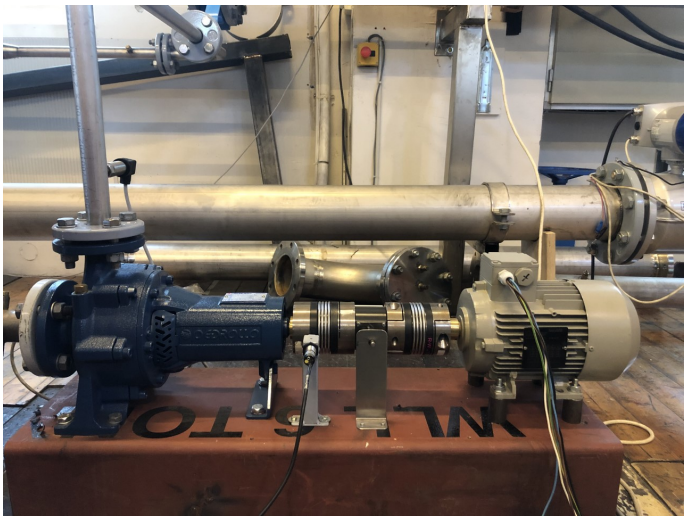

Figure 6.2: Picture of the direct connection of the PAT (to the left) and the induction generator (to the right)

Figure 6.1 also shows the connection of the measuring instruments in the test. A measuring instrument named Power CASSY is used to measure the village and ballast current,

voltage, frequency and power. Three Fluke multimeters are used to measure the phase voltages at the generator terminal. The line currents are measured using a clamp meter. A 50 mm flow meter from Krohne is integrated in the pipeline leading into the inlet of the PAT, measuring the flow rate. The rotational speed of the rotor shaft and the PAT is measured using a speed sensor pointed at a reflective tape attached to the shaft. A torque transducer is also integrated in the rotor shaft, measuring the mechanical torque at the shaft. One pressure sensor is placed at the inlet of the PAT, and another pressure sensor is placed at the outlet of the PAT. The two are measuring the pressure different between the high- and low-pressure side of the PAT. The net head, H_n can be calculated, using equation (6.1) [55].

$$\Delta p = p_{inlet} - p_{outlet} = \rho \cdot g \cdot H_n \tag{6.1}$$

Where Δp is the pressure different in kilo pascal [kPa], ρ is the water density [kg/m^3], and g is the acceleration of gravity [m/s^2]. The pressures, flow rate, speed and torque are logged using LabVIEW.

Both pressure transducers were first designed for 0-5 bar gage pressure, but during the tests it was clear that in order to reach the desired head, ensuring the rated load power, the pressure needed to be increased further. The inlet pressure transducer was therefore switched to a 0-10 bar absolute pressure transducer.

The phase connection of the generator is as found in the previous chapter, shown in Figure 4 in Appendix G. The phase numbering is shown in Figure 6.1.

In addition to the equipment shown in Figure 6.1, a three-phase switch is inserted between the generator and the capacitors. If both the village load and the ballast load are suddenly disconnected during the test, the system will go to runaway conditions, meaning that the rotational speed of the system will increase rapidly. This will increase the frequency, thus also the voltages and currents in the system. In real life, the plant must have overvoltage or overcurrent protection in case of situations like this. In this laboratory test the manual three-phase switch mentioned is used instead.

6.1.1 Calibration

Before the pressure transducers where connected to the rig, they were calibrated. This was done by connecting them to a digital pressure indicator. The produced voltage signal at different pressures was noted, and the best fit line was used as calibration line. Afterwards the calibrations were verified by comparing the pressure measured by the digital pressure indicator with the calibrated measured pressure in LabVIEW. The error between the actual pressure and the measured pressure were calculated to be maximum 0.091 $\%$ for all three pressure transducers used.

Because the pressure transducer at the inlet of the PAT was changed to an absolute pressure transducer and the pressure transducer at the outlet of the PAT was gage, the

air pressure in the laboratory had to be known as the tests were run. This because both of the measured pressures should either be gage or absolute, in order to calculate the difference in pressure across the PAT. The air pressure was therefor noted from a sensor in the laboratory. If the air pressure changed between the different tests, the calibration equation had to be corrected.

Calibration of the flow meter and the torque transducer are both time consuming calibrations and was not be done before executing this laboratory test. Therefore, the calibration certificates from earlier calibrations were used. The torque meter was calibrated by Sondre Skjoldli and Øyvind Albert in [4], last time it was used. The calibration data of the torque transducer, obtained in [4] is attached in Appendix I. The calibration data of the flow meter is also attached in Appendix I. During the tests it turned out that the calibration of the flow meter was not correct. The flow rate [l/s] was therefore read from the display of the flow meter instead. The display only shows one digits.

6.2 Procedure

The laboratory test is started by increasing the rotational speed of the auxiliary pumps slowly. The village load is disconnected from the system at startup, by disconnecting the load switch in the IGC cabinet. The ballast load is connected, but will not consume any power until the voltage is at least 230 V. At one point the head and flow is high enough to start rotating the PAT and the rotor of the SEIG. The rotational speed of the auxiliary pump is further increased, and the voltage rises slowly, until the generator is self-excited. A this point the currents are not balanced. To avoid high currents in the generator phases, the village load is connected before reaching the desired head. After the connection of the village load, the head is further increased, thus increasing the speed of the PAT, the voltage and frequency in the system. The rotational speed of the auxiliary pump is increase until the phase voltage across the loaded phase is 230 V, and the system is balanced. It is also tested to increase the head further, but then the ballast load starts consuming and the system becomes unbalanced. After finding the desired head for ensuring stable operation of the generator, 230 V and 50 Hz, the village load is decreased, and the behavior of the system is studied.

Figure 6.3 shows the control window of the Pelton Rig in the Waterpower Laboratory. In the figure, the piping system to the right do not represent the piping system as it is in reality. The actual piping system is as shown in Figure 6.1.

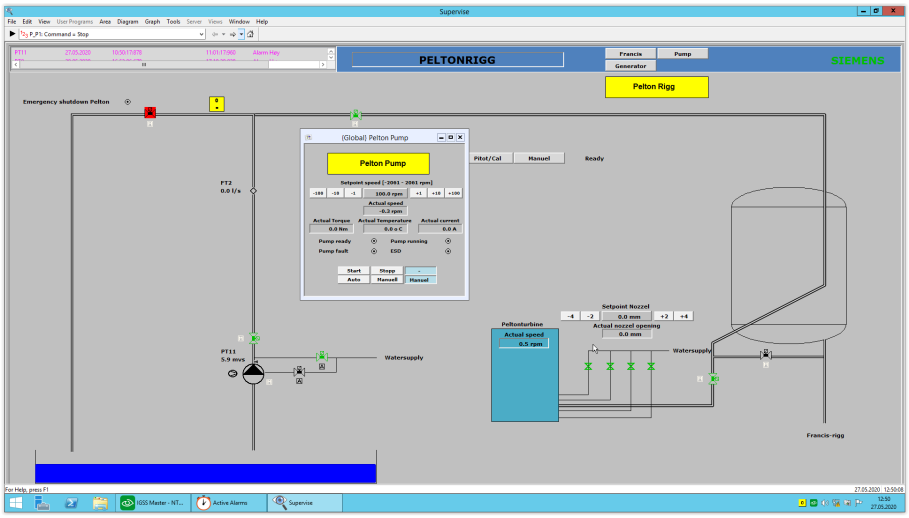

Figure 6.3: Overview of the control panel of the Pelton Rig in the Waterpower Laboratory at the Norwegian university of Science and Technology

During the tests there were some trouble with the pressure transducer over the auxiliary pump, named *PT11* in Figure 6.3. The transducer was only rated to 0 - 4 bar, while the rig is designed to withstand at least 10 bar. To reach the desired head at the PAT, the pressure over the Pelton pump had to be increased beyond 4 bar, which meant that the pressure measurement at the auxiliary pump was as not available.

After preforming the tests, the rotational speed of the auxiliary pumps was decreased slowly, and the village load was switched out, around the same operating point it was switched in, to keep the phase currents low. When the rotational speed of the auxiliary pumps is as low as 100 rpm the system is turned off.

The test is done several times, for the purpose of ensuring that the system behaves equally every time, and to obtain a good test result. Different states of the fine tuning, F, were also tested. First it was tested to increase the F, but it turned out that the voltage at rated power then became lower than 230 V, and the frequency was lower than 50 Hz. In this state, the voltage and frequency were closer to the rated values hen both the village load and the ballast load consumed, compared to when F is in normal state or decreased. Regardless of the position of F, the voltage and frequency increased as both the ballast load and village load consumed. It is therefore decided that the fine tuning should be equal to the stat *F normal*, as shown to the left in Figure 5.8.

6.3 Results

The needed head in order to get a balanced system is found to be 65 m. The measured data of the auxiliary pump, the PAT, the SEIG, the village load, and the ballast load, at this operating point, as the village load is varied, are given in table 6.1. The measured voltage in the loaded phase and the frequency are highlighted in blue. The balanced currents are highlighted in green. The total load power and the speed of the system are highlighted in orange.

Table 6.1: Test results when testing the SEIG, PAT and IGC at the Waterpower laboratory with variation in the village load.

Measured data in test 5							
Test number		5.1	5.2	5.3	5.4	5.5	5.6
Auxiliary pumps							
Rotational speed	[rpm]	1786	1786	1786	1786	1786	1786
PAT							
Speed	[rpm]	1577.1	1619.1	1665.5	1667.2	1612.8	1578.1
Head	[m]	65.1	65.1	65.3	65.2	65.1	65.1
Flow rate	[m^3/s]	0.0956	0.0956	0.0956	0.0956	0.0956	0.0956
Torque	[Nm]	13.7	13.7	13.7	13.7	13.7	13.7
$P_{hydraulic}$	[W]	6102.1	6106.9	6121.1	6112.5	6102.9	6103.5
$P_{turbine}$	[W]	2260.3	2323.9	2392.6	2389.4	2317.6	2268.4
Turbine efficiency, η_t	[%]	37.0	38.1	39.1	39.1	38.0	37.2
SEIG							
RMS Phase voltage 1-2	[V]	229.5	234	235.6	235.2	234.1	229.0
RMS Phase voltage 3-1	[V]	229.7	232.9	233.9	233.8	231.7	228.5
RMS Phase voltage 2-3	[V]	229.6	237.4	245	245.3	236.7	228.8
RMS Line current 1	[A]	7.2	7.1	7.1	7.1	7.6	7.3
RMS Line current 2	[A]	7.2	7.0	6.6	6.4	7.0	7.3
RMS Line current 3	[A]	7.2	7.8	8.4	8.6	7.8	7.3
Frequency	[Hz]	50.4	51.8	53.2	53.3	51.5	50.4
Village load							
Resistance	[Ω]	37	ca 40	56	79	∞	37
RMS voltage	[V]	229.3	234.23	236.07	235.67	0	228.83
RMS current	[A]	6.17	5.79	4.16	3.00	0.00	6.18
Consumed power	[W]	1414	1355	980	704	0	1413
Ballast load							
Resistance	[Ω]	35	35	35	35	35	35
RMS voltage	[V]	0	60.1	134.38	165.63	226.3	0
RMS current	[A]	0	1.65	3.75	4.64	6.37	0
Consumed power	[W]	0	97	500	764	1439	0
Total power	[W]	1414	1453	1480	1468	1439	1413
Generator efficiency, η_g	[%]	62.6	62.5	61.9	61.4	62.1	62.3
Total efficiency	[%]	23.2	23.8	24.2	24.0	23.6	23.2

As the village load is varied, the speed, voltage and frequency of the system is observed, to investigate if there occur changes. The logged output of the speed sensor during the test is shown in Figure 6.4. It can be seen that the measuring signal from the rig is very noisy. The same happens for the torque and pressure signals. The measuring signal is therefore logged and transferred to MATLAB, where the average value for each steady measurement are calculated and presented as shown in table 6.1. However, Figure 6.4 gives a good picture of the variation in speed during test 5. The x-axis shows the time in seconds. From 0 s to 7 s the figure shows the speed in test 5.1. At 7 s, the village load is decreased and the speed of test 5.2 is shown. At 25 s the village load is decreased again, and the figure shows the speed of test 5.3. At ca 40 s the village load is further decreased, and the figure shows the speed of test 5.4. At 55 s, the village load is disconnected, and the speed of test 5.5 is shown. From 80 s to almost 100 s, the figure shows the speed of test 5.6.

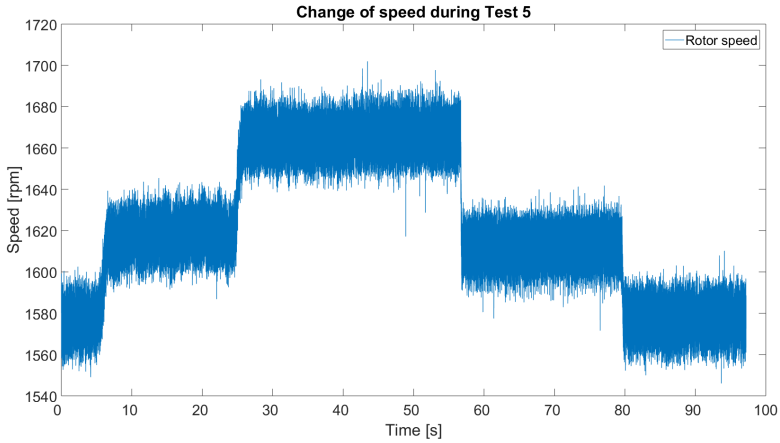

Figure 6.4: The measured speed during the test with varying village load. 0 s - 7 s equal to test 5.1, 7 s - 25 s equals test 5.2, 25 s - 40 s equals test 5.3, 40 s - 55 s equals test 5.4, 55 s - 80 s equals test 5.5 and 80 s - ca 100 s equals test 5.6.

Figure 6.5 shows the village voltage and the frequency during test 5 as the village load varies. The x-axis show time [ms] and the y-axis to the left show voltage, and the y-axis to the right show frequency. Figure 6.6 shows the measures village load and ballast load as the village load varies. In both figures test 5.1 starts at time 0 s, test 5.2 starts at 10 s, test 5.3 starts at ca 30 s, test 5.4 starts at 45 s, test 5.5 starts at 60 s and test 5.6 starts at 85 s.

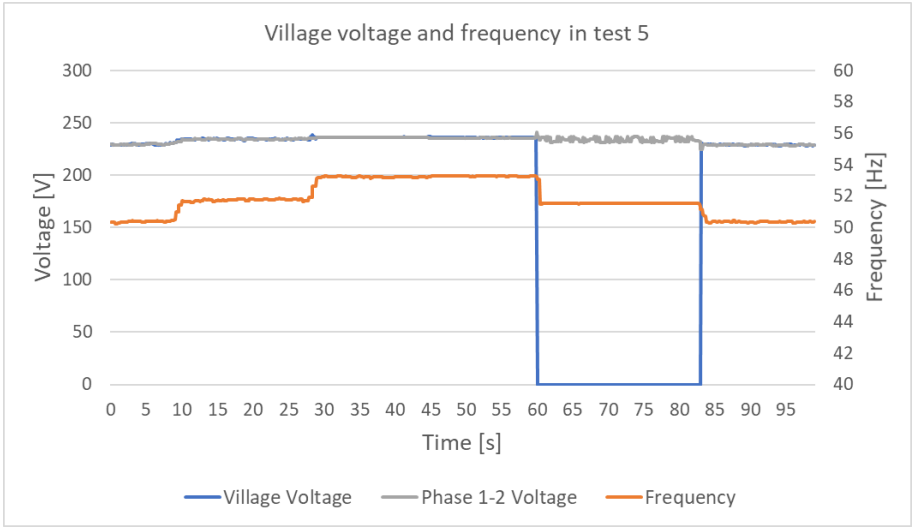

Figure 6.5: Measured village voltage (blue), frequency (orange) and generator phase voltage (gray) as the village load varies.

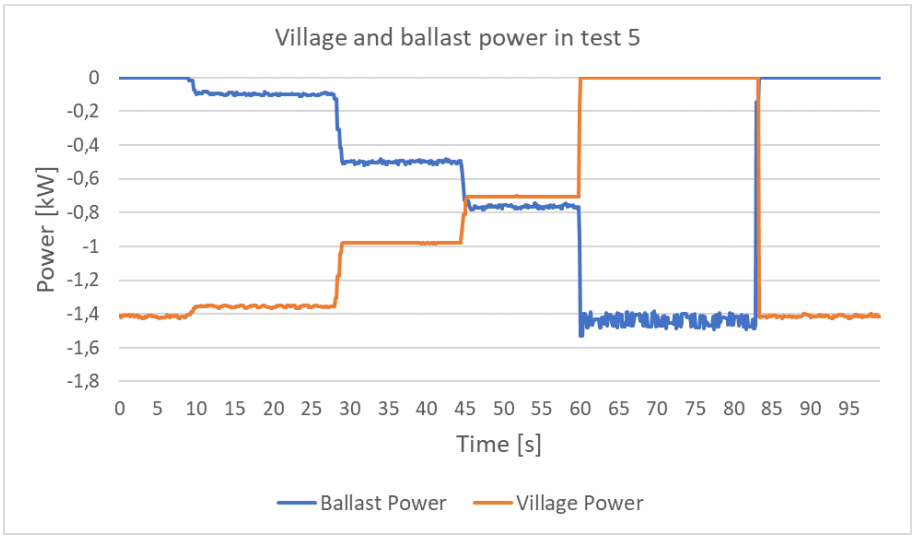

Figure 6.6: Measured village power (red) and ballast power (blue) as the village load varies.

6.3.1 Waveform distortion

The currents and voltages in the evaluated system is sinusoidal when the ballast load is not consuming. As village load decreases, and the ballast load is switched on at different

phase angles, the waveform of the signals changes. During similar tests as test 5.1, 5.2, 5.4 and 5.5 Power CASSY is used to track the instantaneous signals over the village load, the ballast load and the loaded phase, phase 1-2. The RMS measured results are the same as presented in table 5.2, but in this section the waveform of the signals is in focus. To observe the waveform of the signals the sampling time of the Power CASSY was set to 20 μs, and the sampling period was 600 ms. The figures presented only the first 40 ms of the measured signal.

Figure 6.7 shows the instantaneous village voltage and village current during test 5.1. In test 5.1 the village load is equal to 1414 W, and the ballast load is equal to 0 W. Since the ballast load is zero, the ballast voltage and current are not interesting.

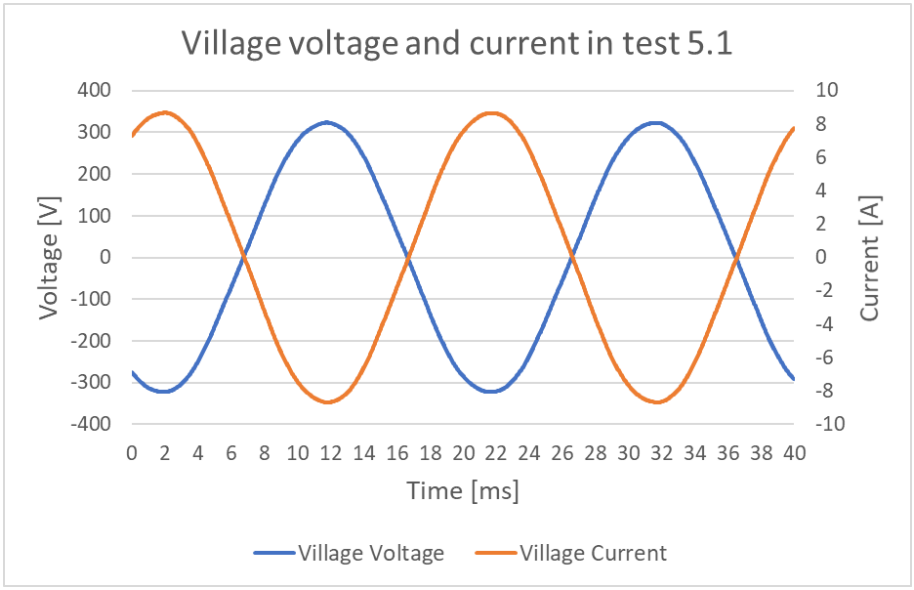

Figure 6.7: The village voltage and the village current in test 5.1. $P_{village}$ = 1414 W, $P_{ballast}$ = 0 W, P_{tot} = 1414 W

Figure 6.8a shows the instantaneous village voltage and village current during test 5.2. Figure 6.8b shows the instantaneous ballast voltage and ballast current during test 5.2. In this test, the village load is equal to 1355 W, and the ballast load is equal to 97 W.

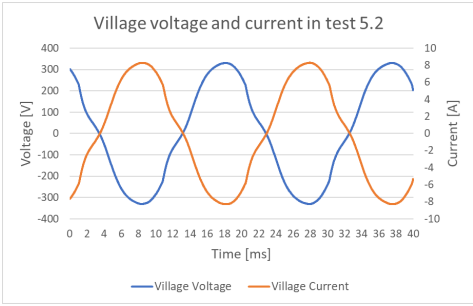

(a) The village voltage and the village current in test 5.2. $P_{village}$ = 1355 W, $P_{ballast}$ = 97 W, P_{tot} = 1453 W

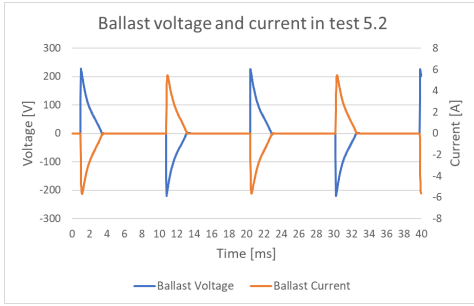

(b) The ballast voltage and the ballast current in test 5.2. $P_{village}$ = 1355 W, $P_{ballast}$ = 97 W, P_{tot} = 1453 W

Figure 6.8: Village voltage and current in Test 5.2 (a) and ballast voltage and current in Test 5.2 (b)

Figure 6.9a shows the instantaneous village voltage and village current during test 5.4. Figure 6.9b shows the instantaneous ballast voltage and ballast current during test 5.4. The village load is in this test equal to 704 W, and the ballast load is equal to 764 W.

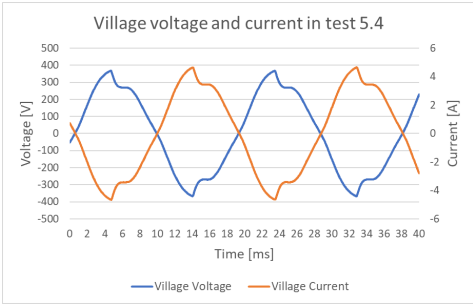

(a) The village voltage and the village current in test 5.4. $P_{village}$ = 704 W, $P_{ballast}$ = 764 W, P_{tot} = 1468 W

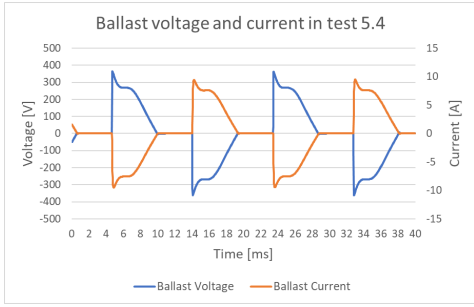

(b) The ballast voltage and the ballast current in test 5.4. $P_{village}$ = 704 W, $P_{ballast}$ = 764 W, P_{tot} = 1468 W

Figure 6.9: Village voltage and current in Test 5.4 (a) and ballast voltage and current in Test 5.4 (b)

Figure 6.10a shows the instantaneous village voltage and village current during test 5.5. Figure 6.10b shows the instantaneous ballast voltage and ballast current during test 5.5. In this test, the village load is disconnected, and the total load power is equal to the ballast load, equal to 1439 W.

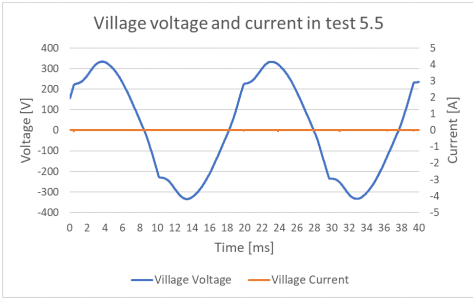

(a) The village voltage and the village current in test 5.5. $P_{village}$ = 0 W, $P_{ballast}$ = 1439 W, P_{tot} = 1439 W

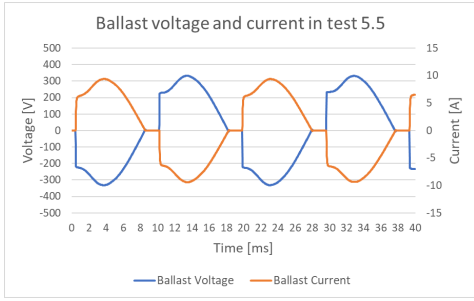

(b) The ballast voltage and the ballast current in test 5.5. $P_{village}$ = 0 W, $P_{ballast}$ = 1439 W, P_{tot} = 1439 W

Figure 6.10: Village voltage and current in Test 5.5 (a) and ballast voltage and current in Test 5.5 (b)

6.3.1.1 Fast Fourier Transform

As explained in Chapter 5, it possible to estimate the THD in the village voltage and village current in the tested system by investigating the FFT of the signal.

By using Power CASSY the FFT of the measured voltage signal and current signal in the village load is found. The result is shown in table 6.2.

Table 6.2: The calculated THD of the measured signals

Calculated THD [%]				
Test no.	5.1	5.2	5.4	5.5
Voltage THD [%]	3.65	4.22	4.34	4.12
Current THD [%]	3.72	4.30	4.33	-

6.4 Discussion

In this test setup there were several uncertainties related to the measuring equipment and the calibration of the sensors and transducers. The flow meter and the torque transducer were not calibrated, which means that the measured values are somewhat uncertain. The signals from the measured speed, pressure transducers and the torque transducer had a lot of noise, which can be seen from Figure 6.4. The LabVIEW measurements where therefore transferred to MATLAB, where the average value of the signal was found, by calculating the mean value of the measured signal over a specific time where the system was known to be in steady state, see Figure 6.4.

During the testing there where some trouble with the flow sensor. When using the measured flow rate and head to calculate the hydraulic power, the calculated hydraulic

power was much lower than the mechanical power at the shaft and the load power, which is not realistic. Since the pressure transducers were calibrated before implemented in the system, and the measured value of the flow rate was unrealistic low, it was concluded that the flow sensor was not calibrated correctly. The flow rate was instead read of the display of the flow meter when the system was operating in steady states. During steady state operations, it was possible to go to the flow meter and read the corresponding flow rate in liters per seconds [l/s] on the display. The uncertainties of the displayed flow rate are not known. The display only shows one decimal, which made it impossible to see small changes in the flow rate.

Due to the uncertainty of the flow rate and the torque transducer, the calculation of the hydraulic power and the delivered power by the PAT must be seen as indicative calculations or rough measurements. For example, the flow rate is assumed constant during the test, as the village load is varied. This because the flow meter only showed one decimal. In reality the flow rate decreases with increasing speed, as shown in Figure 2.4. Even though the measurements are not a 100 $\%$ correct, they show the behavior of the PAT, which is very similar to the behavior elaborated in Chapter 2.1. For instance, it can be seen from the test results shown in table 6.1 that the head increase slightly with increasing rotational speed. This correlates to the fact that the site curve has a parabolic form, and when the speed increase, the flow rate decreases and the head increase. The test results also show that the efficiency of the PAT is lower than the maximal pump efficiency of 55 $\%$, which is expected. This because the PAT BEP is at a head much lower than the head in these tests, at the tested operating speed. The BEP at the tested head, is at a speed much higher than the operating speed. From Figure 2.3 it clear that the efficiency decreases with increasing head beyond the BEP. The test result also shows that the efficiency increases for increasing rotational speed. Figure 2.4 shows the same behavior where the operating point changes from point 4 to point 3. This can be related to the situation because the operating point 4 is far to the left from the BEP at the η_t curve, at 1500 rpm. It is important to notice that even though the efficiency increase for increasing speed, the efficiency at one speed be beyond the best efficiency point and the efficiency decreases rapidly. This can be seen from the same figure, i.e. Figure 2.4, if the speed is increased from point 3 to operating point 2. The same figure also shows that the flow rate changes for different speeds. Since the flow rate is constant in these tests, and thus is assumed constant in the calculations of the efficiency, the efficiency would probably not increase as much as shown in the obtained results, in table 6.1, since the flow rate is in fact decreased.

When the speed increases in these tests, the delivered power by the PAT is also increased because the efficiency increases. This can also be explained by the power speed characteristic of the PAT shown in Figure 2.5 and the torque balance equation (2.8). In this test the behavior of the PAT is explained by use of Figure 6.11. Where point 1 is the starting point at test 5.1, point 2 represent test 5.4 and operating point 3 represent test 5.5. When the total load power is decreased, the PAT rotational speed increases towards runaway speed, shown as speed n_R, in order to find a new equilibrium and a new operating point, where

the mechanical torque matches the electrical torque. If the total load power is increased the operating point will move in the other direction.

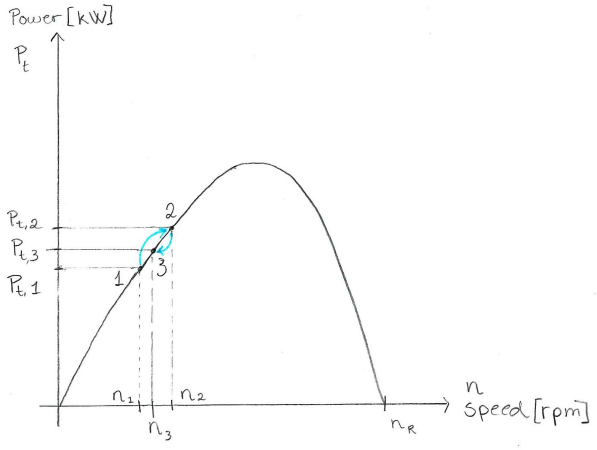

Figure 6.11: The behavior of the PAT in test 5, when the village load is decreased, and the total load power is increased

The behavior of the tested system is quite different in test 5 than in test 2, 3 and 4, shown in Figure 5.9, where the IM was used as prime mover. The characteristic of the PAT clearly affect the behavior of the system, as well as the IGC. Usually the operating point of the PAT is closer to the maximum power output, meaning that the increase in delivered power is limited. It should therefore be considered to change the PAT used in the tested system to another PAT with the maximum power closer to the tested head and flow at the operating speed of the evaluated system. This way the total efficiency of the plant increases, and the maximum delivered power is more limited.

The operating speed in the tested system differs somewhat from the estimated rated operating speed, which was calculated to be 1569 rpm. From table 6.1 it can be seen that the speed of the PAT and SEIG in test 5.1 was 1577 rpm, which is close to the estimated speed. From table 6.1 it can be seen that as the village load decreases the rotational speed increases. The difference between the actual speed and the estimate speed, can be a result of the small increase in frequency and differences in the total load connected to the system.

From table 6.1 it can be seen that, as the connected village load decreases, the phase voltages increase. As the speed of the turbine increases, so does the delivered power by the turbine. At the same time the ballast load will be increased until the load power equals the turbine power, only now the turbine power has increased, and the load power is therefore also increased. This makes the system unbalanced, as can be seen from the measured phase currents shown in table 6.1. The aim of the IGC is to ensure constant

power seen from the generator, by ensuring constant voltage across the village load. The IGC fails to do so perfectly, but it ensures a limited range of total power variation. If both the increase of maximum power is more limited, and the operation of the IGC is improved, the unbalance of the system may be avoided.

The disadvantages of an unbalanced system were presented in Chapter 2.4. The system can operate as an unbalanced system, as long as the current not exceeds the rated current. When operating the PAT at the chosen operating conditions as the ones tested in this laboratory test, the current in the generator exceeds the rated current of the machine, even at balanced operation as shown in green in table 6.1, test 5.1. When the system gets unbalanced, the current in phase 3 increases even more. This can be damaging for the generator, the generator can get overheated, and the lifetime of the generator is significantly affected if operated like this over time. The temperature of the generator increased significantly when running the test in the laboratory. Especially when it was operating with unbalanced current over several minutes. The test where therefore kept short, and the generator had time to cool down between different tests. It can be seen from the test results in table 6.1 that the calculated generator efficiency is a slightly lower than the assumed generator efficiency. This can be a result of the fact that the motor is over loaded. It is therefore recommended to change the SEIG used in this test, to a SEIG with either less strict magnetizing curve or higher rated current. It can also be considered to use a SEIG with higher power ratings. This would decrease the overloading of the SEIG an can also lead to an reduction of the overloading of the PAT as well, since the generator efficiency may increase, which means the net head can be reduced. Another recommendation is to reduce the excitation capacitors integrated in the system. This reduces the rated power in order to ensure balanced operating, which reduces the generator currents and the needed head. In Chapter 3.1.4 is was proposed to use 38 μF capacitors instead of 50 μF capacitors, and to chose the rated power to be 1094 W. This could be further considered.

In test 5.1, it can be seen that the total load power is equal to 1414 W. This is less than the rated power calculated in Chapter 3.1.3 in order to ensure a balanced system, which was calculated to be 1440 W. It can also be seen that the system is in fact balanced in test 5.1. In test 4.5, it can be seen that the total load power is 1440 W, but the system is unbalanced. The reason for this can be due to uncertainties in the capacitor size, the accuracy of the measurements in the laboratory and by Power CASSY, or it could be because there are current related losses in the system, making the generator "see" a higher total load power, than what is measured.

The working of the IGC is not as good as expected. The speed of the PAT and SEIG increases with decreasing village load. The frequency is consequentially also increasing. From the test result presented in blue in table 6.1, it can be seen that the frequency is varied between 50.4 Hz, and up to 53.3 Hz. The maximum increase in frequency is then 6.6 $\%$ from the rated frequency 50 Hz. The voltage increases with decreasing village power as well. The maximum measured RMS village voltage is 236 V, which is 2.6 $\%$ higher than the rated voltage, i.e. 230 V. The minimum village voltage was 229.3 V. This

means that both the frequency and the voltage is within the limits of the desired power quality of the system, defined in Chapter 4. The distribution lines are, on the other hand, not included in the test-setup, and it should be expected that by introducing the lines, the voltage drop will be higher at the end consumer. This, however, was also taken into account when deciding the power quality requirements.

It is important to know that the voltage and frequency were measured within a limited range of village load resistances. This because the available resistors were limited, and the maximal village resistance was 79 Ω. This means that there is a gap in the measurements between 79 Ω and village load disconnection, ∞ Ω. Anyhow, it can be seen from the instantaneous voltage signal across the ballast load in test 5.4 that the switching occurs right before the peak of the voltage wave. This indicates that the test was performed almost during the worst case.

From the instantaneous voltage and current measurements over the ballast load at test 5.4, shown in Figure 6.9b, it can be seen that there are some spikes in the voltage and current amplitudes. This was also the case in test 2.2, shown in Figure 5.7b, which is the similar test only with the IM as prime mover. From the instantaneous voltage and current measurements over the ballast load at test 5.5, shown in Figure 6.10b, it can be seen that the ballast load can consume even more power than it does in this test 5.5, in order to ensure the phase 1-2 voltage is almost 230 V. This because the ballast load is a 35 Ω resistor, designed to be able to consume more than the rated power.

The maximal THD in the village voltage signal and the village current signal in the test are 4.34 $\%$ and 4.33 $\%$ respectively. This is within the defined harmonic limitation of the system, which was defined to be 8 $\%$. The THD results shows that the THD increases from test 5.1 to 5.4. This increase in THD could also be assumed by comparing the instantaneous village signals in Figure 6.7, 6.8a, 6.9a and 6.10a to each other. The THD in test 5.4 is almost the same as the THD in test 2.2, shown in table 5.3, which is done with the same loads connected.

The runaway speed was not tested in this laboratory test. This because the runaway speed is probably much higher than the normal runaway speed which is around 160 $\%$ of the nominal speed. This because the head is much higher than at the BEP. Due to this uncertainty the runaway test is not preformed. Before implementing such system in a real site, the runaway speed should be tested.

Since the operation of the system becomes unbalanced anyways, it could be considered reducing the rated village load connected to the system. This will make the system unbalanced for all operations, but it would also reduce the required head, and the currents can be decreased to below the rated current. It can be seen in test 2.2 and 2.3 in table 5.2, that the currents are closer to the rated current for a lover total load power, than in laboratory test result shown in table 6.1. By doing so, both the overloading of the PAT and

the SEIG will be reduced, but the available load power is also reduced, and the system will be unbalanced.

CHAPTER 7

SIMULATION OF TESTED SYSTEM

A simulation model of the tested system is made in SIMULINK, SIMSCAPE environment in MATLAB, for the purpose of compering the simulation results to the laboratory tests. If the simulation results reflect the results obtained from the laboratory test, the simulation model can be used to further analysis the system with other loads than pure recessive loads and with the implementation of distribution lines, but this is outside the scope of this thesis. In this chapter the simulation model will be explained, and the simulation results will be presented and discussed. The input parameters of this model will be based on the laboratory test results obtained earlier inn this thesis and in the specialization project [1].

7.1 The Model

The simulation model of the tested system is shown in Figure 7.1. A solver, shown as the box with *f(x) = 0*, must be present and connected to the model to be able to run the simulation. The solver configuration is set to the default values. An electrical reference must also be connected to the model and can be seen below the yellow box in the figure. Three voltage sensors measure the phase voltages and a three-phase current sensor measure the line currents from the generator. These measuring sensors are present in the pink box in Figure 7.1. The blue box in Figure 7.1 represent the PAT in the tested system. The green box in Figure 7.1 represent the SEIG, the yellow box consists of the C-2C connected capacitors, the red box is the village load, the orange box represents the IGC and the ballast load. The model of each component will be further explained below.

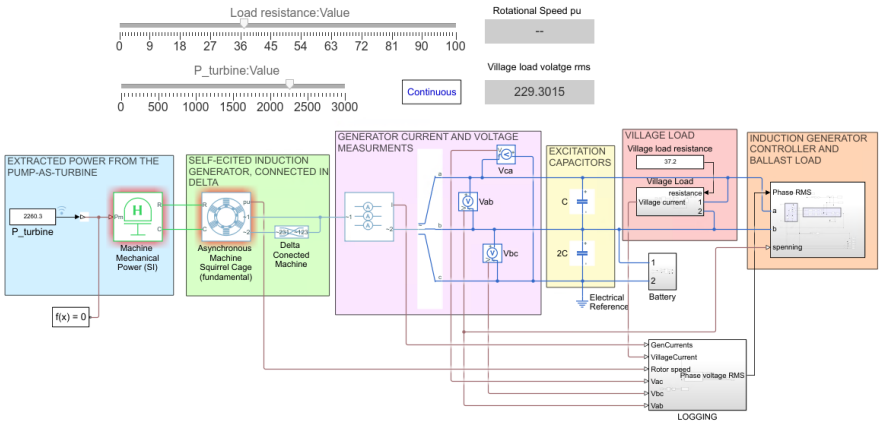

Figure 7.1: The simulation model of the tested micro hydropower system in Simulink. Where the blue box consists of the PAT, the green box consists of the SEIG, the purple box consists of the measuring instruments, the yellow box consists of the excitation capacitors, the red box consists of the village load, the orange box consists of the ballast load and the IGC.

The assumptions in this simulation models are itemized below.

- Only steady states simulation results are considered.
- The solver type is *ode45*.
- $P_{turbine}$ is constant in each simulation.
- Distribution lines is not included.
- The village load and the ballast load are assumed pure resistive loads.
- It is assumed that in the IGC, the triggering angle is decided using a PI-regulator. Since the working of the IGC is not known precisely and the simulation results only considers steady state simulations, the PI-regulator is not tuned more than ensuring that the error becomes zero.

7.1.1 The Pump-as-Turbine

In order to simulate the behavior of the PAT the speed-power curve at the tested head should be known. If this characteristic is not added to the simulation, meaning that the power from the PAT is assumed constant the runaway speed will become much higher than in real life, and the dynamic behavior of the system will not be representative compared to a real-life system. Even so the speed-power characteristics of the PAT is not known for other power-speed operating points than the ones tested in the laboratory. The simulation study the steady state of the simulation tests, in order to recreate the test which was done in the Waterpower Laboratory. The delivered power from the turbine is therefore change

for each simulation to the corresponding measured delivered power from the test results, and is assumed constant during the simulation.

In the simulation model of the PAT, a block named "Machine Mechanical Power (SI)" is used to supply specified power to the induction generator and includes the representation of machine inertia. This block calculates the torque applied to the inertia, by dividing the supplied power by the present speed of the rotor, as shown in equation (2.6). In order to do so, the peak torque to rated torque ratio, the actual inertia and the damping coefficient needs to be defined by the user. The damping coefficient, D [Nm/(rad/s)] represent the viscous friction in the rotor. The damping coefficient is assumed to be 0.005 [pu], by trial and error in the simulation model.

The inertia of the IM used in the tested system is assumed to be in the same order as for similar machines with the same number of poles and rated power found in [56] and is assumed equal to 0.004 [kgm^2]. A rough calculation in order to validate the assumed value was also done. The inertia of the PAT is assumed to be 20 $\%$ of the inertia of the generator, which make the total actual inertia equal to 0.0048 [kgm^2]. In the same motor catalogue [56] the peak torque to rated torque ratio for many machines can be found, the ratio for machines with the same number of poles and power ratings are in between to 2.6-2.8, and it is therefore assumed that the ratio is equal to 2.7 for the machine considered in this system. The input parameters for the "Machine Mechanical Power (SI)" are shown in table 7.1.

Table 7.1: The input parameters of the SIMSCAPE block named Machine Mechanical Power (SI)

Block Parameters: Machine Mechanical Power (SI)	
Main	
Input power sign convention	Generator
Rated apparent power, S_{rated} [VA]	1851.85
Rated electrical frequency, f_{rated} [Hz]	50
Number of pole pairs	2
Peak torque to rated torque ratio	2.7
Inertia	
Actual inertia, J [kgm^2]	0.0048
Per-unit damping coefficient, F	0.005

7.1.2 The Self-Excited Induction Generator

A pre-designed induction machine block, named "Asynchronous Machine Squirrel Cage (fundamental)" is connected in delta and used to simulate the SEIG. The circuit parameters and the magnetizing curve of the IM used in the tested system were found in the specialization project [1] and is presented in Appendix C and in Appendix B respectively. These circuit parameters are implemented in the simulation model of the SEIG. This

magnetizing curve is also implemented in the SEIG block to represent saturation in the machine. The input parameters of the SEIG model is shown in table 7.2.

The rated apparent power of the generator is assumed equal to the rated apparent power when used as a motor. The rated apparent power of the IM, S_{motor} is assumed calculated as shown in equation (7.1).

$$S_{motor} = \frac{P_{shaft,m}}{cos(\phi) \cdot \eta_g} \tag{7.1}$$

Where the $P_{shaft,m}$ is the rated power at the shaft of the motor, $cos(\phi)$ is the full load power factor listed in the name plate data of the motor and η_g is the assumed motor efficiency of 80%.

Table 7.2: The input parameters of the SIMSCAPE block named Asynchronous Machine squirrel Cage (fundamental)

Block parameters: Asynchronous Machine squirrel Cage (fundamental)	
Main	
Rated apparent power, S_{rated}	2314.8 [VA]
Rated RMS line-line voltage, V_{rated}	230 [V]
Rated electrical frequency, f_{rated}	50 [Hz]
Number of pole pairs	2
Type of squirrel cage of the machine	Single squirrel cage
Include of exclude zero sequence	Exclude
Impedances	
Stator resistance, R_s	5.56 [Ω]
Stator leakage reactance, X_s	3.76 [Ω]
Referred rotor resistance, R'_r	4.01 [Ω]
Referred rotor leakage reactance, X'_r	5.64 [Ω]
Magnetizing reactance, X_m	90 [Ω]
Stator zero-sequence reactance, X_0	[Ω]
Saturation	
Magnetic saturation representation	Open-circuit lookup table (v versus i)
No-load stator current saturation data, i (RMS) [A]	Appendix B
Terminal voltage saturation data, v (phase-phase, RMS) [V]	Appendix B

It is important to notice that the magnetizing curve of the induction machine must be implemented as line current versus RMS line voltage for a star connected machine, even if this machine is connected in delta. This is not stated anywhere but was figured out by testing the model when run as motor.

7.1.3 The Capacitors

The three 50 μF excitation capacitors are C-2C connected as explained earlier. Trial and error were used in order to know the right connection of the capacitors, for ensuring the right phase sequence. Two capacitors are connected between phase b and c in the model. One capacitor is connected between phase a and b in parallel with the IGC and the village load.

7.1.4 The Battery

In order to magnetize the IG a DC-source, a battery, must be connected to the terminals of the generator at the beginning of the simulation. This is done because there is no residual flux in the generator at the start, so the generator must be connected to a DC-source in order to get the self-excitation started. The battery is only connected in 0.01 second and the nominal voltage of the battery is set to 24 V, with an internal resistance equal to 2 Ω.

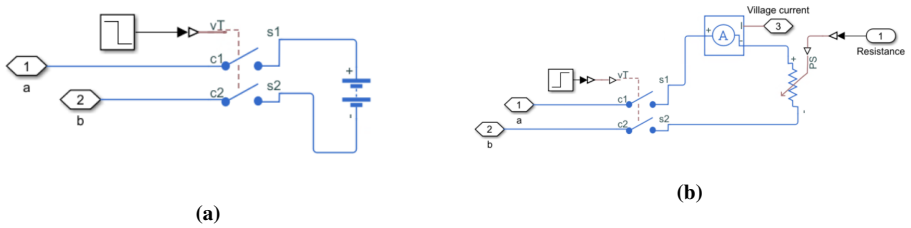

(a) (b)

Figure 7.2: Closeup of the simulation model of the battery (a) and a close up of the simulation model of the village load (b)

7.1.5 The Village Load

The village load consists of a variable resistor, which is disconnected from the model in the beginning of the simulation. This because the generator shall be excited properly. The load is connected after 0.5 second. A voltage sensor and a current sensor measured the voltage, current and the consumed power in the village load. It is possible to vary the village load during the stimulation, but this is not done in these simulations.

7.1.6 The Induction Generator Controller

In order to get simulation results which is comparable with the test results obtained in the laboratory, the IGC is also included in the model. The IGC model presented here, is inspired by a simpler model made by E. Bye and A. Andersson in [6]. In their model the gate signals are set manually, while in the simulation model presented in this chapter, a proportional-integral(PI) regulator controls the gate signals.

Even though the vendor of the IGC was contacted the actual working principal of the IGC is not known. What is known is that the IGC uses phase angle control and that triacs are

used as switching devices. How the gate signals are decided are in this model assumed based on theoretical insight of other phase angle controlled IGCs.

The carrier signal is made by a Phase Locked Loop (PLL), which determine the frequency and the fundamental components of a sinusoidal signal. From the PLL block the angular speed varying for 0 to 2π synchronized with the zero-crossing of the signal. This signal is then multiplied with $\frac{360}{2\pi}$, in order to get the carrier signal to cover 0 ° - 360 ° triggering angle. The carrier signal is then compared to the output from PI controller. The positive sequence triac triggers when the carrier is higher than the PI-regulator output, while the negative sequence triac triggers if the carrier signal is lower than the PI-regulator output. The monostable block then gives a true pulse when it detect a rising change in the input. The pulse duration of the monostable block is set to 0.001 s to be sure that the change is detected.

The frequency is logged as an output from the PLL. It is important to state that the PLL works only properly within a certain range of frequencies. The minimum frequency in the PLL is set to 45 Hz and the initial input frequency is set to 50 Hz. The rest of the parameters are set to the default values.

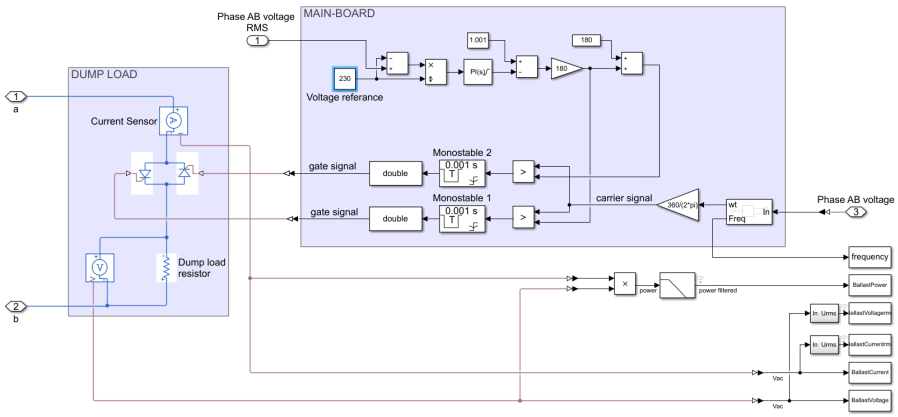

Figure 7.3: Closeup of the IGC model and the ballast load.

The triggering point of the triacs are, as already mentioned, decided by using a PI-regulator. The RMS phase voltage in per-unit (pu) across phase a-b is compared to the desired line voltage, i.e. the reference voltage, of 230 V, equals 1 pu. The obtained error between the voltages is the input of the PI regulator. The input will be multiplied by the proportional gain, K_p, in parallel to being multiplied by the integral gain, K_i which also is integrated. The output is the sum of the two terms. In this model the proportional gain is equal to and the integral gain is equal to 3. The anti-windup method of the PI-regulator is set to *clamping*, so that the integrator will stop integrating

when it reaches the clamp value. The triggering angle for the positive sequence must occur between 0 and 180 degrees. The triggering angel for the negative sequence must occur between 180 to 360 degrees. Therefore, the output signal must be saturated. The upper limit is set to 1, and the lower limit is set to 0 before the output is multiplied with 180 for the positive sequence, and again added to 180 for the negative sequence.

Since the focus in this thesis is the stabilized values, the tuning of the PI-regulator is not in this scope. This is also partly due to the little information of the IGC. However, it is ensured that the error between the measured line voltage and the desired line voltage becomes zero within the simulation time.

7.2 Simulation Results

The simulations are done by applying the measured hydraulic power from one of the steady state measurements done in the laboratory test to the PAT. The village load resistance in the model is selected to the load resistance corresponding to the same steady state measurement in which the delivered power from the turbine was found. Simulation 6.1 corresponds to test 5.1 in the laboratory. Simulation 6.2 represent test 5.2 in the laboratory. Simulation 6.3 represent test 5.3 in the laboratory. Simulation 6.4 represent test 5.4 in the laboratory. Simulation 6.5 represent test 5.5 in the laboratory.

As shown in the laboratory test, the IGC did not manage to ensure 230 V in line AB. The IGC in this simulation model is ideal and manage to eliminate the error. Therefore, the voltage reference in each simulation is set to the line voltage the IGC achieved to maintain in each test result.

The result from each simulation are presented in table 7.3. The input parameters which are taken from the test results in the laboratory, which are change for each simulation, are presented in the beginning of the table.

Table 7.3: Test simulation results when simulating the tested system, with input from the laboratory results

Simulation results at steady state (test 6)						
Test number		6.1	6.2	6.3	6.4	6.5
Input						
$P_{turbine}$	[W]	2260.3	2323.9	2392.6	2389.4	2317.6
Village load resistance	[Ω]	37.2	40.5	56.86	79	∞
Ballast load resistance	[Ω]	35	35	35	35	35
Voltage reference, V_{ref}	[V]	230	234	236	235	234
Output from the SEIG						
RMS Phase voltage 1-2	[V]	230.99	233.98	235.96	234.83	247.27
RMS Phase voltage 3-1	[V]	241.02	242.20	237.40	232.31	250.72
RMS Phase voltage 2-3	[V]	244.37	251.24	257.66	252.35	245.92
RMS Line current 1	[A]	8.16	8.40	8.53	8.32	7.99
RMS Line current 2	[A]	6.28	6.21	5.80	5.78	7.78
RMS Line current 3	[A]	7.79	7.86	7.50	7.48	7.87
Frequency	[Hz]	50.6	51.2	51.8	51.3	50.2
Output from the Village load						
RMS voltage	[V]	230.0	234.0	236	235	247
RMS current	[A]	6.18	5.78	4.15	2.97	0.0
Consumed power	[W]	1421	1352	979	698	0
Output from Ballast load						
RMS voltage	[V]	55.7	75.3	131.1	164.4	244.7
RMS current	[A]	1.59	2.15	3.74	4.70	7.02
Consumed power	[W]	89	162	490	773	1718
Total power	[W]	1510	1514	1469	1471	1718
Generator efficiency, η_g	[%]	66.8	65.2	61.4	61.6	74.1
Speed	[rpm]	1581.9	1602.9	1622.1	1612.05	1574.3

Figure 7.4a shows the instantaneous village voltage and village current during simulation 6.4. Figure 7.4b shows the instantaneous ballast voltage and ballast current during simulation 6.4. In test 6.4 the village load is equal to 698 W, and the ballast load is equal to 773 W.

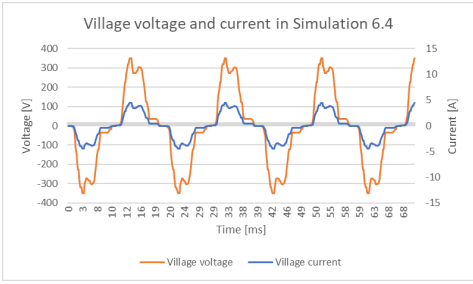

(a) The village voltage and the village current in simulation 6.4. $P_{village}$ = 698 W, $P_{ballast}$ = 773 W, P_{tot} = 1471 W

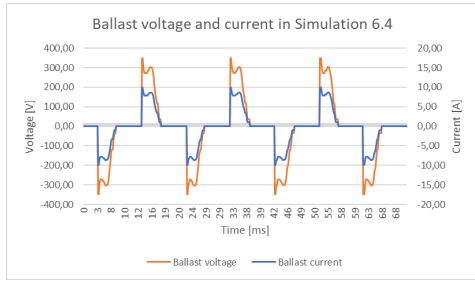

(b) The ballast voltage and the ballast current in simulation 6.4. $P_{village}$ = 698 W, $P_{ballast}$ = 773 W, P_{tot} = 1471 W

Figure 7.4: Village voltage and current in simulation 6.4 (a) and ballast voltage and current in simulation 6.4 (b)

Figure 7.5a shows the instantaneous generator line voltages and Figure 7.5b shows the instantaneous generator line currents during simulation 6.4.

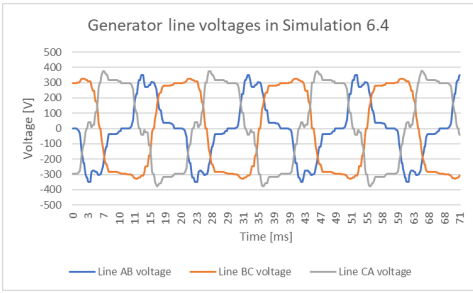

(a) The generator voltage in simulation 6.4. $P_{village}$ = 698 W, $P_{ballast}$ = 773 W, P_{tot} = 1471 W

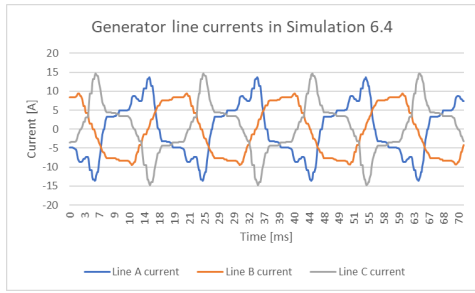

(b) The current voltage in simulation 6.4. $P_{village}$ = 698 W, $P_{ballast}$ = 773 W, P_{tot} = 1471 W

Figure 7.5: Generator line voltages (a) and line currents (b) in simulation 6.4

Figure 7.6a shows the instantaneous village voltage and village current during simulation 6.5. Figure 7.6b shows the instantaneous ballast voltage and ballast current during simulation 6.5. In test 6.5 the village load is equal to 698 W, and the ballast load is equal to 773 W.

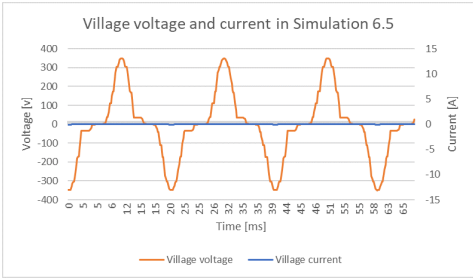

(a) The village voltage and the village current in simulation 6.5. $P_{village}$ = 0 W, $P_{ballast}$ = 1718 W, P_{tot} = 1718 W

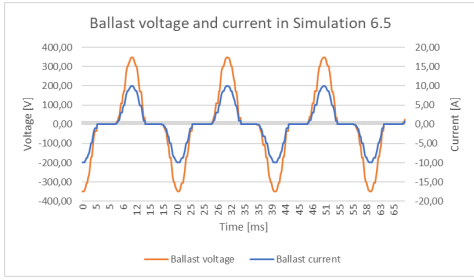

(b) The ballast voltage and the ballast current in simulation 6.5. $P_{village}$ = 0 W, $P_{ballast}$ = 1718 W, P_{tot} = 1718 W

Figure 7.6: Village voltage and current in simulation 6.5 (a) and ballast voltage and current in simulation 6.5 (b)

Figure 7.7a shows the instantaneous generator line voltages and Figure 7.7b shows the instantaneous generator line currents during simulation 6.5.

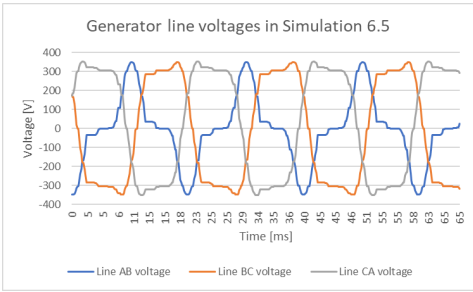

(a) The generator voltage in simulation 6.5. $P_{village}$ = 0 W, $P_{ballast}$ = 1718 W, P_{tot} = 1718 W

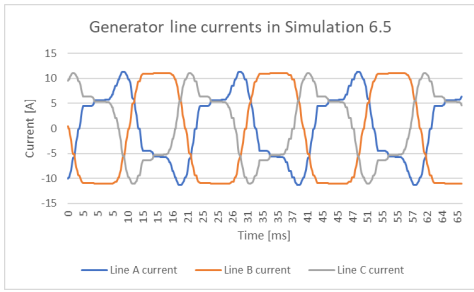

(b) The current voltage in simulation 6.5. $P_{village}$ = 0 W, $P_{ballast}$ = 1718 W, P_{tot} = 1718 W

Figure 7.7: Generator line voltages (a) and line currents (b) in simulation 6.5

7.3 Discussion

Test 6.5 is different than the others, so first only simulation 6.1-6.4 are discussed, and later simulation 6.5 will be discussed. From the simulation results shown in table 7.3, it can be seen that the village voltage, the village current and thus the village power in simulation 6.1, 6.2, 6.3 and 6.4 (highlighted in green) are almost equal to the results obtained in test 5.1, 5.2, 5.3 and 5.4 shown in table 6.1. However, this is because the IGC ensures the voltage is equal to the reference voltage, and the simulated phase voltage in phase 1-2 (highlighted in green) is therefore equal to the phase voltage 1-2 from the laboratory tests. The voltage and current in the ballast power in simulation 6.3 and 6.4

(highlighted in green) are also equal to the measured ballast voltage and current in the laboratory test. Simulation 6.2 achieve almost the same values, while in simulation 6.1 the ballast power should be zero, but is instead 89 W. This can also be seen from the total power. The total power in simulation 6.1 and 6.2 are higher than in the tested results, shown in table 6.1. This is probably because there are losses which are not included in the simulation. For instance the parameters of the SEIG are assumed temperature invariant, but since the generator currents are higher than the rated currents, the temperature of the SEIG increases. The obtained circuit parameters from the specialization project [1] could also be somewhat incorrect. The iron losses are also neglected in this model. Since the efficiency of the tested system is better in the simulation model, the ballast load must consume power in order to obtain 230 V across the village load in test 6.1. From the previous chapter it was also clear that the calculation of the hydraulic power and the delivered power by the PAT must be seen as indicative calculations or rough measurements, due to the uncertainty of the flow rate and the torque transducer,

Since the total power is higher in simulation 6.1 than in test 5.1, the generator becomes unbalanced in test 6.1, as seen from the simulated generator currents table 7.3. The generator voltages are also unbalanced. Even though the line voltage in the loaded line is equal to the voltage in the laboratory tests, the voltage in the other phases is generally higher than the voltages obtained in the laboratory for the corresponding tests. The same applies for the currents, except in line 2, where the current is lower than in the tested results. Generally, all the generator line voltages are both higher and more unbalanced in the simulations compared to the laboratory tests.

In simulation 6.5, the total power is much higher than in the other tests. In this simulation the voltage is also very high in all the three phases. It can be seen from the instantaneous voltage signal in Figure 7.6b that the IGC does not trigger the same way as in test 5.5, shown in Figure 6.10b. This indicates that there is something in the IGC model which is not working properly.

It can also be observed that the speed varies less in the simulations compared to the tested result. It can also be seen that the speed obtained in simulation 6.2, 6.3, 6.4 and especially in 6.5 are lower than the ones from the laboratory tests. This can indicate that the damping coefficient or the inertia constant is higher than it should be. On the other hand, by increasing the speed, the voltages are also increased, and the total power would be even higher. The difference in frequency between the simulation and the test are also affected by the different in speed.

In test 6.5 it can be observed that the line currents are almost balanced, highlighted in yellow. Using equation (2.26) with phase voltage 250 V, frequency equal to 50 Hz, and capacitor equal to 50 μF it can be shown that the rated load power ensuring a balanced operation of the generator operated under these conditions is equal to 1700 W. The power in the ballast load is measured to be 1717 W. Even though the system is balanced, the

voltage is beyond the power quality voltage limits, and the currents are even higher than in test 5.1, shown in table 6.1. In other words, this is not a desired operating point. Simulation 6.5 clearly does not represent the same behavior of the system as shown in test 5.5 in the laboratory.

The simulation model does not represent the behavior of the tested system perfectly, however, simulation 6.1, 6.2, 6.3 and 6.4 gives almost the same results in the village load as the results from laboratory test 5.1, 5.2, 5.3 and 5.4 presented in table 6.1. Further this simulation model should be improved to evaluate the voltage and power in the village load for other loads than a resistive load, or when including distribution lines. It should be clarified why there are differences in the power in simulation model compared to the tested system, so that the simulation model can be further developed in order to observe balanced operation.

CHAPTER 8

CONCLUSION

This thesis has addressed the main challenges for designing and operating an isolated micro hydropower plant consisting of a SEIG, a PAT and an IGC, supplying a varying single-phase village load. The variables of the system are mutually dependent, and it is sufficient to say that the frequency and the voltage are both complex functions of the machine parameters, the excitation capacitor connected and both the size and the type of load that is attached to the system. This makes the system difficult to control. The main focus in this thesis has been to analyze the operation of the evaluated system consisting of the components available, with focus on the relation between voltage, frequency, load consumption, reactive consumption and rotational speed.

In Chapter 3 and Chapter 4 the operating conditions and the power quality requirements of the tested system were defined. The operating conditions were selected in order to ensure balanced operation of the generator. Since the consumers are directly connected to the terminals of the generator, the operating voltage in the microgrid is defined to be 230 V and the operating frequency is defined to be 50 Hz. The power quality requirements of such isolated systems were also defined. It is not necessary to demand the same criteria for the power quality for this system as for bigger and more complex power systems. For the evaluated system the voltage variation should not exceed the range of 220-240 V, and the frequency should be held within 49-60 Hz.

Both the laboratory tests and the simulations show that the tested system, consisting of the pre-selected PAT, the pre-selected three-phased SEIG and the available IGC, are able to supply a varying single-phase resistive load within the voltage and frequency requirements defined for such isolated system, and with the operating conditions defined. However, the

voltage, the frequency vary as the total consumed power by the loads varies. The maximal measured village RMS voltage deviation was 2.6 % from the rated voltage during the tests, and the maximum measured frequency deviation from the rated frequency was 6.6 %. The frequency was never below the rated frequency of 50 Hz. The THD of the village voltage and village current were found to be maximum 4.34 % and 4.33 % respectively. The maximum THD was found when the triacs in the IGC triggered near worst case, at the peak of the voltage wave. This means that the village RMS voltage of the tested system, the frequency of the tested system and the THD of the village voltage and village current of the tested system are within the power quality limits defined. However, the system will at some operating points be unbalanced. By introducing the IGC the aim was to ensure constant total power consumption seen from the generator, which was not perfectly achieved. Since the tested system consists of a three-phase generator converted to a single-phase generator the total load power must satisfy the conditions established in Chapter 2.2.2.1 in order to obtain balanced operation of the generator. The test showed that a balanced operation was possible, when the village load was the only consumer. As the load power was divided in both the village load and the ballast load, the system got unbalanced. This is because the total load power seen from the generator is not held perfectly constant. This is partly because the IGC does not maintain 230 V across the loaded phase, and partly that the operating point of the PAT is far from the maximum power operating point in the power-speed characteristic of the PAT. Meaning that the delivered power from the turbine increases with an increasing speed, due to the steep power-speed characteristic far from the BEP.

In addition to unbalanced operation, the phase currents exceed the rated current of the machine. This results in higher power losses and lower efficiency of the generator. Since the efficiency of the PAT is low as well, the overall efficiency of the tested hydropower plant was calculated to be between 23.2 - 24.2 %. The reason why the currents are so high is mainly because of the size of the excitation capacitors integrated in the IGC. The rated load power necessary to achieve a balanced operation is therefore too high compared to the general tip of derating the motor power to 80 % when used as a generator. It could therefore be considered to either reduce the size of the excitation capacitors or change the SEIG to a SEIG with higher rated current or a less steep magnetization curve, before implementing the evaluated system at a site.

From the PAT section in Chapter 2 it was clear that the prediction of the operation of the PAT is not available. The rotational speed of the PAT and SEIG is dependent on the required operating frequency and the load attached to the generator. The predicted BEP for the PAT at the rated operating speed, corresponds to a far too low delivered power by the PAT compared to the required load power ensuring balanced operation of the generator. The PAT was therefore used for values of the head and flow much higher than at the BEP. This affects the behavior of the system as already mentioned, and as the village load is varied, the delivered power and the speed of the tested system also vary. This is probably one of the reasons why the system is so unbalanced. The required net head when the system was tested in the laboratory was 65 m, and the flow rate was 9.5 l/s.

For these values of the head and flow the PAT worked well, but the efficiency was very low, only between 37-39 $\%$. It can therefore be considered to change the PAT to a PAT which has BEP closer to the operating point tested in the laboratory, because this can both increase the efficiency of the PAT, and limit the increase in delivered power from the PAT.

By using an IGC it has been shown that it is possible to use an uncontrolled PAT to drive an induction generator, without losing control of the voltage and frequency in the system. The number of moving parts in the system is then also reduced and so are the maintenance expenses. This report also shows that it is possible to facilitate the operation in order to use a motor as generator, and to self-excite the induction generator by the C-2C connection of the capacitors.

The main findings in this thesis shows that the PAT behaves as expected. This also counts for the SEIG which is able to self-excite but is overloaded due to the objective of ensuring balanced operation of the system with oversized capacitors. The IGC, on the other hand, does not operate perfectly. However, the tested system could be used as it is, but there should be a better match of the components for a better overall performance of such a system. The overloading of the components reduces the lifetime of the system, meaning that the robustness decreases, and the reliability becomes even lower than it already is. Due to the mismatch of the components, the power quality for loads that are not purely resistive, as assumed in this thesis, could be poor. For more sensitive loads another solution should be considered. Since the system is unbalanced anyways, it could also be considered to reduce the rated load power and head of the system, for the purpose of decreasing the overloading of the PAT and SEIG. Both the frequency and the voltage could still be within the limitations, as shown in the test of only the IGC and the SEIG. The current may then be below the rated currents of the SEIG. The simulation model could be handy for such further evaluations.

CHAPTER 9

FURTHER WORK

In this chapter recommendations for further work are presented.

- Consider if the SEIG, the IGC or the PAT should be changed.
- Evaluate the protection needed for safe operation of the evaluated system, if the system is to be deployed at a real site (overcurrent trips, overvoltage protection, earthing, etc.).
- Design the intake structure and penstock of the micro hydropower plant (the civil work), if the system is to be deployed at a real site.
- Implement transmission lines in the simulation model.
- In order to create a more realistic simulation model, the speed-power characteristic of the PAT should be found by testing, without the IGC, at constant head.
- The PI-regulator should also be tuned, and the implementation of the IGC should be investigated further. By implementing the power-speed characteristic of the PAT, and the correct working of the IGC a more realistic dynamic behavior of the tested system can be simulated
- The performance curve of the PAT could be predicted using computational fluid dynamics (CFD) simulation or other more advanced prediction methods than Sharma.
- Performer a transient analysis of the tested system.
- Consider the behavior of the system when an inductive load is connected.
- Test the evaluated micro hydropower plant when supplying small pumps or fans.

- Consider using a three-phase IGC.
- Consider using an IGC with another control method, like mark-space ratio control. Such IGC may be more expensive, however, it may control the system better.
- Consider increasing the redundancy of the system. The IGC used now have no redundancy, while electric load controllers produced and used by Remote hydro Lights focus more on redundancy, shown in [57].
- Do a similar analysis, only start with a potential site, do a feasibility study, in order to detect the required power from the village and the site head a flow, and then choose a PAT and SEIG accordingly.

BIBLIOGRAPHY

[1] Ragnhild Petterteig Mo. Analysis of a self-excited induction generator used in a micro hydropower plant. Specialization project, Norwegian University of Science and Technology, December 2019.

[2] H. Ritchie and M. Roser. Access to energy. Published online at OurWorldInData.org. Retrieved from: https://ourworldindata.org/energy-access [Online Resource, Accessed 17.12.19], 2019.

[3] S. Evans. Around the world, more than a billion people still lack access to electricity". Published online at carbonbrief.org. Retrieved from: https://www.carbonbrief.org/renewables-will-help-more-people-access-electrcity-than-coal-iea [Online Resource, Accessed 17.12.19], 2017.

[4] S. Skjoldli and Ø. Albert. Pump as turbine, symmetry prediction method for pump as turbine characteristics. Master's thesis, Norwegian University of Science and Technology, June 2018.

[5] N. M. Wahl. Frequency control of a hydro turbine by the use of dump-load to a high temperature heat storage. Specialization project, Department of Energy and Process Engineering, Norwegian University of Science and Technology, December 2018.

[6] E. Bye and A. Andersson. Analysis of self-excited induction generator for use in rural area with electronic load controller and additional compensation methods. Master's thesis, Norwegian University of Science and Technology, June 2016.

[7] A. A. Williams. Pumps as turbines for low cost micro hydro power. *Renewable Energy*, 9(1):1227 – 1234, 1996.

[8] A. Williams. *Pumps as Turbines, A user's guide*. Intermediate Technology Publications, 1997.

[9] N. Smith. *Motors as generators for Micro-hydro power*. Practical Action Publishing, 2008.

[10] J. Björnstedt. Island operation with induction generators - frequency and voltage control. 2009.

[11] S. Evans. Africa deforestation. Published online at wwf.panda.org, Retrieved from: https://wwf.panda.org/our_work/forests/deforestation_fronts2/deforestation_in_the_congo_basin/ [Online Resource, Accessed 17.12.19], 2017.

[12] NVE. Små vannkraftverk. Published online at nve.no. Retrieved from: https://www.nve.no/konsesjonssaker/konsesjonsbehandling-av-vannkraft/sma-vannkraftverk/?ref=mainmenu [Online Resource, Accessed 20.04.2020].

[13] L. Ruisheng L. Fusheng and Z. Fengquan. *Microgrid Technology and Engineering Applications*. Addison Wesley, 1994.

[14] Jorge Parrondo, Sandra Velarde-Suarez, and Carlos Santolaria. Development of a predictive maintenance system for a centrifugal pump. *Journal of Quality in Maintenance Engineering*, 4:198–211, 09 1998.

[15] J Fernández, E Blanco, Jorge Parrondo, Matt Stickland, and T Scanlon. Performance of a centrifugal pump running in inverse mode. *Proceedings of The Institution of Mechanical Engineers Part A-journal of Power and Energy - PROC INST MECH ENG A-J POWER*, 218:265–271, 06 2004.

[16] Natural Resources Canada. *Hydropower Micro-Hydropower Systems: A Buyer's Guide*. 2004.

[17] G. Fischer J.-M. Chapallaz, P. Eichenberger. *Manual on pump used as turbines*, volume 11. Deutsches Zentrum fur Entwicklungstechnologien GATE, 1992.

[18] J. Evans. Centrifugal pump efficiency — specific speed. Retrieved from: https://www.pumpsandsystems.com/centrifugal-pump-efficiency-specific-speed [Online Resource, Accessed 01.05.2020], 2012.

[19] A. Kjølle. *HYDROPOWER IN NORWAY, Mechanical Equipment*. Norwegian University of Science and Technology, 2001.

[20] T. K. Nielsen. Lecture notes. Waterpower Lab. , NTNU.

[21] How to plan a mini hydro power project. Retrieved from: https://energypedia.info/wiki/How_to_Plan_a_Mini_Hydro_Power_Project#toc [Online Resource, Accessed 03.03.2020].

[22] Buono Dario, Emma Frosina, Antonio Mazzone, Umberto Cesaro, and Adolfo Senatore. Study of a pump as turbine for a hydraulic urban network using a tridimensional cfd modeling methodology. volume 82, 09 2015.

[23] Guo Baoling, Bacha Seddik, Mazen Alamir, and Hossein Imaneini. An anti-disturbance adrc based mppt for variable speed micro-hydropower plant. pages 1783–1789, 10 2017.

[24] A A Williams. The turbine performance of centrifugal pumps: A comparison of prediction methods. *Proceedings of the Institution of Mechanical Engineers, Part A: Journal of Power and Energy*, 208(1):59–66, 1994.

[25] Guide vanes in francis turbines. Retrieved from:f http://www.ivt.ntnu.no/ept/fag/tep4195/innhold/Forelesninger/forelesninger%202006/8%20-%20Guide%20Vanes%20in%20Francisturbines.pdf [Online Resource, Accessed 17.02.2020].

[26] A. Doig. *Micro-Hydro Power*. Practical Action, United kingdom, 2009.

[27] Pedrello. Fg standardised en733 centrifugal pump. Published online at termoidraulica2006.com. Retrieved from: https://www.termoidraulica2006.com/pictures/Pedrollo_FG_scheda_UK_32.jpg [Online Resource, Accessed 19.04.2020].

[28] J. B. Ekanayake. Induction generators for small hydro schemes. *Power engineering journal*, pages 61–67, April 2002.

[29] S. J. Chapman. *Electrica Machinery Fundamentals*. McGraw-hill Education, 2012.

[30] I. J. Nagrath D. P. Kothari. *Electrical Machines*. 2018.

[31] Manitoba HVDC Research Centre. Pscad cookbook: Chapter 5 - induction machines. Retrieved from: https://hvdc.ca/knowledge-base/read,article/49/chapter-5-induction-machines/v: [Online Resource, Accessed 05.02.2020].

[32] Bogdan Laurean. Torque and speed in the actuating of mechatronic systems, a case study. *International Journal ROBOTICA MANAGEMENT*, Vol. 20:55, 12 2015.

[33] J. M. Elder, J. T. Boys, and J. L. Woodward. The process of self excitation in induction generators. *IEE Proceedings B - Electric Power Applications*, 130(2):103–108, 1983.

[34] F. A. Farret. M. G. Simões. *Renewable Energy Systems: Design and Analysis with Induction Generators*. CRC Press, 2004.

[35] R.D. Laramore G. McPherson. *An Introduction to Electrical Machines and Transformers*. John Wiley & Sons, 1981.

[36] S. Mababazi and J. Leary. Analysis and Design of Electronic Load Controllers for Micro-hydro Systems in the Developing World. Technical report, University of Sheffield, March 2010.

[37] O. D. THAPAR. Modern hydroelectric engineering practice in india: Electromechanical works. Retrieved from: https://www.iitr.ac.in/departments/HRE/pages/Publications+Modern_Hydroelectric_

Engg_Practice_by_Prof_OD_Thapar.html [Online Resource, Accessed 02.05.2020].

[38] N. W. Aung and A. Ze Ya. Design Calculation and Control System Simulation of a Microcontroller Based Electronic Load Controller for Stand-alone Microhydropower Plant. Technical report, Department of Electrical Power Engineering, Mandalay Technological University Mandalay, Myanmar, December 2018.

[39] N. P. A. Smith. Induction generators for stand-alone micro-hydro systems. In *Proceedings of International Conference on Power Electronics, Drives and Energy Systems for Industrial Growth*, volume 2, pages 669–673 vol.2, Jan 1996.

[40] P. G. A. Kumara. Advance control system for small hydro power project. *National Energy Symposium - 2014*, page 26–38, 2014.

[41] A. Karki B. Pandey. *Hydroelectric Energy: Renewable Energy and the Environment*. CRC Press, 2016.

[42] P. G. A. Kumara. Advance control system for small hydro power project. *National Energy Symposium*, pages 26–38, 2014.

[43] J. B. Ekanayake. Thyristor di/dt and current pulse capability. *Thyristor Physics*, pages 61–67, April 2002.

[44] S. A. Nasar I. Boldea. *The induction machinees design handbook*. Taylor and Francis Groupe, 2010.

[45] C. Z. Kimambo J. Kihedu O. J. Mdee, T. K. Nielsen. Performance evaluation of pump as turbine based on the system curve characteristics. *Renewable Energy*.

[46] P. Kundur. *Power System Stability and Control*. McGraw-hill Education, 1994.

[47] Ieee guide for synchronous generator modeling practices and applications in power system stability analyses. *IEEE Std 1110-2002 (Revision of IEEE Std 1110-1991)*, pages 1–80, 2003.

[48] V. Ajjarapu G. Andersson A. Bose C. Canizares N. Hatziargyriou D. Hill A. Stankovic C. Taylor T. Van Cutsem V. Vittal P. Kundur, J. Paserba. Definition and classification of power system stability ieee/cigre joint task force on stability terms and definitions. *IEEE Transactions on Power Systems*, 19(3):1387–1401, 2004.

[49] David Howe. *Frequency Stability*, page 2. 03 2005.

[50] N. P. A. Smith. Induction generators for stand-alone micro-hydro systems. In *Proceedings of International Conference on Power Electronics, Drives and Energy Systems for Industrial Growth*, volume 2, pages 669–673 vol.2, 1996.

[51] Ieee recommended practice for monitoring electric power quality. *IEEE Std 1159-2019 (Revision of IEEE Std 1159-2009)*, pages 1–98, 2019.

[52] E. Csanyi. How bad harmonics influence the work of motors and generators, transformers, capacitors etc. Retrieved from: https:

//electrical-engineering-portal.com/harmonics-influence [Online Resource, Accessed 04.05.2020], 2017.

[53] Ieee recommended practice and requirements for harmonic control in electric power systems. *IEEE Std 519-2014 (Revision of IEEE Std 519-1992)*, pages 1–29, 2014.

[54] P. B. Andersen. Fft. Published online at snl.no. Retrieved from: https://snl.no/FFT [Online Resource, Accessed 17.02.2020], 2018.

[55] Engineering ToolBox. Static pressure vs. head in fluids. Retrieved from: https://www.engineeringtoolbox.com/static-pressure-head-d_610.html [Online Resource, Accessed 19.05.2020], 2003.

[56] Siemens AG. *IEC Squirrel-Cage Motors, Catalog D 81.1*. 2008.

[57] A. Austegard. Electric load control, elc from remote hydrolight for synchronous generator. Published online at remotehydrolight.com. Retrieved from: http://www.remotehydrolight.com/ELC.php [Online Resource, Accessed 29.01.2020], 2012.

Appendices

A Name Plate Data of Pump and Induction Machine

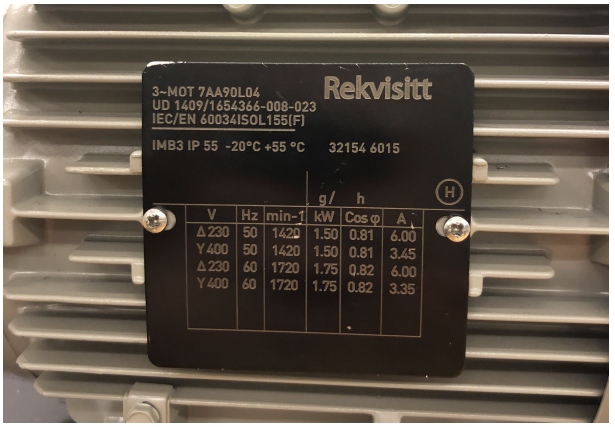

Figure 1: Nameplate data of the induction machine used in this thesis

Figure 2: Nameplate data of the pump used as turbine

B Magnetizing Curve of Tested Induction Machine

The test results from the no-load test done in the specialization project [1] for a star connected machine are presented in table 1.

No-load measurements				
Rotor speed [rpm]	**Phase voltage RMS [V]**	**Phase current RMS [A]**	**Line voltage RMS [V]**	X_m [Ω]
1462	40,4	0,433	70,0	
1477	50,4	0,439	87,3	
1488	61,3	0,459	106,2	129,79
1491	70,9	0,519	122,8	132,85
1494	80,7	0,588	139,8	133,48
1494	90,6	0,641	156,9	137,58
1495	100,3	0,694	173,7	140,76
1499	110,9	0,8	192,1	134,87
1500	120,4	0,867	208,5	135,11
1499	131,8	0,973	228,3	131,70
1499	140,8	1,044	243,9	131,11
1499	149,2	1,103	258,4	131,51
1500	160,5	1,239	278,0	125,78
1499	171,1	1,355	296,4	122,51
1499	180,1	1,438	311,9	121,48
1499	189	1,553	327,4	117,94
1499	200,1	1,737	346,6	111,44
1500	205,9	1,792	356,6	111,14
1500	210,4	1,892	364,4	107,45
1501	215,4	1,98	373,1	105,03
1500	220,2	2,1	381,4	101,10
1499	226,1	2,27	391,6	95,84
1500	231,2	2,4	400,5	92,57
1500	235,7	2,58	408,2	87,60
1499	240,6	2,74	416,7	84,05
1500	245,2	2,93	424,7	79,93
1500	250,9	3,22	434,6	74,16
1500	254,6	3,45	441,0	70,04
1499	260,9	3,83	451,9	64,36

Table 1: Measurements and calculations in the No-load test preformed in the specialization project [1]

The simulation model input for including the saturation of the machine is given below:

- No-load stator current saturation data, i (RMS) [A]:
  [0.00;0.75;1.00;1.25;1.50;1.75;2.00;2.25;2.50;2.75;3.00;3.25;3.50;3.75;4.00]

- Terminal voltage saturation data, v (phase-phase, RMS) [V]: [0.00;183.19;237.59;282.07;318.36;347.89;371.84;391.19;406.74;419.16;428.98; 436.68;42.62;447.10;450.39]

C Circuit Parameters of the Tested Induction Machine

In order to highlight the effect of the assumption of the design class, the parameter result for different designs of the machine is elaborated. The parameters which were found are presented in table 2.

Table 2: The circuits parameters of the induction machine evaluated in ohm, for different designs. Obtained in [1]

Circuit parameters [ohm]			
	Design A	Design B	Design C
R1	5,56	5,56	5,56
R2	4,01	4,01	4,01
X1	4,70	3,76	2,82
X2	4,70	5,64	6,58

D Matlab Script for Finding Magnetizing Curve for Loaded Induction Machine

```
Rs = 5.56;                          %[Ohm] Stator resistance
Xs = 3.76;                          %[Ohm] Stator inductance
Rr = 4.01;                          %[Ohm] Rotor resistance
Xr = 5.64;                          %[Ohm] Rotor inductance
Rload = 110;

Xm = [0,129.79,133.85,137.48,140.58,140.76,134.87,135.11,131.70,
        107.45,105.03,101.10,95.84,92.57,87.60,84.05,79.93,74.16
        ,70.04,64.36];

LABvoltage = 1/sqrt(3)*[0;106.2;122.8;139.8;156.9;173.7;192.1;
        208.5;228.3;243.9;258.4;278.0;296.4;311.9;327.4;346.6;
        356.6;364.4;373.1;381.4;391.6;400.5;408.2;416.7;424.7;
        434.6;441.0;451.9];

LABcurrent = [0;0.459; 0.519; 0.588; 0.641; 0.694;0.8;0.867;
        0.973;1.044;1.103;1.239;1.355;1.438;1.553;1.737;1.792;
        1.892;1.98;2.1;2.27;2.4;2.58;2.74;2.93;3.22;3.45;3.83];

for i = 1:length(LABvoltage)
```

```
    s = -0.002;
    Zgen = (((Rr/s)+j*Xr)*j*Xm(i)/((Rr/s)+j*Xr+j*Xm(i)))+(Rs+j*Xs);
    Itot = LABvoltage(i)/Zgen + LABvoltage(i)/Rload;

        while real(Itot) > 0.01
            s = s - 0.0001;
            Zgen = (((Rr/s)+j*Xr)*j*Xm(i)/((Rr/s)+j*Xr+j*Xm(i)))
                    +(Rs+ j*Xs);
            Itot = LABvoltage(i)/Zgen + LABvoltage(i)/Rload;
        end

    Iload = LABvoltage(i)/Rload;
    Im = (-Iload+Itot) - LABvoltage(i)/((Rr/s)+j*Xr);

    [am,IIm] = cart2pol(real(Im),imag(Im));

    IC50(i) = LABvoltage(i)*2*pi*50*50*10^(-6);
    IC50vol2(i) = LABvoltage(i)*2*pi*45.11*50*10^(-6);
    IC48(i) = LABvoltage(i)*2*pi*50*48*10^(-6);
    IC385(i) = LABvoltage(i)*2*pi*50*38*10^(-6);
    IC33(i) = LABvoltage(i)*2*pi*50*33*10^(-6);
    slip(i) = s;
    Mcurrent(i) = IIm;
    V230(i) = 230;
    Irated(i) = 3.464;
end

 plot(Mcurrent,LABvoltage,'--','LineWidth',2)
 hold on
 plot(LABcurrent,LABvoltage,'LineWidth',2)
 plot(IC50,LABvoltage, 'LineWidth',2)
 plot(IC50vol2,LABvoltage, 'LineWidth',2)
 plot(IC385,LABvoltage, 'LineWidth',2)
 plot(IC33,LABvoltage, 'LineWidth',2)
 plot(LABcurrent,V230,'LineWidth',2)
 plot(Irated,LABvoltage,'--','LineWidth',2)
 plot(3.3,230,'o','LineWidth',2)
 legend('Loaded curve','no-load curve','C3 = 50 micro F (50 Hz)',
        'C3 = 50 micro F (45 Hz)','C2 = 38 micro F',
        'C1 = 33 micro F','230 V line','Rated phase current')
 xlabel('Current [A]')
 ylabel('Voltage [V]')
 title('Magnetizing curve for no-load and loaded machine')
 set(gca,'FontSize',23)
```

E Equipment and Instrument List

Table 3: Equipment used in the test of the IGC

Equipment	ID-number	Used
Variable frequency drive	B03-0144	to control the induction motor
Induction motor	A03-0057	as prime mover
Induction generator	A03-0107	as self-excited induction generator
Tachometer	N06-0094	to measure the rotational speed of the rotor shaft
Variable resistors, 19 ohm and 13 A	K01-0368, K01-0367, K01-0366	as village load
Variable resistors, 23 ohm and 10 A	K01-0373, K01-0374, K01-03	as ballast load
Multimeter	S03-0451, S01-0438	to measure the phase voltages
Direct voltage source	B02-072	as DC source

Table 4: Equipment used in the test of the SEIG, the IGC and the PAT at the Waterpower laboratory

Equipment	ID-number	Used
Pump-as-turbine (Pedrello)	FG 32/160B	as turbine
Torque transducer (HBM T22/200NM)	Iden No: 01709720	to measure the mechanical torque at the shaft
Flow meter (Krohne)	S/N: A07 00394	
Pressure sensor (Druck)	S/N: 4321077, 4321073, 4091551	to measure the inlet and outlet pressure respectively
USB logger box	USB-loggerboks 4	to get the measuring signal into labview
Induction generator	A03-0107	as self-excited induction generator
Speed sensor	No: 01709720	to measure the mechanical speed of the rotor shaft
Variable resistors, 19 ohm and 13 A	K01-0368, K01-0367, K01-0366	as village load
Variable resistors, 23 ohm and 10 A	K01-0373, K01-0374, K01-03	as ballast load
Multimeter	S03-0451, S01-0438,	to measure the phase voltages
Direct voltage source	B02-072	as DC source
Power Cassy		

F Circuit Diagram of Induction Generator Controller

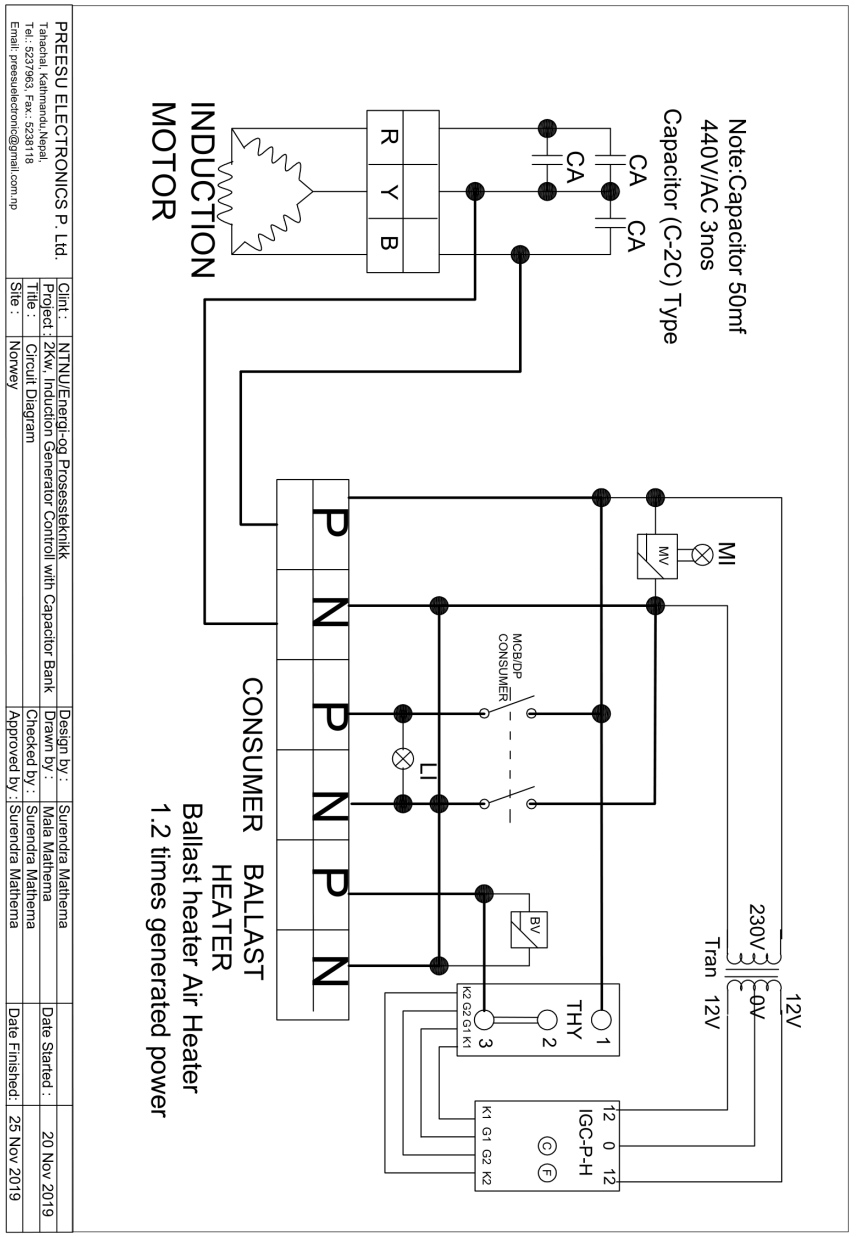

Figure 3: The circuit diagram of the IGC obtained from Preesu Electronics PVTLTD [1]

G Terminal Connections (colour coded)

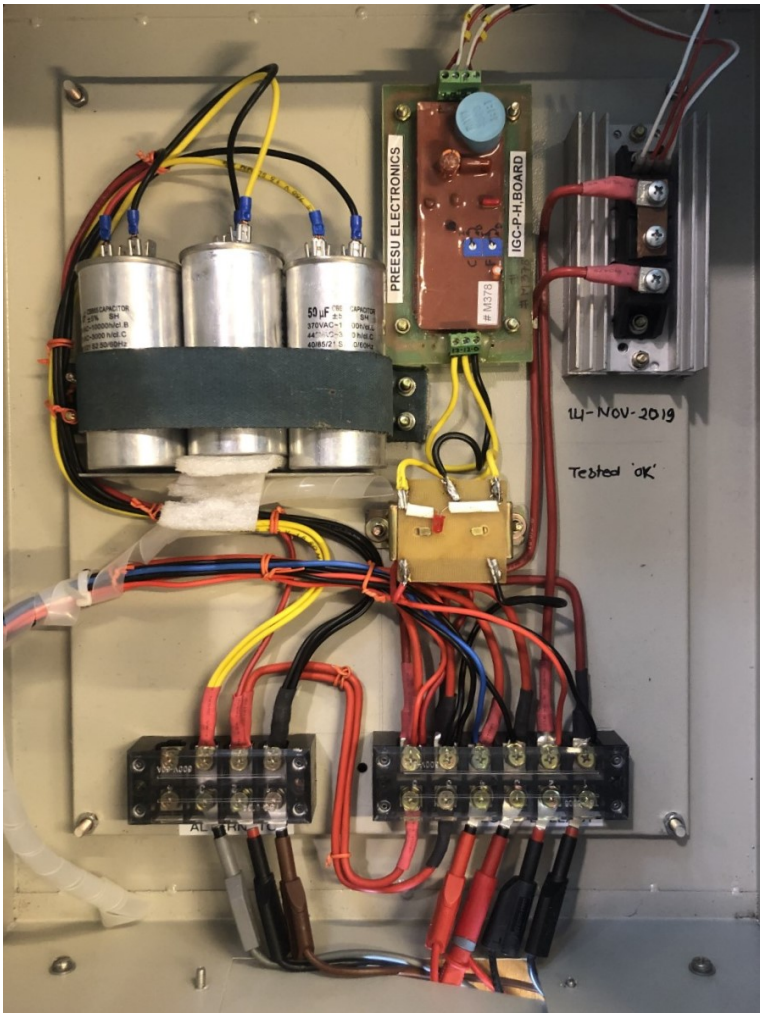

Figure 4: Picture of the connections in the IGC cabinet. The black banana connectors to the right in the connection line in the bottom of the IGC is the ballast load phase. The red banana connectors next to the black once are the village load phase. The white, black and brown banana connector are the three phases of the generator as shown in figure 5.1 and 6.1, where the black connector is referred to as phase 1, the brown connector is referred to as phase 2 and the white connector is referred to as phase 3.

H The Matlab Script for Calculating Mechanical Speed for Achieving Rated Frequency for Given Load

```
clear all
%--------------------Find the speed-------------
% Per unit
fbase = 50;
cos_phi = 0.81;
N = 0.85;                          %0.8-0.85
Vbase = 230;                       % Line to line rms
Sbase = 1500/(cos_phi*N);          % 3-phase
Zbase = Vbase^2/Sbase;             % Z-base
Ibase = Sbase/(Vbase*sqrt(3));
wbase = 1500;                      % nominal rotor speed

%Input data
r_1 = 5.56/Zbase;                  %[pu]
x_1  = 3.76/Zbase;                 %[pu]
r_2 = 4.01/Zbase;                  %[pu])
x_2 = 5.64/Zbase;                  %[pu]
p = 2;                             % Pole pairs

%Chosen values
f1 = 50/fbase;                     %[pu] Stator frequency
r = 110/Zbase;                     %[pu] Load resistance
C = 50*10^(-6);
%[pu] Self-excited capacitor
x_c =(1/(2*pi*f1*fbase*C))/Zbase;



% New circuit parameters
z_L = r*(-i*x_c/f1)/(r-i*x_c/f1);
R_L = real(z_L);
X_L = imag(z_L);
% New circuit parameters
z_l1 = z_L + r_1+ i*f1*x_1;
R_l1 = real(z_l1);
X_l1 = imag(z_l1);


% Roots of the polynomial in order to find the slip
a = f1^2*x_2^2*R_l1;
b = r_2*(R_l1^2+X_l1^2);
c = R_l1*r_2^2;
```

```
P = [a b c];
R = roots(P);
s = max(R);


% Rotor speed
wr = fbase*f1*pi*2*(1-s);        %[rad/s]
nr = 60*wr/(4*pi)                %[rpm]
```

I Calibration of Equipment for Hydraulic Tests

DruckPTX5000calibration 18.05.2020

CALIBRATION REPORT

CALIBRATION PROPERTIES

Calibrated by	: Ragnhild Petterteig Mo
Type/Producer	: UNIK 5000
SN	: 4321073
Range	: 0 – 5 bar g
Unit	: Bar

CALIBRATION SOURCE PROPERTIES

Type/Producer	: Druck Digital Pressure Indicator (DPI601)
SN	: 14206/96-1
Uncertainty [%]	: 0.5

POLY FIT EQUATION

Y = 0.6239 X - 1.2543

CALIBRATION SUMARY

Max Uncertainty	: 0.0503 [%]
Max Uncertainty	: 0.0012 [Bar]
Calibration points	: 8

Figure 5: Calibration data for the pressure transducer used at the outlet of the PAT. SN: 4321073

DruckPTX5000calibration 18.05.2020

CALIBRATION REPORT

CALIBRATION PROPERTIES

Calibrated by	: Ragnhild Petterteig Mo
Type/Producer	: UNIK 5000
SN	: 4321077
Range	: 0 – 5 bar g
Unit	: Bar

CALIBRATION SOURCE PROPERTIES

Type/Producer	: Druck Digital Pressure Indicator (DPI601)
SN	: 14206/96-1
Uncertainty [%]	: 0.5

POLY FIT EQUATION

Y = 0.6242 X - 1.2531

CALIBRATION SUMARY

Max Uncertainty	: 0.0910 [%]
Max Uncertainty	: 0.0014 [Bar]
Calibration points	: 8

Figure 6: Calibration data for the first pressure transducer used at the inlet of the PAT. SN: 4321077

DruckPTX5000calibration 28.05.2020

CALIBRATION REPORT

CALIBRATION PROPERTIES

Calibrated by	: Ragnhild Petterteig Mo
Type/Producer	: Druck PTX 610
SN	: 4091551
Range	: 0 – 10 bar a
Unit	: Bar

CALIBRATION SOURCE PROPERTIES

Type/Producer	: Druck Digital Pressure Indicator (DPI601)
SN	: 14206/96-1
Uncertanty [%]	: 0.5

POLY FIT EQUATION

Y = 1.2486 X – 2.5028

CALIBRATION SUMARY

Max Uncertainty	: 0.0506 [%]
Max Uncertainty	: 0.003 [Bar]
Calibration points	: 10

Figure 7: Calibration data for the first pressure transducer used at the inlet of the PAT. SN: 4091551

CALIBRATION REPORT

CALIBRATION PROPERTIES
Calibrated by: Sondre Skjoldli and Øyvind Albert
Type/Producer: HBM T22/200NM
SN: 01709720
Range: 4-37,5
Unit: Nm

CALIBRATION SOURCE PROPERTIES
Type/Producer: Calibrated Weights
SN: -
Uncertainty [%]: -

POLY FIT EQUATION:
Y= + 1,32395301E+0X^0 + 40,22771287E+0X^1

CALIBRATION SUMARY:
Max Uncertainty : 1,776839 [%]
Max Uncertainty : 0,078748 [Nm]
RSQ : 0,999871
Calibration points : 35

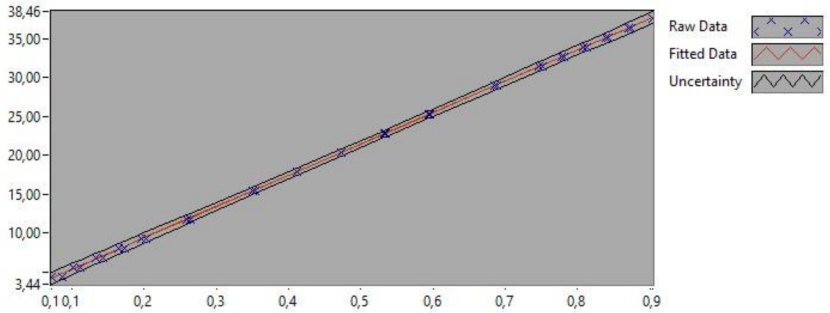

Figure 1 : Calibration chart (The uncertainty band is multiplied by 10)

The uncertainty is calculated with 95% confidence. The uncertainty includes the randomness in the calibrated instrument during the calibration, systematic uncertainty in the instrument or property which the instrument under calibration is compared with (dead weight manometer, calibrated weights etc.), and due to regression analysis to fit the calibration points to a linear calibration equation. The calculated uncertainty can be used as the total systematic uncertainty of the calibrated instrument with the given calibration equation.

Figure 8: Calibration data for the torque transducer. Obtained from [4]

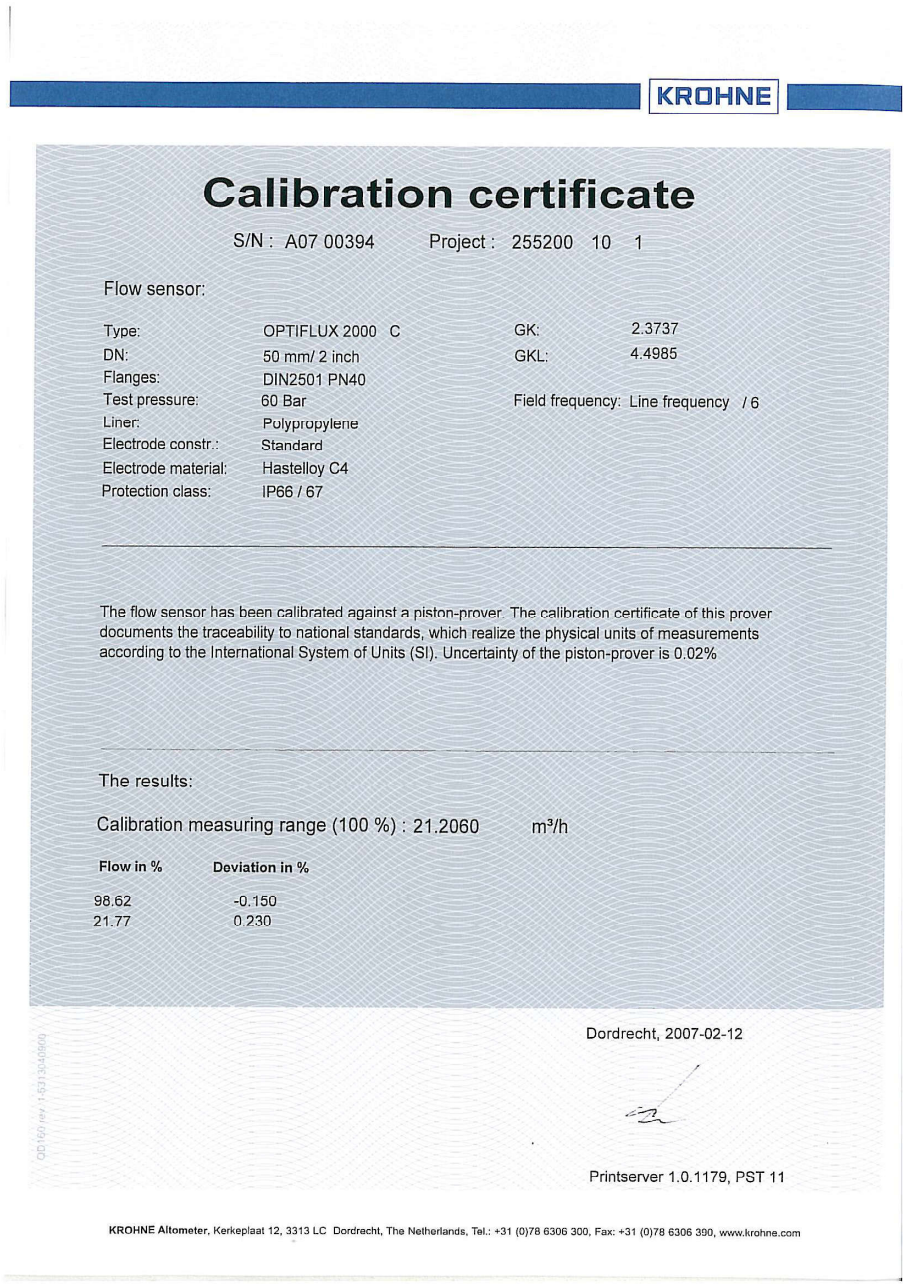

KROHNE

Calibration certificate

S/N : A07 00394 Project : 255200 10 1

Flow sensor:

Type:	OPTIFLUX 2000 C	GK:	2.3737
DN:	50 mm/ 2 inch	GKL:	4.4985
Flanges:	DIN2501 PN40		
Test pressure:	60 Bar	Field frequency:	Line frequency / 6
Liner:	Polypropylene		
Electrode constr.:	Standard		
Electrode material:	Hastelloy C4		
Protection class:	IP66 / 67		

The flow sensor has been calibrated against a piston-prover. The calibration certificate of this prover documents the traceability to national standards, which realize the physical units of measurements according to the International System of Units (SI). Uncertainty of the piston-prover is 0.02%

The results:

Calibration measuring range (100 %) : 21.2060 m³/h

Flow in %	Deviation in %
98.62	-0.150
21.77	0.230

Dordrecht, 2007-02-12

Printserver 1.0.1179, PST 11

KROHNE Altometer, Kerkeplaat 12, 3313 LC Dordrecht, The Netherlands, Tel.: +31 (0)78 6306 300, Fax: +31 (0)78 6306 390, www.krohne.com

Figure 9: Calibration data of the vendor of the flow meter.

J Risk assessment

RISIKOANALYSE (alternativ til bruk av RiskManager)

Enhet/Institutt:	EPT	**Dato opprettet:**	18.05.2020
Ansvarlig linjeleder (navn):	Terese Løvås	**Sist revidert:**	
Ansvarlig for aktiviteten som risikovurderes (navn):	Torbjørn Kristian Nielsen		
Deltakere (navn):	Ragnhild Petterteig Mo		

Beskrivelse av den aktuelle aktiviteten, området mv.:
Risikoanalysen omfatter studentarbeidsoppgaver ved Vannkraft laboratoriet. Det skal gjennomføres testing av et lite vannkraftverk operert i øy drift, bestående av en pumpe brukt som turbin, induksjons generator, eksiterings kondensatorbanker og variable resistorer.

Aktivitet/arbeidsoppgave	**Mulig uønsket hendelse**	**Eksisterende risikoreduserende tiltak**	**Vurdering av sannsynlighet (S)**	**Vurdering av konsekvens (K)** *Vurder en konsevenskategori om gangen. Menneske skal alltid vurderes.*				**Risikoverdi (S x K)**	**Forslag til forebyggende og/eller korrigendene tiltak**	**Restrisiko etter tiltak (S x K)**
			(1-5)	Menneske (1-5)	Øk/materiell (1-5)	Ytre miljø (1-5)	Omdømme (1-5)			
Roterende aksling	Berøringsskade eller skading av utstyr		2	2	1			4	Holde avstand og logge hastighet	2
Støy	Hørselsskade	Hørselsvern/øreplugger	3	1				3		3
Kondensatorbanker	Eksplosjonsfare	Plassert i en beholder	1	2	2			2		2
Berøringsspenning		Beskyttet med avskjerming	1	2				2		2
Høy varme på generator og motstander	Ødeleggelse av utstyr eller brann	Sjekker temperaturen med jevne mellomrom uten å ta direkte på objektene	3	1	1			3		3

Sannsynlighet vurderes etter følgende kriterier:

1 – Svært liten	2 – Liten	3 – Middels	4 – Stor	5- Svært stor
1 gang pr. 50 år eller sjeldnere Ergonomi/psykososialt: Ingen tilfeller	1 gang pr. 10 år eller sjeldnere Ergonomi/psykososialt: Ett enkelt tilfelle	1 gang pr. år eller sjeldnere Ergonomi/psykososialt: Enkelttilfeller	1 gang pr. måned eller sjeldnere Ergonomi/psykososialt: Periodevis	Daglig – hver uke Ergonomi/psykososialt: Kontinuerlig

Konsekvens vurderes etter følgende kriterier:

Gradering	Menneske	Ytre miljø	Økonomi/materiell	Omdømme
5 – Svært alvorlig	Død eller uførhet/ varig nedsatt funksjonsevne	Svært langvarig og ikke reversibel skade	Drifts- eller aktivitetsstans > 1 år	Troverdighet og respekt betydelig og varig svekket
4 – Alvorlig	Alvorlig skade/ belastning som krever medisinsk behandling. Mulig uførhet/ varig nedsatt funksjonsevne.	Langvarig skade Lang restitusjonstid	Driftsstans > ½ år Aktivitetsstans opptil 1 år	Troverdighet og respekt betydelig svekket
3 – Moderat	Alvorlig skade/ belastning som krever medisinsk behandling. Lang restitusjonstid.	Mindre skade og lang restitusjonstid	Drifts- eller aktivitetsstans < 1 måned	Troverdighet og respekt svekket
2 – Liten	Skade/ belastning som krever medisinsk behandling. Reversibel skade. Kort restitusjonstid.	Mindre skade og kort restitusjonstid	Drifts- eller aktivitetsstans < 1 uke	Negativ påvirkning på troverdighet og respekt
1 – Svært liten	Mindre skade/ belastning som krever enkel behandling. Reversibel skade/ belastning. Kort restitusjonstid.	Ubetydelig skade og kort restitusjonstid	Drifts- eller aktivitetsstans < 1 dag	Liten påvirkning på troverdighet og respekt

Risikoverdi = Sannsynlighet x Konsekvens:

KONSEKVENS	**5 – Svært alvorlig**	**5**	**10**	**15**	**20**	**25**
	4 – Alvorlig	**4**	**8**	**12**	**16**	**20**
	3 – Moderat	**3**	**6**	**9**	**12**	**15**
	2 – Liten	**2**	**4**	**6**	**8**	**10**
	1 – Svært liten	**1**	**2**	**3**	**4**	**5**
		1 - Svært liten	**2 - Liten**	**3 - Middels**	**4 - Stor**	**5 - Svært stor**
		SANNSYNLIGHET				

Fargene angir grad av risiko:

Rød		Uakseptabel risiko. Tiltak skal gjennomføres.
Gul		Middels risiko. Tiltak skal vurderes.
Grønn		Akseptabel risiko. Tiltak kan vurderes

Ragnhild Petterteig Mo

NTNU
Norwegian University of
Science and Technology